THE
PHYSICAL REVIEW

A Journal of Experimental and Theoretical Physics Established by E. L. Nichols in 1893

VOL. 55, NO. 6 MARCH 15, 1939 SECOND SERIES

Radioactivity of Li^8

CHARLES KITTEL*
Department of Physics, University of Wisconsin, Madison, Wisconsin
(Received January 25, 1939)

The continuous distribution of alpha-particles observed in conjunction with the beta-decay of Li^8 is examined theoretically from the Fermi theory of beta-decay. It has previously been noted that the Konopinski-Uhlenbeck theory does not give the distribution correctly. An approximate form of the Fermi theory suffices to account for the general form of the distribution. Calculations are presented for $L=0$ and $L=2$, with several values of the nuclear radius. An abnormally small value of Fermi's constant g is found for the beta-decay process, which classes the process as improbable. The consequences of a stable ground state for Be^8 are discussed.

THE bombardment of Li^7 by deuterons produces Li^8,[1,2] a radioactive nucleus which emits beta-rays and has a half-life of 0.88 ± 0.1 sec.[3] This emission of β-particles is accompanied by an alpha-particle activity which decays with the same period. The reactions are:

$$Li^7+D^2=Li^8+H^1$$
$$Li^8=(Be^8)^*+e^-+\nu+Q_1,$$
$$(Be^8)^*=He^4+He^4+Q_2.$$

Breit and Wigner[4] have suggested that the α-particles are emitted from a broad excited virtual state of the intermediate Be^8 nucleus. There is evidence for the existence of such a state, in the neighborhood of 3-Mev excitation energy and with a breadth of about 1 Mev, from the disintegration of B^{11} by protons. Dee and Gilbert[5] showed that the distribution of the three emitted α-particles in the boron reaction could be explained by assuming that one α-particle was first ejected, leaving an excited $(Be^8)^*$ nucleus which then decomposed into two more α-particles. All efforts to detect γ-rays from Li^7 bombarded by deuterons have been unsuccessful;[6,7] it may therefore be concluded that the disintegration into two α-particles is a more probable process than the transition to the ground state of Be^8 with the emission of γ-radiation.

The disintegration sequence is supposed to be: (1) A Li^8 nucleus is formed in a well-defined state; the nucleus subsequently decays with a half-life of 0.88 sec. by beta-neutrino emission. The lower state of this transition does not have a well-defined energy, but corresponds in general to an excited state in the continuum of $(Be^8)^*$. (2) The $(Be^8)^*$ then disintegrates, in a time less than 10^{-20} sec., into two α-particles.

* Wisconsin Alumni Research Foundation Fellow.
[1] H. R. Crane, L. A. Delsasso, W. A. Fowler and C. C. Lauritsen, Phys. Rev. **47**, 971 (1935).
[2] L. H. Rumbaugh and L. R. Hafstad, Phys. Rev. **50**, 681 (1936).
[3] W. B. Lewis, W. E. Burcham and W. Y. Chang, Nature **139**, 24 (1937).
[4] E. Wigner and G. Breit, Phys. Rev. **50**, 1191 (1936); G. Breit and E. Wigner, Phys. Rev. **51**, 593 (1937).
[5] P. I. Dee and C. W. Gilbert, Proc. Roy. Soc. **A154**, 279 (1936).
[6] L. H. Rumbaugh, R. B. Roberts and L. R. Hafstad, Phys. Rev. **54**, 657 (1938).
[7] D. S. Bayley and H. R. Crane, Phys. Rev. **52**, 604 (1937).

The energy distribution of the α-particles has been investigated by several groups of workers.[6, 8, 9] Gamow and Teller[10] have suggested that the observed distributions furnish strong evidence for the Fermi theory of beta-neutrino decay, as opposed to the Konopinski-Uhlenbeck theory, which here leads to predictions in marked disagreement with observation. The main purpose of the present report is to show what general features of the α-particle distribution can be accounted for by the Fermi theory.

The total disintegration energy $Q=Q_1+Q_2=15.9$ Mev is divided between the energy of the light particles $Q_1=E_e+E_\nu$, where E_e is the energy of the electron and E_ν that of the neutrino, and the energy of the two α-particles which is $Q_2=2E_\alpha$ since the two α-particles must receive nearly equal energies if momentum is to be conserved. The probability $N(Q_1)$ of a β-decay process with energy Q_1 in the Fermi theory is roughly proportional to Q_1^5, and therefore to $(Q-2E_\alpha)^5$. For each beta-neutrino process with end point energy Q_1, two α-particles are observed, each with energy E_α. Therefore the number-energy distribution for the α-particles is given by $N(E_\alpha)dE_\alpha \propto (Q-2E_\alpha)^5 dE_\alpha$. This fifth power dependence of the distribution on energy is represented by the straight line A in Fig. 1, and is seen to agree roughly with the experimental points except in the extreme regions of high and low α-energies. The K-U theory predicts a seventh power dependence of distribution on energy, which clearly cannot account for the facts. A log-log plot of number *vs.* energy is equivalent in this problem to a Sargent diagram.

The Fermi theory leads to

$$p(Q_1)=\frac{64\pi^4 g^2}{h^7 c^6}\left|\int u^* v d\tau\right|^2 \frac{(mc^2)^5}{30}(\sinh^5\theta)\mathfrak{F} \quad (1)$$

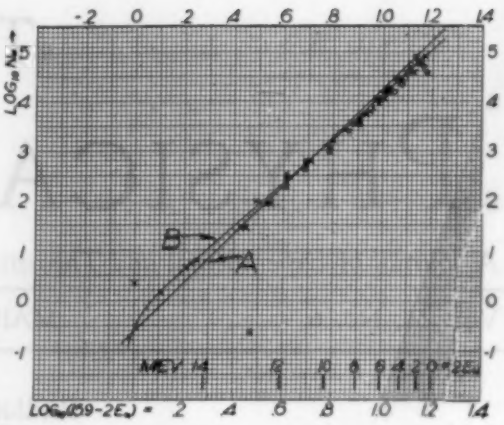

FIG. 1. Number-energy distribution for α-particles. Crosses: R.R.H. counter. Circles: R.R.H. cloud chamber. A. Plot of fifth power approximation. B. Plot of $(\log_{10}\mathfrak{F}\sinh^5\theta)-2.35$.

for the probability per nucleus per unit time that a β-process with energy Q_1 will take place. g=Fermi's constant, u and v are the wave functions of the initial and final states, respectively, and $\cosh\theta=Q_1/(mc^2)$. $\mathfrak{F}$ is given by

$$\mathfrak{F}=\left[1-\frac{5}{2}\frac{1}{\sinh^2\theta}-\frac{15}{2}\frac{1}{\sinh^4\theta}+\frac{15}{2}\frac{\theta\cosh\theta}{\sinh^5\theta}\right].$$

It is a very slowly varying function of the energy, and is effectively equal to one except for low values of Q_1.

For a complete treatment of the problem one would have to evaluate the matrix elements $\int u^* v d\tau$ using solutions of the many-body problem for Li^8 as well as for the continuum of Be^8. It is very difficult at this stage to obtain sufficiently good approximations to these solutions. In the present note, therefore, the effect of the energy of $\int u^* v d\tau$ is taken into account only in a rather rough approximation. It is supposed that, in the region of configuration space which overlaps Li^8, the variation with energy of the amplitude of the many-body wave function of the continuum of Be^8 is proportional to the variation with energy of the two-body function for two alpha-particles having the empirical value of the phase shift. For distances between α-particles greater than the α-particle diameter this procedure can be expected to be fairly accurate, but it is of course very imperfect for smaller distances. Most of the calculations made followed a method in which the interaction

[8] W. A. Fowler and C. C. Lauritsen, Phys. Rev. **51**, 1103 (1937).

[9] C. Smith and W. Y. Chang, Proc. Roy. Soc. **A166**, 415 (1938).

[10] Considerations of G. Gamow and E. Teller quoted by L. H. Rumbaugh, R. B. Roberts and L. R. Hafstad, Phys. Rev. **51**, 1106 (1937). Although the original β-ray theories are being remodeled at present along mesotron lines, the Fermi and K-U theories practically reappear in a new guise. It is of interest that here also the experimental evidence indicates a preference for the Fermi-like type of theory.

potential between the α-particles was adjusted to give the experimental phase shift, and the two-body function corresponding to this potential was used within the nuclear distance. In order to see to what extent the results are dependent on the above-mentioned approximation, a second method was tried in which the two-body functions were continued to $r=0$ as though there were no interaction potential. Several estimates were also made in which the integral of the wave function through the potential well was replaced by the maximum amplitude of the function within the well; the results in these cases were generally similar to those obtained from the first method.

After normalizing the α-wave functions for the continuum in a large sphere, one obtains the approximate form suitable for the present problem:

$$N_\alpha(Q_2)dQ_2=\frac{256\pi^4 g^2 m^5 c^4}{h^5}\times\left(\frac{1}{V_\alpha}\int_0^{r_0}\bar{F}^2dr\right)\frac{\sinh^5\theta}{30}\mathfrak{F}dQ_2,$$

where $N_\alpha(Q_2)dQ_2$ is the probability of an α-process with energy in dQ_2 at Q_2 per nucleus per second, V_α is the relative velocity of the two α-particles, $\bar{F}$ is the α-particle radial wave function, and r_0 is the radius of the nuclear barrier.

There is evidence from the work of Rumbaugh, Roberts and Hafstad, and Fowler and Lauritsen for a maximum in the alpha-particle distribution at $2E_\alpha\sim 2.5$ Mev, with a falling off below the fifth power expression on the low energy side of the maximum. The maximum has appeared only when the distribution is obtained with an expansion chamber; counters do not reveal the maximum, but counter results are known to be uncertain at these low energies. Rather rough calculations have been made of the behavior to be expected theoretically in this region, on the two-body simplification. The term $(V_\alpha^{-1}\int\bar{F}^2dr)$ was calculated for both s waves and d waves with a Coulomb barrier.

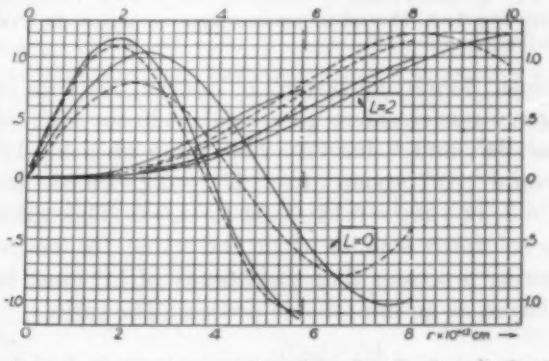

FIG. 2. Internal wave functions for $L=0$ and $L=2$. Solid lines: $Q_2=1.80$ Mev. Broken lines: $Q_2=3.18$ Mev. ($L=0$ functions have been multiplied by -1 for the sake of clarity.)

The internal nuclear wave functions were joined to wave functions for a Coulomb field at the boundary. The internal functions were taken for a flat bottom cylindrical well. No preassigned depth was taken for the well; instead the wave-lengths of the internal functions were adjusted to join smoothly the preassigned external functions at the boundary. The external functions for large arguments can be written as $A(r)\sin[\Phi(r)+K]$ where the amplitude $A(r)$ and phase $\Phi(r)$ have been computed by Wheeler;[11] K is the usual phase shift. The values of the phase shifts which were used are those calculated by J. A. Wheeler[12] from experimental data of the scattering of α-particles in helium. Calculations were made for $L=0$: $r_0=5.00$, 5.68, 6.20, 8.00×10^{-13} cm; and $L=2$: $r_0=5.68$, 8.00, 10.00×10^{-13} cm. The radius is strictly the distance between the centers of the α-particles when confined within the volume of the unstable Li^8 nucleus; the radius is to be compared with the diameter of the Li^8 nucleus, which may be rather large. In Fig. 2 several of the internal radial wave functions $\bar{F}_L$ are shown for $L=0$ and $L=2$. An internal function is determined only by its logarithmic derivative at r_0. If the wave function possesses a node in the neighborhood of r_0, the value of the integral is very sensitive to the interaction around r_0. Since the assumption of a constant interaction inside the well is crude, the results are probably only reliable when the amplitude of the wave function at the boundary is near its maximum.

The calculated curves are joined smoothly to the $\mathfrak{F}sh^6$ curve at $Q_2=2E_\alpha=3.18$ Mev. The main features of the experimental data can be reproduced for either the $L=0$ interaction with a small radius, or the $L=2$ interaction with a

[11] J. A. Wheeler, Phys. Rev. **52**, 1123 (1937).
[12] J. A. Wheeler, private communication.

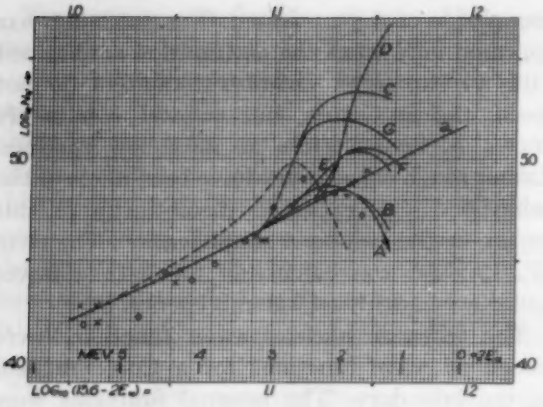

FIG. 3. Number-energy distribution for α-particles. Circles: R.R.H. cloud chamber. Crosses: R.R.H. counter. Dashes: Fowler-Lauritsen cloud chamber (smoothed). a. $(\log_{10} \mathfrak{F}sh^5)-2.35$. A. $L=2$, $r_0=8\times10^{-13}$ cm, B. $L=2$, $r_0=10\times10^{-13}$ cm, C. $L=2$, $r_0=5.68\times10^{-13}$ cm, D. $L=0$, $r_0=8\times10^{-13}$ cm, E. $L=0$, $r_0=5.0\times10^{-13}$ cm, F. $L=0$, $r_0=5.68\times10^{-13}$ cm, G. $L=0$, $r_0=6.2\times10^{-13}$ cm; extended Coulomb function.

larger radius. It is not at present possible to make a definite decision as to the angular momentum of the excited state of $(Be^8)^*$. The best fit seems to be for $L=2$, $r_0=8.00\times10^{-13}$ cm. $L=1$ is ruled out because the wave functions for two α-particles must be symmetrical in the two particles. The general form of the calculated distributions is maintained for the several values of r_0; this is some justification for the use of "one-body" phase shifts in the calculation. The assumption is made that no appreciable resonance effects occur for energies above 3.18 Mev; on the one-body model this is a reasonable assumption.

A further calculation was made in which the Coulomb functions for $L=0$ with the phase shifts as before were extended into $r_0=0$; the radius for the integral was taken as $r_0=6.20\times10^{-13}$ cm. Wheeler's tables for the wave functions may be used as far as about 3.60×10^{-13} cm; from 0 to about 2×10^{-13} cm. The tables of Yost, Wheeler and Breit[13] can be used. Wheeler's $A(r)\sin[\Phi(r)+K]=F\cos K+G\sin K$ in the notation of Y. W. B. The curve in the intermediate region was traced in by eye. The distribution expected for this case is represented by curve G in Fig. 3.

The agreement with experiment in the region of $Q_2>10$ Mev is very sensitive to the value of $Q=Q_1+Q_2$ used. Figs. 1 and 4 are plots of $\mathfrak{F}sh^5$ for $Q=15.9$ and 15.6 Mev, respectively. The former value appears to give improved agreement with the observed distribution in the region of high α-particle energies. Rumbaugh, Roberts and Hafstad[6] give $Q=15.9$ (±0.1) Mev from observed masses.

Fermi's constant g was evaluated for the process by equating the integral $\int_0^Q N_\alpha(Q_2)dQ_2$ to the observed disintegration probability. The integral was evaluated graphically with the theoretical distribution for $L=0$, $r_0=5.68\times10^{-13}$ cm and also for $L=2$, $r_0=8\times10^{-13}$ cm. The disintegration probability is given by $(ln2)/\tau$, where the half-life $\tau=0.88\pm0.1$ sec. For $L=0$ one obtains $g=1.7\pm0.2\times10^{-50}$ erg cm^3; for $L=2$, $g=2.0\pm0.2\times10^{-50}$ erg cm^3. For heavy nuclei Fermi found $g=4.00\times10^{-50}$. Breit and Knipp,[14] however, found with $g=4.00\times10^{-50}$ that He^6, Be^7 and C^{11} have anomalously high values of the matrix elements, and have suggested that there may be a decrease in the intrinsic β-emitting powers of nuclear particles in heavy nuclei. They give $|M|^2=120$ for He^6, 30 for Be^7, and 9 for C^{11}. The value of g for Li^8 would correspond to $|M|^2=0.25\pm0.03$ for $L=2$, or $|M|^2=0.18\pm0.02$ for $L=0$. This value is so much smaller than the value for neighboring processes that the β-decay of Li^8 must be classed as an improbable process. The ratio

$$\frac{|M|^2(Be^7)}{|M|^2(Li^8, L=2)}\sim125\pm15.$$

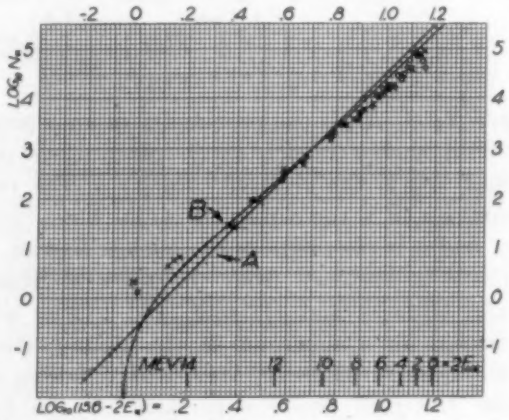

FIG. 4. Shows effect of change of energy scale. Compare with Fig. 1. A. Plot of fifth power approximation. B. Plot of $(\log_{10} \mathfrak{F}sh^5)-2.20$.

[13] F. L. Yost, J. A. Wheeler and G. Breit, Terr. Mag. **40**, 443 (1935).

[14] G. Breit and J. K. Knipp, Phys. Rev. **54**, 652 (1938).

The ratio between two adjacent Sargent curves is about 100. It is not immediately possible to decide whether the improbability in the case of Li^8 is caused by spin changes, geometrical factors, or a combination of both.

The existence of a stable ground state for Be^8 would admit the possibility of β-transitions to the ground state without the emission of α-particles. Allison and co-workers[15] have recently reported that Be^8 is stable with respect to two α-particles by 0.31 ± 0.06 Mev. Rumbaugh, Roberts and Hafstad[6] found that the number of delayed α-particles from the Li^8 reaction is 1.1 times greater than the total number of β-particles observed. They suggest that various corrections would tend to increase the ratio of α to β. The ratio 1.1 : 1 may be regarded as setting a limiting value to the relative probabilities of β-decay to the continuum and to the stable state of Be^8. Beta-decay to the continuum will have to compete with decay to the ground state; this competition will decrease the values of the matrix elements as calculated above, which represent transitions to the continuum only, by a factor of 0.55. One obtains $|M_c|^2=0.10(L=0)$; $=0.14(L=2)$.

The matrix element for transitions to the stable state can be estimated in a similar way. The direct estimate must be corrected for the spreading of the wave function of the ground state beyond the boundaries of the potential well. The ground state is assumed to consist of two α-particles with $L=0$. One gets finally $|M_s|^2\leqq0.04$. On the basis of this low value one might tentatively suggest that the excited state has $L=2$, and β-transitions to the ground state are forbidden by a strong selection rule.

It is a pleasure to thank Professor G. Breit for suggesting this problem, and for his constant advice. I am very indebted to Professor J. A. Wheeler for permission to use his calculations of phase shifts before publication. The Wisconsin Alumni Research Foundation has granted financial support.

[15] S. K. Allison, E. R. Graves, L. S. Skaggs and N. M. Smith, Jr., Phys. Rev. **55**, 107 (1939).

MARCH 15, 1939 PHYSICAL REVIEW VOLUME 55

Total Secondary Electron Emission from Tungsten and Thorium-Coated Tungsten

EDWARD A. COOMES*
George Eastman Laboratories of Physics, Massachusetts Institute of Technology, Cambridge, Massachusetts
(Received January 27, 1939)

The secondary electron emission from polycrystalline tungsten covered with monomolecular films of thorium evaporated onto it from a thoriated tungsten filament, has been investigated over an energy range for primary electrons of 100 to 1000 volts. The state of the target surface was ascertained from thermionic emission measurements. For clean thorium on clean tungsten apparently the secondary emission coefficient did not change with thoriation for primary energies below 200 volts, but decreased at higher voltages with increasing amounts of thorium on the target. No observed increase in secondary emission takes place with a reduction in the work function of tungsten by a monomolecular layer of pure thorium; apparently there is a decrease in secondary emission in this case. When the thorium-coated tungsten was treated with oxygen released from the thoriated tungsten filament the work function increased, but there obtained also an increase in the secondary emission coefficient; further change in work function by evaporation of thorium caused a variation of the secondary emission coefficient that other experimenters also have observed.

INTRODUCTION

SYSTEMATIC studies of the secondary electron emission from composite surfaces bombarded with low energy primary electrons have been carried out by several investigators,[1-3] but conclusions reached are at variance. Data[2] are available which check a theory stating that

* Now at the University of Notre Dame.

[1] Paul L. Copeland, Phys. Rev. **46**, 435 (1933).
[2] L. R. G. Treloar, Proc. Phys. Soc. **49**, 392 (1937).
[3] H. Bruining and J. H. de Boer, Physica **5**, 17 (1938).

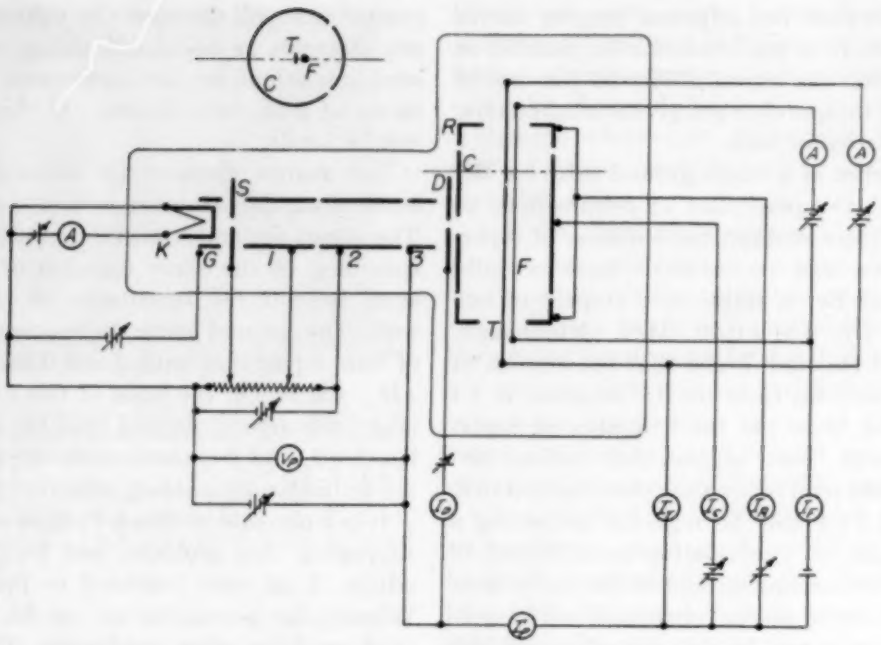

FIG. 1. Schematic diagram of experimental tube and circuit for secondary emission measurements.

changes in secondary emission coefficient result solely from changes in work function when monomolecular impurity films are deposited on a target surface. Other recent work[3] has expressed lack of agreement with this theory, and indicates that at least in the case of metals there is no correlation between change in work function and change in secondary emission coefficient. It is not impossible that some of the apparent disagreement has come about as a result of the technical difficulties encountered in obtaining an initially clean surface, and in clearly defining subsequent conditions brought about by contaminants; therefore, the present work was undertaken in an effort to remove some of the disagreement and possibly to gain a fuller knowledge of the fundamental physics of the secondary emission process.

Measurements were taken of the total number of secondary electrons produced when a well-focused beam of primary electrons was allowed to strike a carefully prepared tungsten target. A one-mm diameter beam cross section was always maintained at the target, and the range over which the primary voltage was varied extended from 100 to 1000 volts. The maximum in the secondary emission characteristic lies in this region. Targets used were in the form of a tungsten ribbon four cm long, 0.2 cm wide and one mil thick. These were initially flashed at 2700°K, which heat treatment produced a polycrystalline tungsten surface and dissuaded further crystal growth on additional heating. The crystalloids formed had faces exposed to the primary beam which were found to be on the average 100 square microns in area, so that about 1000 crystal faces were bombarded by the beam.

Preliminary observations on both clean and thorium-coated tungsten indicated the secondary emission coefficient to be independent of the primary current and target temperature. Measurements were taken for primary voltages of 200, 500 and 1000 volts, respectively, as the primary current was varied from 0.05 to 1.0 microampere, but changes in the secondary emission coefficient greater than one percent did not appear. This procedure was carried out for target temperatures from room temperature to about 1200°K where thermionic emission could be detected, but no changes in secondary emission were observed.

Method and Apparatus

The tube and circuit employed are quite similar to those already described.[3, 4] Fig. 1 is a schematic diagram of the experimental arrangement. The tube design includes the particular features: (1) the *electron gun* has the electrode system (G, S, 1) for concentrating the space charge in the cathode region into the primary beam, and a final retarding potential lens (2, 3) for keeping secondaries produced within the gun out of the primary current. This arrangement allowed wide and independent variations of both primary voltage and beam current density without causing an appreciable spread in electron energies. (2) The *collector system* (C, R) consists of three tantalum cylinders, 1.5 inches in diameter and mounted coaxially with the target along the axis. For thermionic emission measurements the arrangement was connected in the usual fashion with anode (C) and two guard rings (R). The ratio of the cylinder diameter to the target cross-sectional dimensions was made large so that the field a short distance from the target was approximately radial. For secondary emission measurements the anode and guard rings were connected together so as to form a collector almost completely surrounding the target. The primary current was taken as the current I_p entering the collector system when the beam was focused to clear the stop (D). The back quarter of the main collector (C) could be insulated from the rest of the system, and a thin willemite screen sprayed on the inside of this collector was useful in focusing the beam and in observing its cross section. The actual current to this quarter section when the beam was focused on the target supplied additional information concerning the aberrations suffered by the primary beam. For both thermionic and secondary currents the collector system was maintained at 40 volts positive with respect to the target, which potential was sufficient to draw saturation current in both cases.

All experimental tubes were sealed off from the vacuum system before measurements were taken. The only materials besides glass used in construction were tungsten, monel metal, outgassed tantalum, and to a very small extent, outgassed nickel. The technique used in the preparation of structural parts for vacuum and the schedule of evacuation have been described by Nottingham.[5]

The procedure for obtaining a clean surface of pure tungsten was necessarily empirical. The surface was assumed to be in the state desired when the results obtained were reproducible

[4] H. E. Farnsworth, Phys. Rev. **25**, 41 (1925).

[5] W. B. Nottingham, J. App. Phys. **8**, 762 (1937).

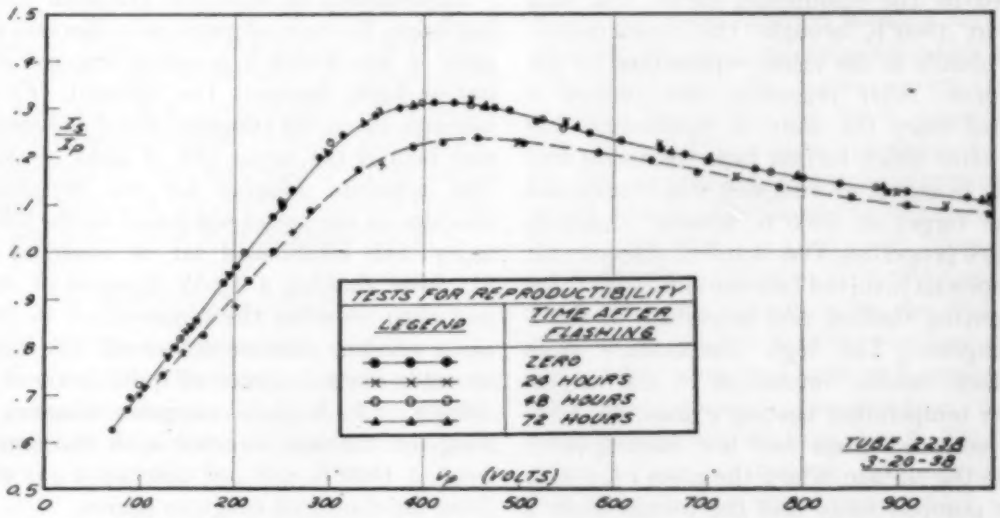

Fig. 2. *Secondary emission characteristic for clean tungsten.* The upper curve represents equilibrium; in this state tungsten could be evaporated from the target at 2800°K without changing the yield of secondary electrons. Dashed line, after flashing at 2700°K and heating at 1800°K for 10 hours. Solid line, equilibrium after successively flashing at 2700°K and heating at 1800°K over a period of 120 hours.

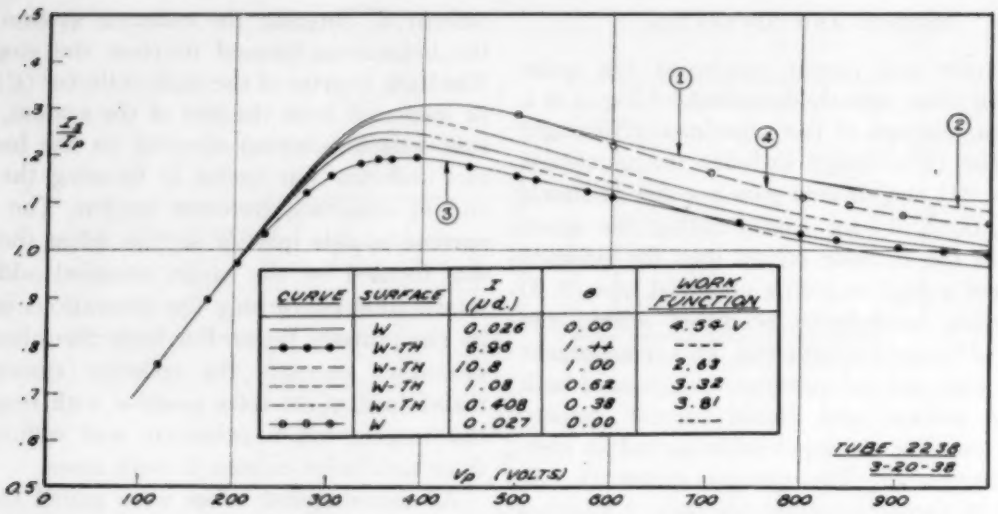

FIG. 3. *Secondary emission characteristic for thorium-coated tungsten.* The primary current was of the order of 1 microampere, at all values of primary voltage. I = emission current at 1200°K. $\theta = (\log I_\theta - \log I_w)/(\log I_T - \log I_w)$.

within one percent regardless of subsequent treatment given the target. This condition was demanded for both thermionic and secondary currents. The procedure finally adopted consisted in successive short period flashings of the target at 2700°K followed by a long period of heating at 1800°K. The final results of this procedure are shown in Fig. 2. The short high temperature heating usually caused a rise in the secondary emission characteristic over that illustrated by the equilibrium curve. The long heating at 1800°K brought the characteristic down gradually to the values represented by the lower curve. After repeating this process a number of times the state of equilibrium was reached after which further heat treatment had no effect; in this state tungsten was evaporated from the target at 2800°K without changing the surface properties. One is led to suspect that the phenomena involved here are similar to those accompanying flashing and activation of thoriated tungsten. The high temperature flash decomposes metallic impurities in the target; the lower temperature heating causes the diffusion of occluded gases and low melting-point metals to the surface, where the gases evaporate and are pumped away and the metals form a monatomic film on the target. This state is represented by the lower curve of Fig. 2. When the target has been freed of body impurities in this manner the final flash cleans adsorbed substances from the surface. That such a process does occur was confirmed by observing patterns from the target undergoing heat treatment in an electron projection tube.[6] The upper curve of Fig. 2. is offered as an accurate secondary emission characteristic for polycrystalline tungsten. It has its maximum at 420 volts where the secondary emission coefficient reaches a value of 1.31.

Experiments on thoriated tungsten filaments led finally to their adoption as a thorium source, after it was found a practical impossibility to outgas bulk thorium. The filament (F) was a one-mm thoriated tungsten spiral mounted two mm behind the target out of sight of the gun. The schedule adopted for the deposition of thorium on the target was based on the following fairly well established set of observed facts: (1) After flashing a Th-W filament at 3000°K, and then reducing the temperature to 2500°K, quite gas-free thorium comes off. (2) Gas, presumably oxygen, comes off quite freely at about 1800°K. (3) A clean tungsten filament, or a tungsten filament covered with thorium when held at 1600°K will not take up a gas evolved from the thoriated tungsten source.

In view of this experimental work the follow-

[6] The tube was a simple electron microscope such as described by R. P. Johnson, J. App. Phys. 9, 508 (1938).

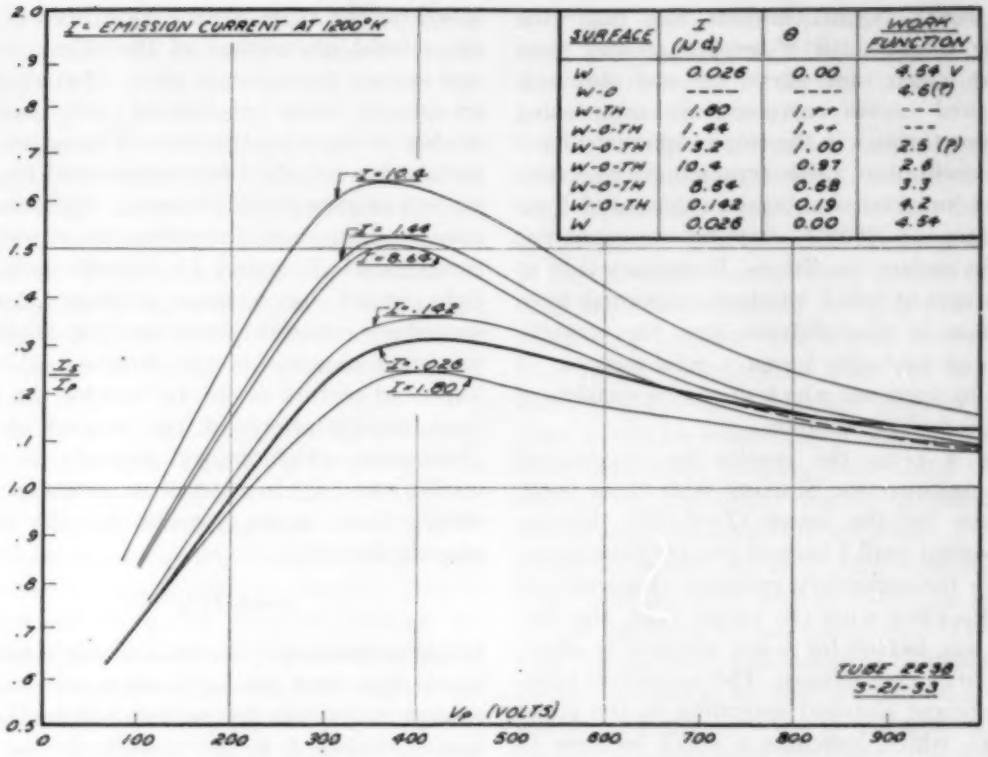

FIG. 4. *Secondary emission characteristic for oxygenated thorium-coated tungsten.*

ing procedure was followed for evaporating thorium in the secondary emission tubes: (*a*) the target T, after heat treatment, was set at 1600°K; (*b*) the Th-W filament F was flashed and then held at 2500°K for evaporation of throium, at which time the target was brought down to about 1000°K; (*c*) after the evaporation period the target was brought up to 1600°K and the Th-W filament reduced to room temperature; (*d*) thermionic current was read from the target at 1200°K to check the condition of the surface, which was not altered at this temperature.

EXPERIMENTAL RESULTS

Figure 3 is a set of secondary emission characteristics for clean thorium on clean tungsten. To represent the degree of thoriation the parameter θ, which is simply related to the work function ϕ, was chosen.[7]

$$\theta=\frac{\log I_\theta-\log I_w}{\log I_T-\log I_w}=\frac{\phi_\theta-\phi_w}{\phi_T-\phi_w},$$

where I_θ = thermionic emission at any state, for which the work function is ϕ_θ; I_w = thermionic emission for clean tungsten, for which the work function is ϕ_w; and I_T = maximum thermionic emission for which the work function is ϕ_T. The table of Fig. 3 gives the values of θ and ϕ for the corresponding graphical representation of the results. The set of (Th-W) curves are for the second cycle of thoriation. Note that the curve for clean tungsten at the beginning of the cycle does not reproduce in the high voltage range when all the thorium is evaporated from the target surface. Curve (1) represents the secondary emission characteristic for clean tungsten reproduced from Fig. 2. Thorium was deposited until θ became greater than unity. When the thorium was evaporated off, curve (2) represents the final state, and this did not change even when the target was raised to 2800°K at which temperature tungsten evap-

[7] S. Dushman, Rev. Mod. Phys. **2**, 381 (1930). It should be understood that θ is not intended to represent the fraction of the tungsten surface covered with thorium; for $\theta=1$ the true coverage is probably about 0.75.

orated freely. Again thorium was deposited onto the target until θ became greater than unity, at which time curve (3) was obtained. The dashed curves represent the intervening stages gone through in the step evaporation back to the equilibrium value represented by curve (4). Here tungsten was again evaporated from the surface at 2800°K without an apparent change in surface conditions. It appears that at temperatures at which thorium evaporates from the surface it also diffuses into the metallic lattice, and probably forms a solid solution of thorium in tungsten which might be considered a constant boiling solution.

Figure 4 gives the results for oxygenated thorium-on-tungsten. Starting with clean tungsten given by the curve ($I=0.026$) thorium was deposited until θ became greater than unity; this gave the secondary emission characteristic ($I=1.80$). Then with the target cold, the filament F was heated for a few minutes at about 1800°K to release oxygen. The secondary emission coefficient changed according to the curve ($I=1.44$), which indicates a small increase in work function and a greatly increased secondary emission coefficient. When thorium was then evaporated from the surface the secondary emission became greater as the work function decreased (table of Fig. 4), and the ability to evaporate the thorium without causing any apparent change in structure except the lowering of work function suggests that the oxygen might be adsorbed to the tungsten under the thorium. For computing the values of the table in Fig. 4 the work function for the $(W-O)$ surface was assumed to reach a value of 4.6 volts, and for monomolecular layer of thorium-on-oxygen-on-tungsten corresponding to $\theta=1$, the work function was taken as 2.5 volts. These values were chosen to give a range of variation of contact potential approximately the same as observed by Treloar[8] in his experiments on thoriated tungsten.

Interpretation of Data

A theory of secondary emission based on the quantum mechanics of metals as initiated by Bloch has been given by Fröhlich.[8] Theories based on the same picture have been given for the related phenomena of thermionic emission and surface photoelectric effect,[9] but all of these treatments have considered only simplified models of the metal surface. The action of the surface has usually been represented by simple smooth or step-potential curves, while in reality even for a pure metal the situation is much more complicated. It would be difficult to give the right model for a more accurate theory of secondary emission; however, one might hope for some progress in the direction of a more improved picture of the surface for the process from considerations of the related electronic phenomena which depend strongly on surface conditions: (*a*) In *thermionic emission* simple theory leads to an equation for the emission current density:

$$I=ADT^2e^{-\phi\epsilon/kT}.$$

While problems of transmission and reflection in the surface field are not understood completely enough to give the precise value of the transmission coefficient D in any individual case, values of the work function ϕ (at least for the case of tungsten) are reproducible, and the variations in emission with work function caused by adding monomolecular films of foreign substances may be fairly well predicted.[10] (*b*) In the case of the *surface photoelectric effect* difficulties are likewise experienced in giving an explanation of transmission coefficients for the real case,[11] but the dependence of current on work function seems to check simple theory.

In the case of *secondary emission* if one does not consider absorption, simple theory shows that at least up to the maximum of the secondary emission curve the current should depend very little on the height of the potential barrier, and hence one could look for little dependence on work function. The results plotted in Fig. 3 certainly do not show any systematic variation when the work function of tungsten is changed by thoriation. Experiment (see Fig. 3) has the secondary emission coefficient decreasing for greater amounts of thorium on the surface, and the

[8] H. Fröhlich, Ann. d. Physik **13**, 229 (1932).

[9] See F. Seitz and R. Johnson, J. App. Phys. **8**, 246 (1937).

[10] See A. L. Reimann, *Thermionic Emission* (John Wiley & Sons, 1934), Chapter III.

[11] A. G. Hill, Phys. Rev. **53**, 184 (1938).

condition $\theta=1$ has no unique significance. Below 200 volts the secondary emission coefficient appears to be independent of the amount of thorium on the surface and is the same as for clean tungsten. One could speculate that this case might correspond to a simple metal, the collision cross section being independent of thoriation, so that the emission process is independent of the nature of the surface barrier. This would be in agreement with the approximate theory of Fröhlich, but it is more probable that a number of conflicting processes average to give the result.

For the range of voltages including the maximum of the curves in Fig. 3 it is significant that the maximum shifts to lower voltages for coverage with thorium. Assuming that the excitation process does not change on thoriation an interesting calculation comes out of classical theory. The dependence of the primary voltage for maximum secondary emission coefficient on the density of the metal has been computed classically.[12] The result is that the primary energy for maximum secondary emission coefficient should vary as the square root of the density of the metal.

Density of tungsten = 18.7 grams/cm³
Density of thorium = 11.2 grams/cm³
V_W = primary voltage for maximum I_s/I_p for tungsten = 420 volts for Fig. 2
V_T = primary voltage for maximum I_s/I_p for thorium = $420\ (11.2/18.7)^{\frac{1}{2}} = 326$ volts.

This value compared with the maximum of 350 volts from curve (4) of Fig 3 is in fair agreement, considering that the target consisted of thorium on tungsten rather than pure thorium. One might go farther with the classical picture and attribute the fewer secondary electrons obtained in the case of thorium-coated tungsten to the liberation of secondaries farther below the surface than in the case of clean tungsten, and hence, the lower probability of escape. It is not improbable that the classical picture fits the experimental data fairly well because it is consistent with the damping of electron waves in crystals as developed by Slater.[13]

A reasonable explanation can be assigned to the variation of secondary emission coefficient with change in work function for the case of oxygenated thorium-coated tungsten expressed in Fig. 4. In the energy band picture this structure would correspond roughly to a semiconducting surface. The Fermi levels for this case would be separated from the first energy band by a forbidden region, and since the lower zone would be completely filled and the upper zone completely empty, transitions would be allowed to the upper region. Besides, if one should view the structure very near the surface probably many impurity states exist, and a large collision cross section would be presented to the incoming primary electrons. The excitation and emission processes in this case could be quite analogous to the surface photoelectric effect, and the secondary emission coefficient would be expected to vary with the work function in the manner that has been predicted.[2]

While it is thus possible to find reasonable explanations for experimental results on the secondary emission from composite surfaces much more data must be taken under controlled conditions before an accurate description of the physical processes can be formed.

I am deeply grateful to the many people who have given me assistance in this work. I wish to thank particularly Professor W. B. Nottingham for his many suggestions; Dr. L. B. Headrick of the RCA Manufacturing Company for his material assistance and advice in the matter of electron gun design; and Dr. R. B. Nelson for his suggestions on the treatment of targets. My thanks are due, also, to Mr. Walter Ennis for his assistance in the glass-working operations demanded in this problem.

[12] D. R. Bhawalkur, Proc. Indian Acad. Sci. **6**, 74 (1937).

[13] J. C. Slater, Phys. Rev. **51**, 840 (1937).

The Molecular Beam Resonance Method for Measuring Nuclear Magnetic Moments

The Magnetic Moments of $_3Li^6$, $_3Li^7$ and $_9F^{19}$*

I. I. RABI, S. MILLMAN, P. KUSCH, *Columbia University, New York, New York*

AND

J. R. ZACHARIAS, *Hunter College, New York, New York*

(Received January 20, 1939)

A new method of measuring nuclear or other magnetic moment is described. The method, which consists essentially in the measurement of a Larmor frequency in known magnetic fields, is of very general application and capable of the highest precision in absolute and relative measurements. The apparatus consists of two magnets in succession which produce inhomogeneous magnetic fields of oppositely directed gradients. A molecular beam of the substance to be studied possesses a sigmoid path in these magnets and is focused on a suitable detector. A third magnet which produces a homogeneous field is placed in the region between the two deflecting magnets. In this strong homogeneous field the nuclear moments are decoupled from other nuclear moments and from rotational moments of a molecule in a $^1\Sigma$ state, and precess with their Larmor frequency $\nu=\mu H/hI$. An oscillating field perpendicular to the homogeneous field produces transitions to other states of space quantization when the frequency of this field is close to ν. If such transitions take place the molecule is no longer focused on to the detector by the subsequent inhomogeneous field and the observed intensity diminishes. The application of the method to the molecules LiCl, LiF, NaF and Li_2 is described. The nuclear moments of Li^7, Li^6 and F^{19} were found to be 3.250, 0.820 and 2.622 nuclear magnetons, respectively.

THE magnetic moment of the atomic nucleus is one of the few of its important properties which concern both phases of the nuclear problem, the nature of the nuclear forces and the appropriate nuclear model. According to current theories the anomalous moment of the proton is directly connected with the processes from which nuclear forces arise. The question whether the intrinsic moments of the proton and neutron are maintained within the nucleus is part of the problem of two and multiparticle forces between nuclear constituents. With regard to the atomic model it is clear that the nuclear angular momentum does not alone suffice to fix the nature of the wave functions which specify the state of the nucleus. The magnetic moment, on the other hand, is sensitive to the relative contributions of spin and orbital moment and, with the advance of mathematical technique, suffices to decide between the different proposed configurations.

In the light of these considerations it is particularly desirable that nuclear moments be known to high precision because small effects may be of great importance. A case in point is that of $_3Li^7$; according to the calculations of Rose and Bethe[1] the contribution of the orbital motions to the moment of this nucleus is about 10 percent of the total moment. The rest is contributed by the intrinsic proton moment. If the nuclear moment were known to only 10 percent, the importance of this datum would be greatly diminished.

In two letters to this journal,[2, 3] we reported briefly on a new precision method of measuring nuclear moment, and on some results. In this paper we shall give a more detailed account of the method, apparatus and results.

METHOD

The principle on which the method is based applies not only to nuclear magnetic moments but rather to any system which possesses angular momentum and a magnetic moment. We consider a system with angular momentum, J, in units of $h/2\pi$, and magnetic moment μ. In an external magnetic field H_0 the angular mo-

* Publication assisted by the Ernest Kempton Adams Fund for Physical Research of Columbia University.

[1] M. E. Rose and H. A. Bethe, Phys. Rev. **51**, 205 (1937).
[2] I. I. Rabi, J. R. Zacharias, S. Millman and P. Kusch, Phys. Rev. **53**, 318 (1938).
[3] I. I. Rabi, S. Millman, P. Kusch and J. R. Zacharias, Phys. Rev. **53**, 495 (1938).

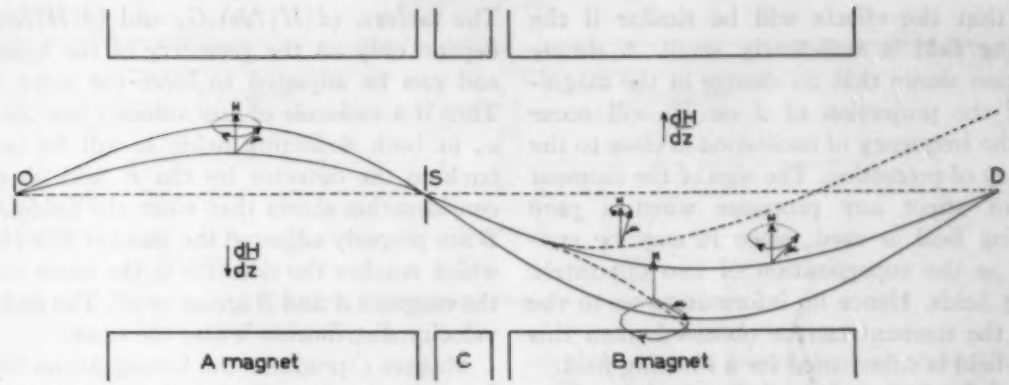

FIG. 1. Paths of molecules. The two solid curves indicate the paths of two molecules having different moments and velocities and whose moments are not changed during passage through the apparatus. This is indicated by the small gyroscopes drawn on one of these paths, in which the projection of the magnetic moment along the field remains fixed. The two dotted curves in the region of the B magnet indicate the paths of two molecules the projection of whose nuclear magnetic moments along the field has been changed in the region of the C magnet. This is indicated by means of the two gyroscopes drawn on the dotted curves, for one of which the projection of the magnetic moment along the field has been increased, and for the other of which the projection has been decreased.

mentum will precess with the Larmor frequency, ν, (in revolutions per sec.) given by,

$$\nu = \mu H_0 / Jh. \tag{1}$$

Our method consists in the measurement of ν in a known field H_0. The measurement of ν is the essential step in this method, since H_0 may be measured by conventional procedures. Using Eq. (1) we obtain the gyromagnetic ratio. If, in addition, the angular momentum, J, of the system is known, we can evaluate the magnetic moment μ. In its present state of development our method is not suitable for the measurement of J.

The process by which the precession frequency ν is measured has a rather close analog in classical mechanics. To the system described in the previous paragraph, we apply an additional magnetic field H_1, which is much smaller than H_0 and perpendicular to it in direction. If we consider the initial condition such that H_1 is perpendicular to both the angular momentum and H_0, the additional precession caused by H_1 will be such as to increase or decrease the angle between the angular momentum, J, and H_0, depending on the relative directions. If H_1 rotates with the frequency ν this effect is cumulative and the change in angle between H_0 and J can be made large. It is apparent that if the frequency of revolution, f, of H_1 about H_0 is markedly different from ν, the net effect will be small. Furthermore, if the sense of rotation of H_1 is opposite to that of the precession, the effect will also be small. The smaller the ratio H_1/H_0 the sharper this effect will be in its dependence on the exact agreement between the frequency of precession, ν, and the frequency f.

Any method which enables one to detect this change in orientation of the angular momentum with respect to H_0 can therefore utilize this process to measure the precession frequency and therefore the magnetic moment. The general method here outlined includes not only the magnitude but also the sign of the magnetic moment since the direction of precession depends on whether the magnetic moment vector is parallel or antiparallel to J.

The precise form of the initial conditions previously described is not important and we may consider H_1 initially at any angle ϕ with the plane determined by H_0 and J but still perpendicular to H_0. In fact, according to quantum mechanics, we must consider the initial conditions of an ensemble of systems with a definite projection of J on H_0 as uniformly distributed over ϕ. This only means that some systems will increase and other systems will decrease their projections in the direction of H_0.

In practice it is frequently more convenient to use an oscillating field H_1 rather than a rotating field. Although the situation is not quite as clear as for the rotating field, it is reasonable to

expect that the effects will be similar if the oscillating field is sufficiently small. A simple calculation shows that no change in the magnitude of the projection of J on H_0 will occur unless the frequency of oscillation is close to the frequency of precession. The sign of the moment does not affect any processes when a pure oscillating field is used, since it may be considered as the superposition of two oppositely rotating fields. Hence no information as to the sign of the moment can be obtained when this type of field is substituted for a rotating field.

Although the reorientations of the system under the combined influence of H_0 and H_1 may be detected in a number of ways,[4] the most delicate and precise is that of molecular beams.

The arrangement used in our experiment is shown schematically in Fig. 1. A stream of molecules coming from the source, O, in a high vacuum apparatus is defined by a collimating slit, S, and detected by some suitable device at D. The magnets, A and B, produce inhomogeneous magnetic fields, the gradients of which, $d|H|/dz$, are indicated by arrows. When these magnets are turned on, molecules having magnetic moment will be deflected in the direction of the gradient if the projection of the moment, μ_z, along the field is positive, and in the opposite direction if μ_z is negative. A molecule starting from O along the direction OS will be deflected in the z direction by the inhomogeneous A field and will not pass through the collimating slit unless its projected moment is very small or it is moving with very high speed. In general, for a molecule having any moment, μ_z, and any energy, $\frac{1}{2}mv^2$, it is possible to find an initial direction for the velocity of the molecule at the source such that the molecule will pass through the collimating slit. This is indicated by the solid lines in the diagram. If d_A denotes the deflection at the detector from the line OSD suffered by the molecule due to the A field alone, it may be expressed by:

$$d_A=(\mu_z/2mv^2)(d|H|/dz)_A G_A.$$

The deflection in the B field will be in a direction opposite to that in the A field and is given by:

$$d_B=(\mu_z/2mv^2)(d|H|/dz)_B G_B.$$

The factors, $(d|H|/dz)_A G_A$ and $(d|H|/dz)_B G_B$, depend only on the geometry of the apparatus and can be adjusted to have the same value. Thus if a molecule of any velocity has the same μ_z in both deflecting fields it will be brought back to the detector by the B field. A simple consideration shows that when the fields A and B are properly adjusted the number of molecules which reaches the detector is the same whether the magnets A and B are on or off. The molecular velocity distribution is also the same.

Magnet C produces the homogeneous field H_0. In addition, there is a device, not pictured in Fig. 1, which produces an oscillating field perpendicular to H_0. If the reorientation which we have described takes place in this region the conditions for deflecting the molecules back to D by means of the B magnet no longer obtain. The molecule will follow one dotted line or the other depending on whether μ_z has become more positive or has changed sign. In fact, if any change in orientation occurs, the molecule will miss the detector and cause a diminution in its reading. We thus have a means of knowing when the reorientation effect occurs.

Since most of the systems in which one is interested have small angular momenta ($<10h/2\pi$) the classical considerations given above have to be reconsidered from the point of view of quantum mechanics. The reorientation process is more accurately described as one in which the system, originally in some state with magnetic quantum number, m, makes a transition to another magnetic level, m'. An exact solution for the transition probability for the case where H_1 rotates and is arbitrary in magnitude was given by Rabi.[5] For the particular case of $J=\frac{1}{2}$ we have,

$$P_{(\frac{1}{2},-\frac{1}{2})}=\frac{\sin^2\theta}{1+q^2-2q\cos\theta}\sin^2\pi tf(1+q^2-2q\cos\theta)^{\frac{1}{2}},$$

where $P_{(\frac{1}{2},-\frac{1}{2})}$ is the probability that the system, originally in the state $m=\frac{1}{2}$ is found in the state $m=-\frac{1}{2}$ after a time t, q the ratio of the frequency of revolution f to the frequency of precession $\nu[\nu=\mu(H_0^2+H_1^2)^{\frac{1}{2}}/Jh]$, and $\tan\theta=H_1/H_0$.

For an oscillating field, in the limit where $H_1/H_0\ll 1$, and in the neighborhood of $f=\nu$ this

[4] C. J. Gorter, Physica 9, 995 (1936).

[5] I. I. Rabi, Phys. Rev. 51, 652 (1937).

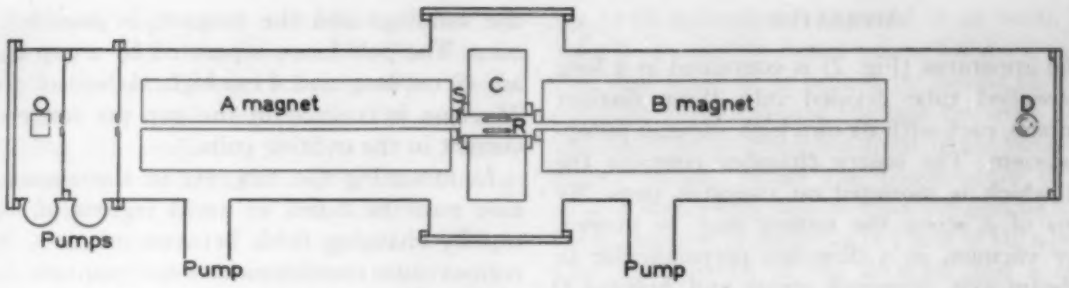

FIG. 2. Schematic diagram of apparatus.

formula becomes:

$$P_{(i-i)}=\frac{\Delta^2}{(1-q)^2+\Delta^2}\sin^2\pi tf[(1-q)^2+\Delta^2]^{\frac{1}{2}}, \quad (2)$$

where $\Delta=H_1/2H_0$, one-half the ratio of the amplitude of the oscillating field to the static field, and the other symbols retain their meaning. For spins higher than $\frac{1}{2}$ the general formula given by Majorana[6] applies, and

$$P_{(a,\ m,\ m')}=(\cos\tfrac{1}{2}\alpha)^{4J}(J+m)!$$
$$\times(J+m')!(J-m)!(J-m')!$$
$$\times\left[\sum_{\nu=0}^{2J}\frac{(-1)^\nu(\tan\tfrac{1}{2}\alpha)^{2\nu-m+m'}}{\nu!(\nu-m+m')(J+m-\nu)!(J-m'-\nu)!}\right]^2, \quad (3)$$

where α is defined through $P_{(i,\ -i)}=\sin^2(\alpha/2)$. That is, we calculate α for a system which has the same μ/i but with a spin of $\frac{1}{2}$ and subject to the same field, and use it in Eq. (3).

The orders of magnitude involved can be seen from a simple example: consider a system with spin $\frac{1}{2}$ and a moment of 1 nuclear magneton in a field of 1000 gauss and an oscillating field of 10 gauss amplitude. We assume that the system is moving at a speed of 10^5 cm per second which is of the order of thermal velocities, and set $t=l/v=10^{-5}l$. The resonance frequency is

$$\frac{uH}{hi}=\frac{(0.5\times10^{-23})(10^3)}{(6.55\times10^{-27})(\frac{1}{2})}\sim1.5\times10^6 \text{ cycles per sec.},$$

which fortunately is in a very convenient range of radiofrequencies. To make the $\sin^2$ terms a maximum at $q=1$ we set

$$\pi\times10^{-5}l\times1.5\times10^6\times0.5\times10^{-3}=\pi/2.$$

Solving for l, we obtain $l=6.6$ cm, which is a very convenient length for the oscillating field.

The theoretically simplest systems to which these ideas may be applied in the study of nuclear moment are atoms which are normally in a state with electronic angular momentum equal to zero. If the electronic J is not zero, the interaction of the nuclear spin with the electronic angular momentum is of the order of magnitude of its interaction with the applied field H_0. Moreover, the electronic magnetic moment is so much larger than nuclear moment that the deflections in the A and B fields will be almost entirely due to this electronic moment and the apparatus will accordingly be insensitive to changes in nuclear orientation. Resort must therefore be had to atoms in a state $J=0$ or to molecules in a $^1\Sigma$ state in which all electronic angular momentum is neutralized to the first order. These considerations do not preclude the study, with these methods, of atoms with electronic angular momentum, as such, but rather point out that they are not the most suitable systems for the investigation of nuclear magnetic moment.

As elementary calculations show, the interactions between the nuclear moments of the nuclei in a molecule in a $^1\Sigma$ state and the other angular momentum vectors, such as molecular rotation, are of the order of magnitude of 100 gauss or less. External fields of a few thousand gauss will therefore decouple all the nuclear spins from each other and from the molecular rotation to such a degree that they may be regarded as free. The other interactions will result in a fine structure of constant or decreasing width as H_0 is increased. These effects on the precision can, therefore, be reduced to any assigned value merely by working at suitably high field.

[6] E. Majorana, Nuovo Cimento 9, 43 (1932).

Apparatus

The apparatus (Fig. 2) is contained in a long brass-walled tube divided into three distinct chambers, each with its own high vacuum pumping system. The source chamber contains the oven which is mounted on tungsten pegs. By means of a screw the mount may be moved, under vacuum, in a direction perpendicular to the beam axis. Stopcock grease and Apiezon *Q* on the screw preserve vacuum even when the screw is turned. The interchamber contains no essential parts of the apparatus, but provides adequate vacuum isolation of the receiving chamber from the gassing of the heated oven, by means of a narrow slit on each end of the chamber. These slits may be moved under vacuum in a manner similar to the oven mount. The receiving chamber contains most of the essential parts of the apparatus: the two deflecting magnets, *A* and *B*, the magnet, *C*, which produces the constant field, the radio-frequency oscillating field, *R*, the collimating slit, *S*, and the 1-mil tungsten filament detector, *D*.

The *A* and *B* fields are electromagnets of the type described by Millman, Rabi and Zacharias[7] and are 52 cm and 58 cm long, respectively. The gap is bounded by two cylindrical surfaces, one convex of radius 1.25 mm, and the other concave of radius 1.47 mm. The gap width in the plane of symmetry, defined by the axes of the two cylindrical surfaces, is 1.0 mm. The nature of the field obtained is approximately the same as that produced by two parallel wires with centers 2.5 mm apart and carrying current in opposite directions. Each magnet has four turns of copper windings; current is supplied by a 3000-ampere-hour, 2-volt storage cell. A current of 300 amperes in the windings yields a field of over 12,000 gauss and a gradient of about 100,000 gauss/cm in the gap.

The *C* magnet, which produces the homogeneous field, is made of annealed Armco iron and is of conventional design. It is wound with 12 turns of $\frac{3}{16}''$ square copper rod to which $\frac{3}{16}''$ copper tubing has been soldered for cooling purposes. Insulation between turns, and between the windings and the magnet, is provided by mica. The pole faces, separated by a gap of $\frac{1}{4}''$, are 10 cm long and 4 cm high. A field of about 23 gauss is realized in the gap per ampere of current in the exciting coils.

In mounting the magnets in the apparatus, care must be taken to avoid regions of weak, rapidly changing fields between magnets. Such regions cause transitions between quantum states of the various magnetic moments associated with the molecule and prevent good refocusing of the beam by the *B* field. Although the gradient in the *B* field is necessarily in a direction opposite to that in the *A* field, the magnetic fields in the planes of symmetry of the two magnets are in the same direction and parallel to that in the *C* magnet. The magnets are placed as close to each other as the windings will permit. Moreover these windings are completely hidden from the "view" of the molecular beam by mounting slabs of iron as extensions on both ends of the *C* magnet and on the ends of the *A* and *B* magnets facing the *C* magnet. This arrangement insures a fairly strong field along the entire path of the molecular beam where changes in the over-all magnetic moment of the molecule affects its position at *D*, i.e., from the beginning of the *A* field to the end of the *B* field, and thus limits transitions between the quantum states to the region of the *R* field, where they may be controlled and studied.

The oscillating field, *R*, consists of two $\frac{1}{8}''$ copper tubes, 4 cm long, carrying current in opposite directions. These tubes are flattened to permit their insertion between the pole faces of the *C* magnet when a space of about 1 mm between the tubes is left for the passage of the beam. The plane defined by the centers of these tubes is horizontal and is adjusted to be closely the same as the planes of symmetry of the *A* and *B* magnets. These tubes are supported by heavy copper tubing through which electrical and water connections may be made outside the apparatus.

The magnetic field, H_1, produced by a current in the tubes is about 2 gauss/amp. and is approximately vertical and therefore at right angles to the field H_0 produced by the *C* magnet. The high frequency currents in the tubes are obtained by coupling a loop in series with them

[7] S. Millman, I. I. Rabi and J. R. Zacharias, Phys. Rev. **53**, 384 (1938).

to the tank coil of a conventional Hartley oscillator in which an Eimac 250 TL tube is used. The frequencies used for these experiments range from 0.6 to 8 megacycles. The currents producing the oscillating field may be varied from 0 to 40 amperes; the higher currents are more easily obtained at low frequencies.

Procedure

A preliminary line-up of magnets, slits and detector is made by optical means while the apparatus is assembled. If this line-up is sufficiently good, a beam may be sent through the apparatus and a more precise line-up made by means of a triangulation process utilizing the property of rectilinear motion of the molecules in the beam.

The A and B magnets have knife edges at both ends which overlap the gap on the side of the convex pole face by known amounts and extend above the gap into the region above the magnet by a known amount. Since it is impossible to sight through the gaps with a telescope, the preliminary optical line-up is made by sighting on the extensions of the edges in the region above the magnets. In this way it is possible to adjust the plane of symmetry of magnet A to coincide with that of magnet B. The optical line-up is sufficient for this purpose, since no very great precision is needed for this adjustment. It is also possible to adjust optically the lateral position of the magnets as well as the slits and detector to permit a beam to pass through the magnet gaps. The C magnet is lined up so that the median plane of its gap coincides with the centers of the gaps of the A and B magnets. The two wires which produce the radiofrequency field, R, are suspended from a brass plate which is mounted on top of the vacuum chamber, and are so constructed that the width of the assemblage is only very slightly less than the width of the gap in the C magnet. The field R is then arranged in the gap so that it does not short to the poles of the C magnet. Since the width of the gap between the two wires is greater than that of the available working gap in the A and B magnets, this line-up is sufficient for the field R.

A sample of the molecular compound, the magnetic moments of whose constituent nuclei are to be determined, is placed in an oven. The oven is completely closed except for a slit about 0.03 mm wide. It is heated by means of spiral tungsten heaters passed through the oven block and electrically insulated from it by means of quartz tubing. When the temperature of the oven is sufficiently high so that the sample has a vapor pressure of the order of 1 mm of Hg a beam may be observed at the detector and a more precise line-up may be initiated.

In the present apparatus the B magnet is permanently fixed inside the vacuum chamber and all other line-up operations are made with respect to it. By suitable movements of the oven, the collimating slit, and the detector, the beam is shifted until it is cut by each of the two fiduciary knife edges on the B magnet in turn. From a knowledge of the distances separating the various elements involved in a cut-off, it is possible to set the beam parallel to the plane defined by the two edges and to ascertain the distance of the beam from that plane. The only measurements that must be made during this line-up process are the readings of detector positions by means of a calibrated tele-microscope. By successive movements of the oven, collimating slit and detector the beam can be translated parallel to itself by any desired amount. It is thus brought into a position at which one would like to have the plane of the edges of the A field. This field is then moved, in a manner similar to that described for the motion of the oven mount, until its fiduciary edges cut the beam. This operation sets the plane defined by the edges on the A field parallel to the corresponding plane of the B field and at a predetermined distance from it. The beam is then translated to a position approximately midway between these planes.

The experimental criterion which determines the exact position of the beam is that the weakening of a molecular beam at the detector by the A and B fields taken separately must be equal. This may easily be accomplished by a lateral displacement of the beam, since for any such displacement the gradient increases in one of the fields and decreases in the other. When this criterion is satisfied the intensity of the refocused beam with a current of about 300 amp. in the windings of each of the two inhomogeneous

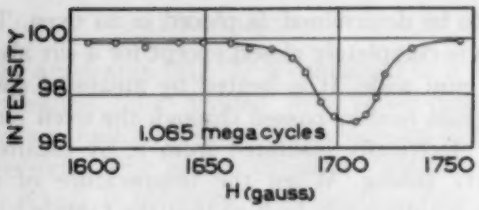

FIG. 3. Resonance curve of the Li^6 nucleus observed in LiCl.

fields is about 95 percent of the beam observed in the absence of fields.

As has been pointed out, the refocusing condition obtains only when there is no change in the space quantization of any of the moment vectors associated with the molecule. If weak fields occur in the region between the *A* and *B* fields, transitions may occur. The refocusing becomes good only when the *C* field itself is fairly large, and the intensity of the refocused beam is an increasing function of the *C* field up to a value of about 500 gauss. The resonance minima to be described subsequently are usually observed at fields larger than 1000 gauss.

Because the amplifier is not completely shielded from the oscillator and because the steady deflection of the galvanometer associated with the amplifier due to the oscillator is a function of the frequency, observations are made of the beam intensity as a function of the magnetic field, H_0, when the frequency is held fixed. Curves relating the beam intensity to the field H_0, taken for $_3Li^7$, $_3Li^6$ and $_9F^{19}$ are shown in Figs. 3, 4 and 5.

MAGNETIC AND FREQUENCY MEASUREMENTS

Since the value of the magnetic moment of any nucleus is calculated from an observed magnetic field and an observed frequency it is essential that these quantities be known to a high degree of precision. The frequency of the oscillating magnetic field is determined to better than 0.03 percent by measuring the frequency of the oscillator with a General Radio Type 620A heterodyne frequency meter. It was found that the frequency of the oscillator varied by no more than 0.01 percent during the time required to obtain data on one resonance curve (~15 minutes).

A calibration of the magnetic field of the homogeneous *C* magnet in terms of the current through the exciting coils was made in the usual way by measuring the ballistic deflection of a galvanometer when a flip coil was pulled from the magnetic field. The galvanometer was calibrated by the use of a 50-millihenry mutual inductance, good to ½ percent. Several flip coils were constructed in this laboratory by winding various types and sizes of insulated wire on carefully measured brass spools. Errors in the magnetic field due to uncertainties in flip coil areas are probably not greater than 0.2 percent.

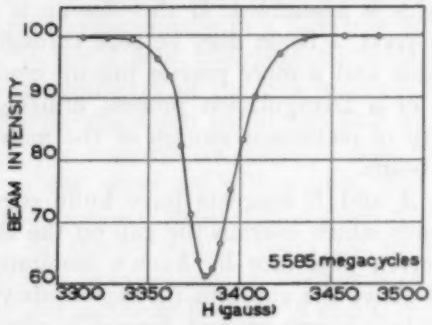

FIG. 4. Resonance curve of the Li^7 nucleus observed in LiCl.

A type K potentiometer was used to measure the potential drop across a shunt in series with the *C* magnet windings. The same shunt was used both in the calibration and in subsequent work, thereby eliminating the necessity of knowing its resistance accurately.

It is important that the magnetic field always return to the same value for a given magnetizing current. It was found that when a definite, reproducible procedure was used for demagnetizing the homogeneous field and for bringing it up to any state of magnetization, this condition was fulfilled to better than 0.1 percent.

A considerable variation in the value of the mutual inductance was observed, apparently depending on the humidity. The absolute value of the magnetic field is indeterminate to about 0.5 percent due to the uncertainty in the value of the mutual inductance and uncertainty in the areas of the flip coils. This, of course, introduces a corresponding uncertainty in the absolute values of the magnetic moments.

RESULTS

The first nuclei to be studied by this method were $_3Li^6$, $_3Li^7$ and $_9Li^{19}$ in the LiCl, LiF, NaF and

Li_2 molecules. The resonance minima which are obtained are shown in Figs. 3, 4 and 5. For each nucleus the f/H values corresponding to the resonance minima are constant to a very high degree for wide variations of frequency. This shows that we are dealing with a change of nuclear orientation and not with some molecular transition, since such a transition would not possess a frequency proportional to H. A representative sample of the results is shown in Table I. The constancy of f/H also shows that our method of calibration of the C magnet yields accurate results, at least for relative values of the homogeneous field.

The nuclear g is obtained from the observed f/H values by use of the formula

$$g=\frac{4\pi}{e/Mc}\cdot\frac{f}{H}=1.3122\times10^{-8}\frac{f}{H},$$

which follows immediately from Eq. (1) if the magnetic moment μ is measured in units of $eh/4\pi Mc$, the nuclear magneton, and $f=\nu$. The specific charge of the proton in electromagnetic

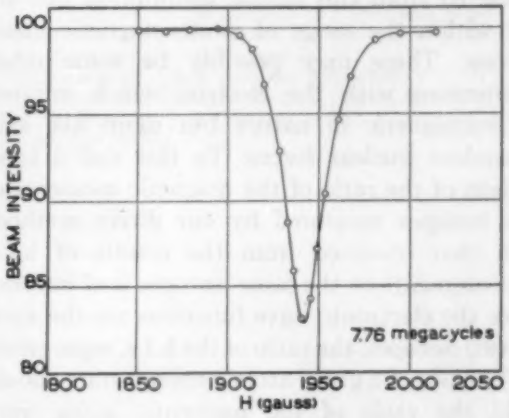

FIG. 5. Resonance curve of the F^{19} nucleus observed in NaF.

units, e/Mc, is obtained directly from the value of the Faraday[8] (9648.9 e.m.u.) and the atomic weight[9] of hydrogen (1.0081). Expressed in this form our experimental results do not depend upon any inaccuracies in e, h or m/M, the ratio of the electronic mass to the mass of the proton. The nuclear spins of Li^6 and Li^7 are known from atomic beam measurements,[10, 11] and that of F^{19} from band spectra.[12] The nuclear moments are obtained directly by multiplying g by i. The nuclear g's, the spins and the magnetic moments are listed in Table II. The values here given are about 0.5 percent lower than, and are to supersede, those published in the preliminary report.[3] The differences are due to the use of a more trustworthy mutual inductance in the calibration of the magnetic field and to an error in the value of the constant $4\pi/(e/Mc)$ previously used. The identification of the resonance minimum with a particular nucleus is made by using the same element in more than one molecule. For example, two of the resonance minima, observed for each of the molecules,[13] LiCl, LiF and Li_2 have f/H values which are the same in all three cases. These must be attributed to the nuclei of the two isotopes of lithium. Since Li^7 is about 12 times as abundant as Li^6 and since the intensity drop at resonance for one of these minima is as much as 60 percent of the refocused beam, this minimum can only be assigned to Li^7. No minimum is definitely assigned to a nucleus unless it has been observed in at least two different molecules.

The accuracy of the nuclear moment values depends solely on a knowledge of the magnetic field, H, at which the Larmor frequency associated with the nuclear magnetic moment is equal to the frequency of the oscillating field. The absolute moment values depend upon the absolute calibration of magnetic standards and cannot at present be taken to be better than 0.5 percent. The relative moment values, on the other hand, do not depend on such standards but merely on the accuracy of the shape of the, magnetization curve for the homogeneous field on the reproducibility of a definite field with the same current in the exciting coils of the homoge-

[8] R. T. Birge, Rev. Mod. Phys. **1**, 1 (1929).
[9] Eighth Report of the Committee on Atomic Weights of the International Union of Chemistry, J. Am. Chem. Soc. **60**, 737 (1938).
[10] J. H. Manley and S. Millman, Phys. Rev. **51**, 19 (1936).
[11] M. Fox and I. I. Rabi, Phys. Rev. **48**, 746 (1935).
[12] H. G. Gale and G. S. Monk, Astrophys. J. **69**, 77 (1929).
[13] The Li_2 molecules are obtained by heating lithium metal to about 1000°K. At vapor pressures of one mm the beam contains about 0.5 percent molecules. The lithium atoms have magnetic moments of the order of one Bohr magneton and suffer such large deflections in the A field that they do not reach the detector. The problem of working with alkali molecules of the type of Li_2 is solely one of obtaining enough intensity for the molecular beam. The atoms do not interfere with the experiment in any way.

neous field, on the location of a minimum in the resonance curve and on the assumption that any form of interaction tending to broaden the resonance curve and not considered in the simple theory will introduce no asymmetry into the curve. The criterion for the first three points mentioned is the internal consistency of the f/H values obtained under varied conditions. This leads to a precision of about 0.1 percent for the relative moment values of Li^6, Li^7 and F^{19}. From a consideration of the small half-widths observed for the resonance curves ($\sim$1 percent) and their symmetrical character it seems unlikely that any interactions are present which will tend to shift the minimum by more than 0.2 or 0.3 percent, if at all.

The simple model which we have used to discuss the principles of the method is, no doubt, insufficient to describe the finer details of the results, such as the width and shape of the resonance curves. For this purpose one must consider the various interactions between the nuclear spins of the different nuclei and their interactions with the rest of the molecular structure. The nature of other perturbations and the physical information which can be obtained from detailed observation of resonance minima will be discussed in another paper.

TABLE I. *Representative values of f/H for Li^6, Li^7 and F^{19}.*

NUCLEUS	MOLECULE	f MEGACYCLES PER SECOND	H GAUSS	$\frac{f}{H}$
Li^6	LiCl	2.127	3405	624.6
		2.127	3400	625.6
		2.155	3455	623.8
		2.155	3446	625.3
	Li_2	1.714	2742	625.0
		1.714	2744	624.7
	LiF	2.193	3506	625.5
		2.193	3501	626.5
Li^7	LiCl	5.611	3399	1651
		5.610	3400	1650
		6.587	3992	1650
		2.113	1278	1654
		5.552	3383	1651
	LiF	5.621	3401	1653
		6.580	3981	1653
		3.517	2133	1649
	Li_2	3.056	1862	1651
		3.084	1879	1652
		3.129	1907	1651
F^{19}	NaF	5.634	1407	4001
		5.634	1409	3998
		7.799	1949	4001
		7.799	1953	3992
		7.799	1952	3995
	LiF	4.204	1053	3994
		4.204	1055	3986

TABLE II. *Nuclear g's and magnetic moments.*

NUCLEUS	g	SPIN	MOMENT
$_3Li^6$	0.820	1	0.820
$_3Li^7$	2.167	$\frac{3}{2}$	3.250
$_9F^{19}$	5.243	$\frac{1}{2}$	2.622

DISCUSSION

One of the important objects of nuclear moment investigations is to ascertain whether the hyperfine structure of atomic energy levels can be accounted for entirely by the assumption that the nucleus interacts with the external electrons as a small magnet. The effects arising from the finite size of the nucleus and its charge distribution (isotope effect and electric quadrupole moment effect) modify slightly the h.f.s. predicted from this simple assumption but are still within the range of electromagnetic interactions. There may possibly be some other interactions with the electron which are not electromagnetic in nature but more like spin dependent nuclear forces. To this end a comparison of the ratio of the magnetic moments of two isotopes measured by our direct methods with that obtained from the results of h.f.s. measurements on the same isotopes is of interest. Since the electronic wave functions are the same for two isotopes, the ratio of the h.f.s. separations $(\Delta\nu)_1/(\Delta\nu)_2$ of a given atomic energy state should yield the ratio of the moments, μ_1/μ_2, very accurately if no other effect enters. It is to be expected that a discrepancy between these two moment ratios will be very small because of the short time which an electron spends in the region very close to the nucleus.

The ratio of the moments of the lithium isotopes, μ_7/μ_6, found by Manley and Millman[10] by the atomic beam zero moment method of measuring h.f.s. separations is 3.89. Our value is 3.963, which is about two percent higher. It is difficult to be certain, at the present time, that this difference represents a real physical

effect rather than an experimental error. Although our value can hardly be off by as much as 0.3 percent, the value given by Manley and Millman may possibly be in error because the Li^6 zero moment peak was not completely resolved from the Li^7 background. Further work along this line is clearly desirable. Another method of studying this question is through very accurate calculations of atomic wave functions (particularly in the case of Li) from which the nuclear moment can be calculated from h.f.s. data to a precision comparable with that of our direct measurements. The present status of this side of the problem is that our value of 3.250 for Li^7 is to be compared with 3.29 obtained from the measurements of Granath[14] on the h.f.s. of Li II, and the calculations of Breit and Doerman.[15] Fox and Rabi[11] find 3.14[16] from atomic beam experiments on Li I and the theory of Goudsmit[17] and that of Fermi and Segrè,[18] while Bartlett, Gibbons and Watson[19] calculate 3.33 from the same data. These differences, though small, may be significant; however, they are, as yet, within the range of accuracy claimed by the calculations.

For $_9F^{19}$, Brown and Bartlett[20] calculate values ranging from 1.9 to 3.8 from the h.f.s. data of Campbell[21] which are to be compared with our value of 2.622. For a discussion of the accuracy and reliability of these calculations see the conclusions of the papers by Bartlett and his co-workers.

From the standpoint of current nuclear theory our results for the ratio of the moments μ_{Li^7}/μ_{Li^6} diverge even more widely from the calculations of Rose and Bethe,[1] than did the previous results of Manley and Millman. In a recent paper, Bethe[22] has sought to improve the previous calculation by the use of an α-particle model. The agreement with experiment is more satisfactory than for the previous theory of Rose and Bethe. Whether this result is accidental remains to be seen from future calculations of other moments with a similar model.

This research has been aided by a grant from the Research Corporation.

[14] L. P. Granath, Phys. Rev. **36**, 1018 (1930).
[15] G. Breit and F. W. Doerman, Phys. Rev. **36**, 1732 (1930).
[16] The value 3.20 cited by Fox and Rabi for the moment of Li^7 is in error due to a mistake in sign of ds/dn in the factor $(1-ds/dn)$ of the formula of Fermi and Segrè. The effect of the correction factor $(1-ds/dn)$ is to decrease the moment and not to increase it.
[17] S. Goudsmit, Phys. Rev. **43**, 636 (1933).
[18] E. Fermi and E. Segrè, Zeits. f. Physik **82**, 729 (1933).
[19] J. H. Bartlett, J. J. Gibbons and R. E. Watson, Phys. Rev. **50**, 315 (1936).
[20] F. W. Brown and J. H. Bartlett, Phys. Rev. **45**, 527 (1934).
[21] J. S. Campbell, Zeits. f. Physik **84**, 393 (1933).
[22] H. A. Bethe, Phys. Rev. **53**, 842 (1938).

Concerning the Nature of Radio Fade-Out

L. V. BERKNER
Department of Terrestrial Magnetism, Carnegie Institution of Washington, Washington, D. C.

(Received January 21, 1939)

Radio fade-outs in the Earth's sunlit hemisphere coincident with bright solar chromospheric eruptions are examined by means of vertical-incidence recording of ionospheric echoes with a wide range multifrequency technique. It is concluded from the series of observations examined that a fade-out is best described as an upward projection of the lower or absorption limit of echo-return, and that the fade-out is caused by intense absorption of ionizing radiation, emanating from bright chromospheric eruptions, at the base of, or below, the E region, that is, below the 110-km level. It is shown that no appreciable absorption of chromospheric-eruption radiation takes place at levels higher than that of the E region; therefore, a process of selective absorption must operate. Since the principal geomagnetic effect associated with fade-outs is an augmentation of the diurnal variation of terrestrial magnetism, it appears that only the Stewart-Schuster "atmospheric-dynamo" theory of diurnal variation is possible under the restrictions imposed by these observations.

THE radio fade-out is defined qualitatively as a sudden marked diminution or complete cessation of echoes of radio waves from the ionosphere over the Earth's sunlit hemisphere. It is now well established that the fade-out coincides with bright solar chromospheric eruption and with certain geomagnetic effects of a specific character.[1–4] The experiments described in this paper are directed toward localization of the fade-out effect in the ionosphere, and to its description in quantitative terms.

When radio waves of intermediate or high frequencies are propagated during daylight, there is an upper and lower limitation on the range of wave frequencies at which echoes from the ionosphere can be observed. These limits depend on structure of the ionosphere and can be defined in terms of dispersion-theory.[5–8] When the wave is propagated along the normal to the ionosphere (as in the experiments herein described), the upper frequency limit for return of echo is the critical frequency required for penetration through the maximum ion density encountered in the ionosphere. Maximum of ion density is ordinarily reached in the outer (F_2) region (for otherwise this region could not be observed). Then at normal incidence the upper frequency limit depends only on maximum ion-density of the outer region. Wave frequencies higher than this simply penetrate the ionosphere. The lower frequency limit is imposed in the lower ionosphere by absorption of waves[9] passing through it. This absorbing region must be below the lowest level at which reflections can be observed and is therefore in the base of, or below, the E region. The lower frequency limitation on echo-return is therefore an absorption limit.[10]

These limitations on the range of wave frequency over which echoes can be observed are illustrated in Fig. 1*A*. They are drawn for the average of six successive control-days of observation adjacent to, but not including, a day during which fade-out occurred on July 31, 1937. The shaded portions give the range of wave frequency over which echoes were observed. Both upper and lower limiting frequencies undergo more or less regular diurnal variation under normal circum-

[1] J. H. Dellinger, Science **82**, 351 (1935); Phys. Rev. **48**, 705 (1935); Terr. Mag. **42**, 49–53 (1937); Nat. Bur. Stand. J. Research **19**, 111–141 (1937).
[2] O. W. Torreson, W. E. Scott and H. E. Stanton, Terr. Mag. **41**, 199–201 (1936). See also O. W. Torreson, F. T. Davies, W. E. Scott and H. E. Stanton, Terr. Mag. **41**, 409–410 (1936).
[3] J. A. Fleming, Terr. Mag. **41**, 404–406 (1936).
[4] A. G. McNish, Nature **139**, 244 (1937).
[5] G. Breit and M. A. Tuve, Phys. Rev. **28**, 554–575 (1926).
[6] E. V. Appleton, J. Inst. Elec. Eng. **71**, 642–650 (1932).
[7] G. Goubou, Hoch:tech. u. Elek:akus. **45**, 179–185 (1935).
[8] H. G. Booker, Proc. Roy. Soc. **A150**, 267–286 (1935).
[9] E. V. Appleton, Proc. Roy. Soc. **A162**, 451–479 (1937).
[10] If the wave frequency is continually decreased, a frequency range will be reached when reflection from the ionosphere is again observed. Waves from these low frequencies no longer pass into absorbing region in the same sense as the shorter waves, but are reflected by it. This provides the mechanism utilized by J. E. Best, J. A. Ratcliffe and M. V. Wilkes, Proc. Roy. Soc. **A156**, 614–633 (1936), in investigation of very low ionospheric regions.

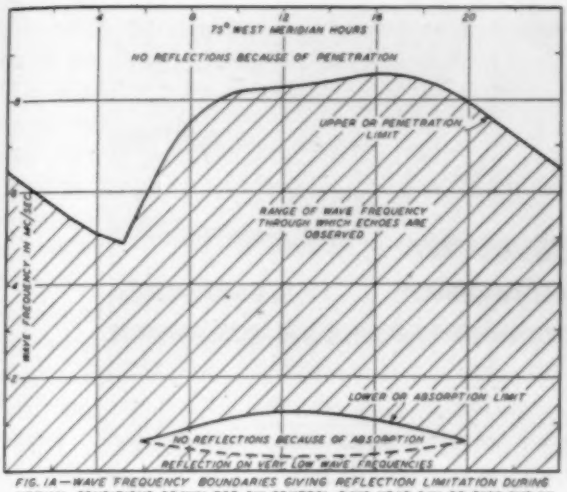
75° WEST MERIDIAN HOURS
NO REFLECTIONS BECAUSE OF PENETRATION
UPPER OR PENETRATION LIMIT
RANGE OF WAVE FREQUENCY THROUGH WHICH ECHOES ARE OBSERVED
WAVE FREQUENCY IN MC/SEC.
LOWER OR ABSORPTION LIMIT
NO REFLECTIONS BECAUSE OF ABSORPTION
REFLECTION ON VERY LOW WAVE FREQUENCIES

FIG. 1A—WAVE FREQUENCY BOUNDARIES GIVING REFLECTION LIMITATION DURING NORMAL CONDITIONS; DRAWN FOR SIX CONTROL-DAYS NEAR DAY OF FADE-OUT OF JULY 31, 1937, KENSINGTON, MARYLAND

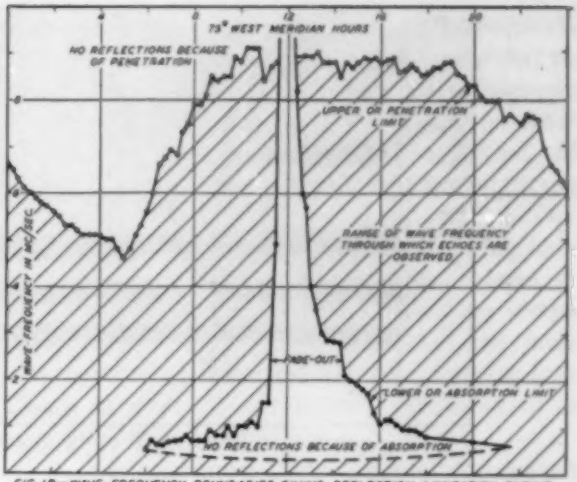
75° WEST MERIDIAN HOURS
NO REFLECTIONS BECAUSE OF PENETRATION
UPPER OR PENETRATION LIMIT
RANGE OF WAVE FREQUENCY THROUGH WHICH ECHOES ARE OBSERVED
WAVE FREQUENCY IN MC/SEC.
FADE-OUT
LOWER OR ABSORPTION LIMIT
NO REFLECTIONS BECAUSE OF ABSORPTION

FIG. 1B—WAVE FREQUENCY BOUNDARIES GIVING REFLECTION LIMITATION DURING FADE-OUT; ILLUSTRATING UPWARD PROJECTION OF LOWER OR ABSORPTION LIMIT FOR FADE-OUT OF JULY 31, 1937, KENSINGTON, MARYLAND

stances, the lower disappearing at night. Such data are obtained using an automatic multi-frequency technique so that echoes are recorded once each quarter-hour on each of all wave frequencies between 0.516 and 16.0 mc/sec. In this way the whole structure of the ionosphere is examined at regular intervals.

With this technique, it has been shown by Berkner and Wells[11] that fade-out is principally defined as an upward projection of the lower absorption limit of echo-return. This is illustrated in Fig. 1*B* drawn for the fade-out of July 31, 1937, as seen at Kensington, Maryland (39° north and 177° west). This fade-out coincided with a bright chromospheric eruption reaching maximum intensity at about the midpoint of fade-out. Fade-out was also recorded simultaneously at the Huancayo (Peru) Magnetic Observatory of the Department of Terrestrial Magnetism (12° south and 75° west). At commencement of fade-out (and coinciding closely with the outburst of the bright chromospheric eruption) this lower or absorption limit rises rapidly, intersecting the upper or penetration limit in the case of intense events, so that no echoes on any wave frequency can then be observed. At the end of fade-out, the absorption limit decreases in an approximately exponential manner, so that echoes at successively lower and lower wave frequencies come into view. Thus, while the commencement of fade-out is usually almost simultaneous on all wave frequencies because of rapidity of rise of absorption limitation, its termination and duration depend upon wave frequency at which observation is made. Fade-out of echoes on a fixed wave frequency of 4.8 mc/sec. is illustrated in Fig. 2. Had observation been made on a lower frequency, termination would have been later and duration longer.

While echoes are obliterated during the more intense effects, it is possible to infer, from observation immediately before and after fade-out, effects which have occurred in each ionospheric region during the event. Using both fixed and multifrequency observations, Berkner and Wells[11, 12] have shown that both the outer (F_2 and F_1) regions reappear substantially unchanged after fade-out. On the contrary, the lower (E) region reappears after fade-out with some increase in maximum ion density and in virtual height. Because atmospheric density in higher regions is very much less than in the E region, one may justifiably argue that equilibrium conditions would be established in the higher regions more slowly than in the E region. Therefore, because the outer regions reappear unchanged after fade-out, no substantial change can have occurred in them during the event.

Similarly, maximum ion density of the E region returns to normal some time (usually an hour or more) before the lower absorption limit has dropped to its normal value. This demonstrates

[11] L. V. Berkner and H. W. Wells, Terr. Mag. **42**, 301–309 (1937).

[12] L. V. Berkner and H. W. Wells, Terr. Mag. **42**, 183–194 (1937).

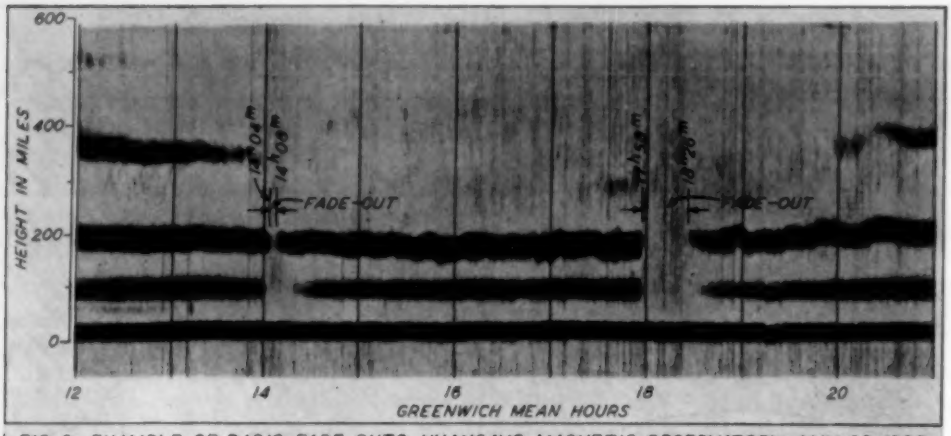

FIG. 2—EXAMPLE OF RADIO FADE-OUTS, HUANCAYO MAGNETIC OBSERVATORY, MAY 28, 1936

that absorption of the wave must occur principally *below* the level of E region maximum and cannot be attributed simply to the increase of maximum ion density of the E region which is observed.

These observations permit certain generalizations. (1) Ionizing radiation emanating from the bright chromospheric eruption and responsible for the fade-out is not noticeably absorbed in the upper but only in the lower ionospheric region. (2) Fade-out occurs because of intense absorption at the base of, or below, the E region, that is, below the 100-km level in the ionosphere. The former implies that the ionizing emanation traverses the upper regions without appreciable absorption, but that it is selectively absorbed in the base of or below the E region. The latter indicates increased ionization in the absorbing region where energy of radio waves passing through it is dissipated by frequent collision of ionized particles in relatively dense atmosphere.

A question concerning absorption of light emanating from bright chromospheric eruption in the upper regions of the ionosphere has been raised by observations of Martyn, Munro, Higgs and Williams.[13] Making their experiments on a fixed frequency, they observed effects almost coincident with a bright chromospheric eruption and with the associated diminution of echo intensity which they interpret as a decrease of ion density associated with an increase of virtual height of the F_2 region. They attribute the effect to absorption of part of the light emanating from the chromospheric eruption in the outer atmospheric regions, and suggest heating and expansion of these regions to explain the effects observed. This appears to be in contradiction to the results of experiments outlined above where absorption of light emanating from the chromospheric eruption in the outer ionospheric regions was found almost negligible. This distinction is an important one, for upon it hinges the localization of the effect in the ionosphere, with consequent decision concerning processes of light-absorption, layer-formation, and mechanism producing the associated geomagnetic effect.

Further investigation of this point has been made by observations on a number of fade-outs at the Watheroo (Western Australia) Magnetic Observatory (30° south, 116° east) of the Department of Terrestrial Magnetism, Carnegie Institution of Washington. Observations were made simultaneously with the automatic multifrequency technique and with a continuous recorder on a fixed wave frequency of 4.8 mc/sec. While the multifrequency method defines the heights and ion densities of each region as well as the absorption limitation at regular quarter-hourly intervals, the fixed-frequency recorder gives a continuous and exact chronology of events on the particular wave frequency to which it is adjusted. The two methods are complementary in producing a picture of the event.

The fade-out of September 20, 1938, is shown in Figs. 3 and 4. This fade-out was of sufficient intensity that echoes on lower wave frequencies

[13] D. F. Martyn, G. H. Munro, A. J. Higgs and S. E. Williams, Nature **140**, 603–605 (1937).

were obliterated but such that echoes on upper wave frequencies, showing details of the outer (F_2) region, remained throughout the event. The upper region in question was therefore measurable during the whole of the fade-out, so that nothing is left to inference. The event consisted in reality of two fade-outs, one closely following the other, but neither obscuring the upper region. Variation of penetration-frequency and of the lower or absorption limit is shown in Fig. 3. Means of values for each quarter-hour for ten control-days, five before and five after the day of fade-out, are shown by solid lines, while individual values observed on the day of fade-out are plotted. In Fig. 4 similar data are given for the minimum virtual heights of the regions.

No significant change in the upper regions during fade-out is apparent. The F_2 critical frequency follows the mean of the control-days very closely, with fluctuation not exceeding 0.1 mc/sec. during the main phase of the fade-out. The criterion by which the significance of fluctuation of F_2 critical frequency can best be judged, may be had by reference to observation made on control-days. Fig. 5*A* shows the fluctuation of F_2 critical frequency with respect to the mean for the five control-days before and Fig. 5*B* for the five days after the fade-out, respectively. Examination of these data demonstrates that the performance of the F_2 penetration-frequency during fade-out cannot be considered as otherwise than normal from simple inspection. All control-days show apparently random fluctuation of the F_2 penetration-frequency up to 1.0 mc/sec. so that the relatively small change during fade-out cannot be said to be significant from inspection alone. Similarly the minimum virtual height (Fig. 4) conforms closely to the mean throughout the event, certainly not varying from it by as much as the deviation experienced on many of the control-days.

It might be argued that the minimum virtual height was representative only of the lower portions of the F_2 region, and that the upper portions observed on the higher frequencies might be affected without a corresponding change in minimum virtual height. The virtual heights observed on a frequency of 9.5 mc/sec. during the afternoon of September 20, 1938, and including the interval of the fade-out, are shown in the upper portion of Fig. 6. This wave frequency was selected as the highest wave frequency on which echoes could be observed throughout the interval because of the normal diurnal change in pene-

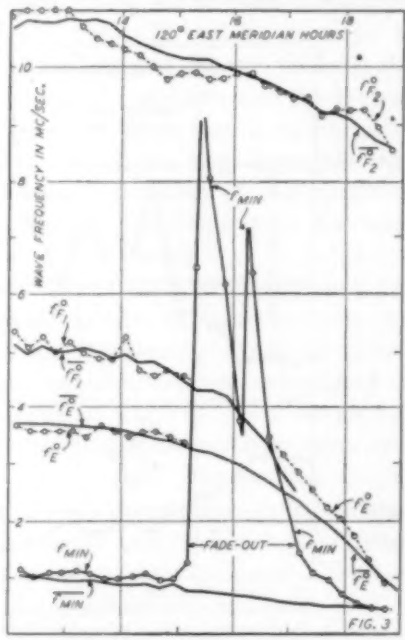

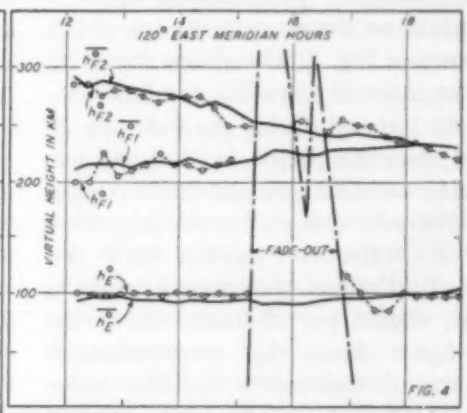

FIG. 3—CRITICAL FREQUENCIES OF IONOSPHERE SHOWING RADIO FADE-OUT OF SEPTEMBER 20, 1938, DETERMINED FROM AUTOMATIC MULTIFREQUENCY REGISTRATIONS, WATHEROO MAGNETIC OBSERVATORY, WESTERN AUSTRALIA (116° EAST, 30° SOUTH)

FIG. 4—VIRTUAL HEIGHTS OF IONOSPHERE SHOWING EFFECT OF RADIO FADE-OUT OF SEPTEMBER 20, 1938, DETERMINED FROM AUTOMATIC MULTIFREQUENCY REGISTRATIONS, WATHEROO MAGNETIC OBSERVATORY, WESTERN AUSTRALIA (116° EAST, 30° SOUTH)

LEGEND
- OBSERVED VALUES FOR "O" WAVE COMPONENT, SEPTEMBER 20, 1938
- MINIMUM FREQUENCY FOR WHICH REFLECTION OBSERVED, SEPTEMBER 20, 1938
- MEANS OF OBSERVED VALUES FOR 10 CONTROL DAYS AROUND SEPTEMBER 20, 1938

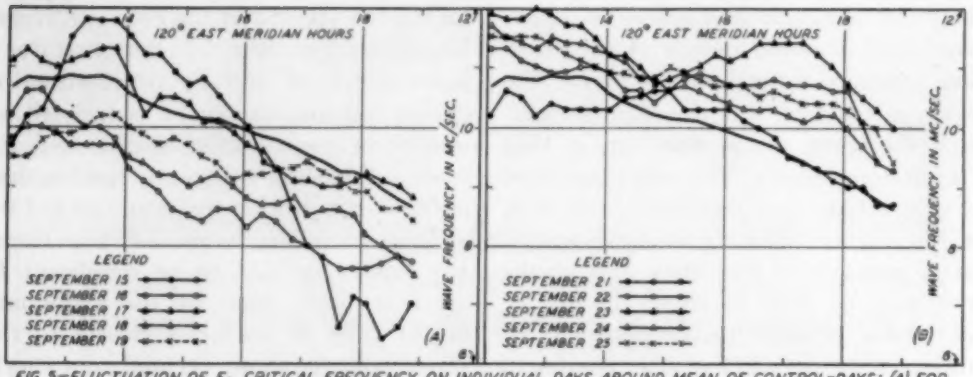

FIG. 5—FLUCTUATION OF F_2 CRITICAL FREQUENCY ON INDIVIDUAL DAYS AROUND MEAN OF CONTROL-DAYS; (A) FOR FIVE DAYS PRIOR TO FADE-OUT, SEPTEMBER 15-19, 1938, AND (B) FOR FIVE DAYS AFTER FADE-OUT, SEPTEMBER 21-25, 1938, WATHEROO MAGNETIC OBSERVATORY, WESTERN AUSTRALIA

tration-frequency illustrated in the lower portion of the figure. As the penetration-frequency becomes identical to the wave frequency in question, the virtual height tends to infinity. The question is whether the virtual heights on this frequency of 9.5 mc/sec. are significantly different during the fade-out from heights to be expected if the fade-out had not occurred. It is clear that the major influence on virtual height on this wave-frequency is the proximity of the penetration-frequency, but we must determine whether any additional retardation occurs during fade-out.

The relation between penetration-frequency and virtual height on the wave frequency of 9.5 mc/sec. is shown in Fig. 7. The circles show the relation for the interval preceding the fade-out, the dots for the interval during the fade-out. If it is assumed that the distribution of the ion density remains substantially the same during the interval, the dots and circles should follow the same curve. On the other hand, a rise in the upper portion of the region, that is, an increase in its diffuseness, should put the dots above the circles. The figure shows that no substantial difference in the relation before and after commencement of fade-out can be seen—though there is a tendency for the dots to fall slightly below the circles. It can be shown that this tendency occurs on any afternoon in the manner shown in the figure as a consequence of increase of ion gradient with approach of nightfall. One can certainly conclude, however, that there is no indication of increased diffuseness during this fade-out.

Because the fade-out just illustrated occurred in the afternoon and extended until nearly sunset, the F_1 and F_2 regions had merged at its termination so that no decisive conclusions can be drawn concerning the F_1 region. The performance of the F_1 region can better be seen from another fade-out illustrated in Figs. 8 and 9 for November 26, 1938. During this event neither F_1 nor F_2 regions show any noticeable deviation from the normal trend at its termination.

The conclusions to be drawn from these data (which are representative of a series of such observations) are that no obvious change occurs in the outer (F_1 and F_2) regions during the bright

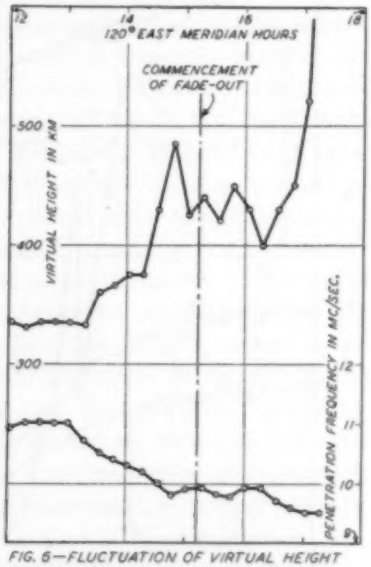

FIG. 6—FLUCTUATION OF VIRTUAL HEIGHT ON 9.5 MC/SEC. COMPARED TO CHANGE OF PENETRATION FREQUENCY ON AFTERNOON OF FADE-OUT OF SEPTEMBER 20, 1938, WATHEROO MAGNETIC OBSERVATORY, WESTERN AUSTRALIA

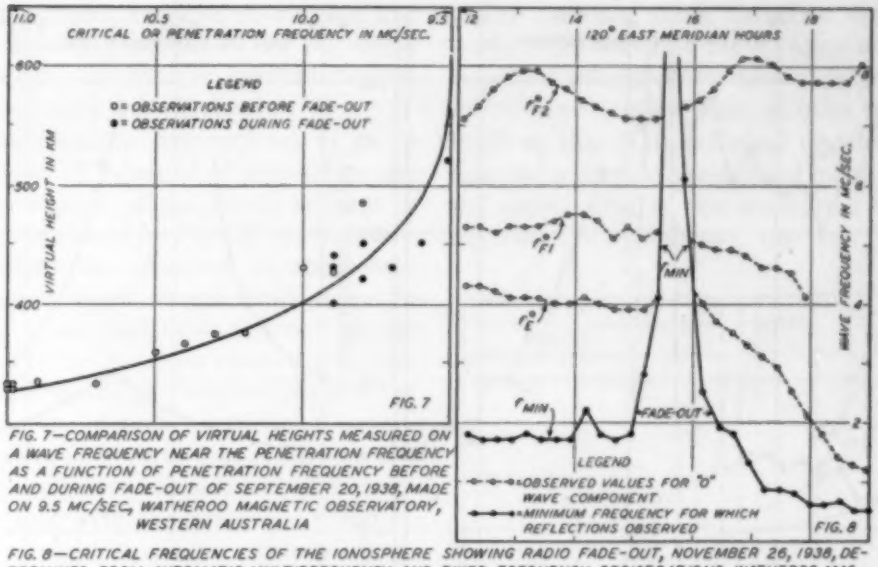

FIG. 7—COMPARISON OF VIRTUAL HEIGHTS MEASURED ON A WAVE FREQUENCY NEAR THE PENETRATION FREQUENCY AS A FUNCTION OF PENETRATION FREQUENCY BEFORE AND DURING FADE-OUT OF SEPTEMBER 20, 1938, MADE ON 9.5 MC/SEC., WATHEROO MAGNETIC OBSERVATORY, WESTERN AUSTRALIA

FIG. 8—CRITICAL FREQUENCIES OF THE IONOSPHERE SHOWING RADIO FADE-OUT, NOVEMBER 26, 1938, DETERMINED FROM AUTOMATIC MULTIFREQUENCY AND FIXED FREQUENCY REGISTRATIONS, WATHEROO MAGNETIC OBSERVATORY, WESTERN AUSTRALIA (118°EAST, 30° SOUTH)

chromospheric eruption and coincident fade-out. As a consequence, the absorption of light emanating from the chromospheric disturbance in these outer regions must be negligible; a consistent change of more than about 0.1 mc/sec. would be evident from inspection of a few diagrams of fade-outs such as shown. If any small change, which would indicate slight absorption, does actually occur, it cannot be determined from inspection of the data. It will be possible to detect it only by averaging departures from the mean for a number of fade-outs and by demonstration that resultant departure is significantly different from a corresponding departure obtained from similar treatment of appropriately selected control-days. Sufficient data for such analysis are not yet available.

We have yet to explain the discrepancy between the observations of Martyn and his colleagues and the experiments described above. Their published observations are reproduced as nearly as possible in Fig. 10. This shows the variation of virtual height observed by them on a frequency of 9.75 mc/sec. The sudden rise in virtual height of both components, with passage of the "o" to infinity and its subsequent reappearance, indicates a dip in penetration-frequency reaching a minimum at about $9^h\ 47^m$. They point out also that the layer-height increased simultaneously, basing this conclusion on the fact that the virtual heights of the end of the record are greater than at the beginning, though the separation of "o" and "x" wave components is in both cases about the same.

It is necessary first to evaluate the decrease of penetration-frequency which must have occurred during their observations. No direct method is available, so we resort to a method of comparison. For this purpose a dip of penetration-frequency centering at about $14^h\ 20^m$ on September 17, 1938, and shown in Fig. 5*A*, is selected. This dip occurred on one of the control-days near the day of the fade-out of September 20, 1938. Five sweeps of the multifrequency equipment during this dip are illustrated in Fig. 11 where the virtual heights of both "o" and "x" wave components on the wave frequencies above 8 mc/sec. are graphically reproduced from the records. Suppose that recording of virtual heights on some fixed wave frequency had been in progress during this interval. Three such selected wave frequencies, namely, 10.20, 10.35 and 10.50, are indicated on Fig. 11 by vertical lines. The intersections of the selected fixed frequency with multifrequency curves give the virtual height observed on this wave frequency at succeeding epochs. From these values it is possible to reproduce the principal features of curves which would be recorded by a fixed-frequency recorder on any particular wave frequency during the interval. This is done in

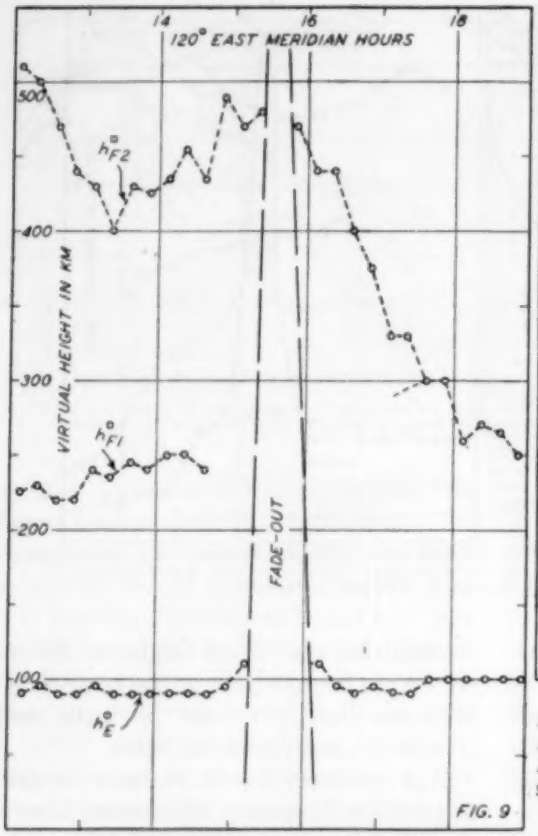

FIG. 9—VIRTUAL HEIGHTS OF IONOSPHERE SHOWING EFFECT OF RADIO FADE-OUT, NOVEMBER 26, 1938, DETERMINED FROM AUTOMATIC MULTIFREQUENCY AND FIXED FREQUENCY REGISTRATIONS, WATHEROO MAGNETIC OBSERVATORY, WESTERN AUSTRALIA (116°EAST, 30°SOUTH)

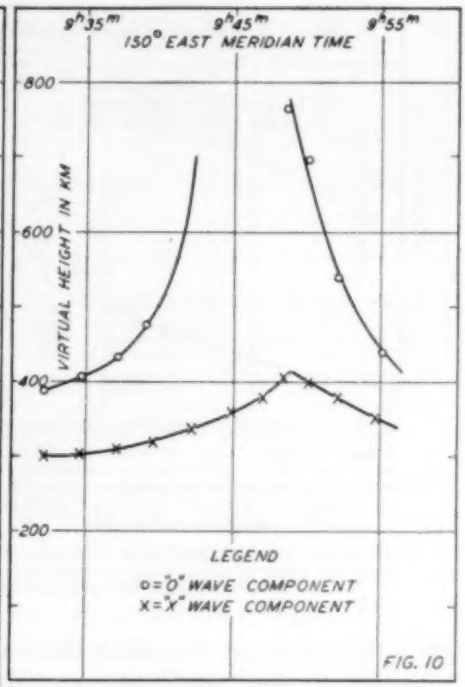

FIG. 10—GRAPH AFTER MARTYN, MUNRO, HIGGS, AND WILLIAMS SHOWING VIRTUAL HEIGHT OBSERVED ON WAVE FREQUENCY 9.75 MC/SEC. DURING RADIO FADE-OUT OF MAY 15, 1937

Fig. 12 for three frequencies indicated above. Thus by trial selection of a suitable fluctuation of F_2 critical frequency it is possible to practically produce a replica of the fixed-frequency observations of Martyn and his colleagues from multifrequency data. Critical frequencies for the multifrequency data are completely known, so that by comparison the change which the data of Fig. 10 represent can be estimated quite closely. The central portion of Fig. 12 covers the same range of virtual height which they observed and their observations are closely duplicated in this figure on the frequency of 10.35 mc/sec.

Reference to Fig. 11 shows that the performance of the graphs of Fig. 12 was induced by a decrease of penetration-frequency of about 0.6 mc/sec. during the quarter-hour before the minimum, followed by an increase of 0.25 mc/sec. during the next quarter-hour. From this, one may infer that the decrease in penetration-frequency inducing the effects observed by Martyn and his colleagues was of about the same magnitude, and that at the commencement of their observation the critical frequency for the "o" wave component was less than 0.45 mc/sec. above their wave frequency. This is consistent with the fact that they observed no echoes on 10.7 mc/sec.

There are certain other features of Fig. 12 worthy of attention. After the minimum of dip of penetration-frequency has been passed, the height of the region appears greater than before for frequencies near the penetration-frequency. This is based on the same criterion as the similar deduction from Fig. 10, namely, that greater heights occur for an equivalent separation of "o" and "x" wave components after the dip than before it. Furthermore, the increase in height is about the same as that shown in Fig. 10. Therefore, one is led to the conclusion that the fluctuation of the F_2 penetration-frequency illustrated in Fig. 12 is very similar, if not identical, to the

change noted by Martyn and his co-workers. The outstanding difference is that it did not occur during a fade-out, and that no marked diminution in echo intensity was observed.

Fluctuations (usually diminutions) of penetration-frequency of F_2 region of as much as one megacycle per second (of magnitude as large or larger than that deduced for Fig. 10) are frequent. Such fluctuations are observed at apparently random intervals, often several times during a day—in fact, these variations are one of the characteristics of the F_2 region which distinguish it from the more regular performance of the lower regions. A number of such fluctuations are apparent in the data for control-days of Fig. 5*A* and *B*. A certain number of coincidences of fluctuations of this sort with fade-outs are therefore inevitable. As nearly as can be estimated from present data, one marked incidence should be observed in about five or six fade-outs.

From the series of observations just described, it is concluded that there is no obvious change in F_1 and F_2 regions during most fade-outs. If any consistent change of penetration-frequency does occur, it must be of the order of about 0.1 mc/sec. or less, or it should be evident from inspection of the observed multifrequency records. It is suggested that such small changes as have been reported may be due to (1) coincidence of the fade-out with random fluctuation of the F_2 region such as occurs frequently, or to (2) an increased emission spectrum from occasional chromospheric eruptions leading to absorption in the F_2 region only for certain fade-outs. The former appears the most favorable explanation, as random fluctuation of the F_2 region is sufficiently frequent to make occasional coincidence inevitable. Furthermore, this random fluctuation appears to be of the same nature as that reported as coinciding with fade-out. So far, no mechanism has been proposed to explain apparently random fluctuation of the F_2 region such as illustrated. Nevertheless, if it were possible to accept the dip in F_2 penetration-frequency which is occasionally observed coincident with fade-out as due to absorption in the F_2 region of radiation emanating from bright chromospheric eruption, it would yet be necessary to introduce an additional mechanism to explain effects which appear identical, but do not coincide with fade-out.

The fade-out effect therefore appears to be confined primarily to the E region and below. It is defined principally by upward projection of the lower or absorption limit of echo return. Inasmuch as this is its principal manifestation, the fade-out might well be defined quantitatively by the upper value of this absorption limit during the event. Furthermore, one can localize the

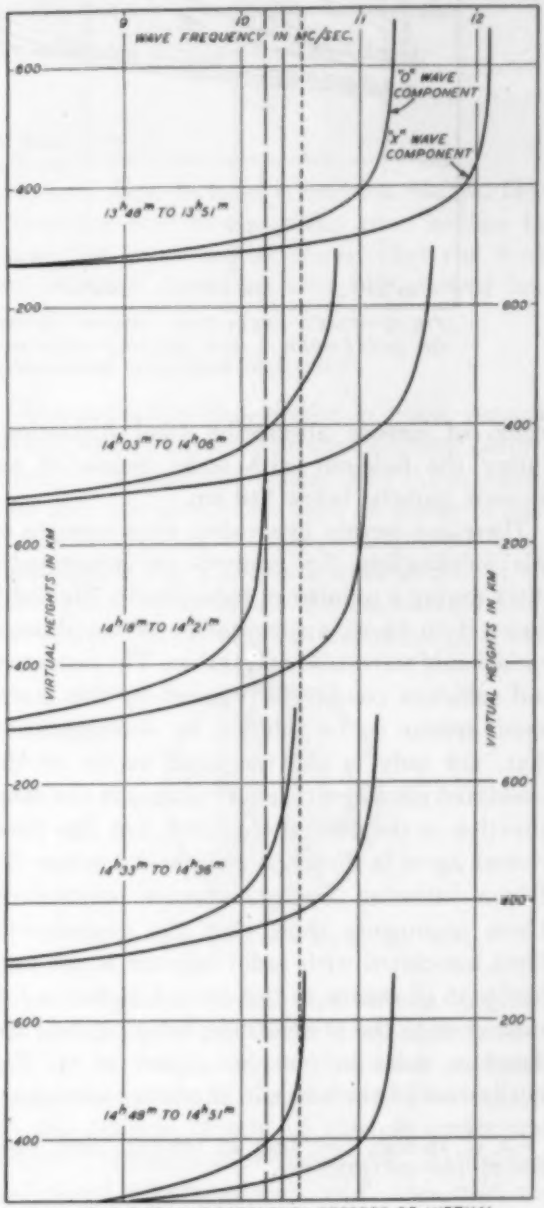

FIG. 11—GRAPHS OF MULTIFREQUENCY RECORDS OF VIRTUAL HEIGHTS FOR WAVE FREQUENCIES ABOVE 8 MC/SEC. TAKEN AT QUARTER-HOURLY INTERVALS DURING FLUCTUATION OF PENETRATION FREQUENCY, SEPTEMBER 17, 1938, WATHEROO MAGNETIC OBSERVATORY, WESTERN AUSTRALIA

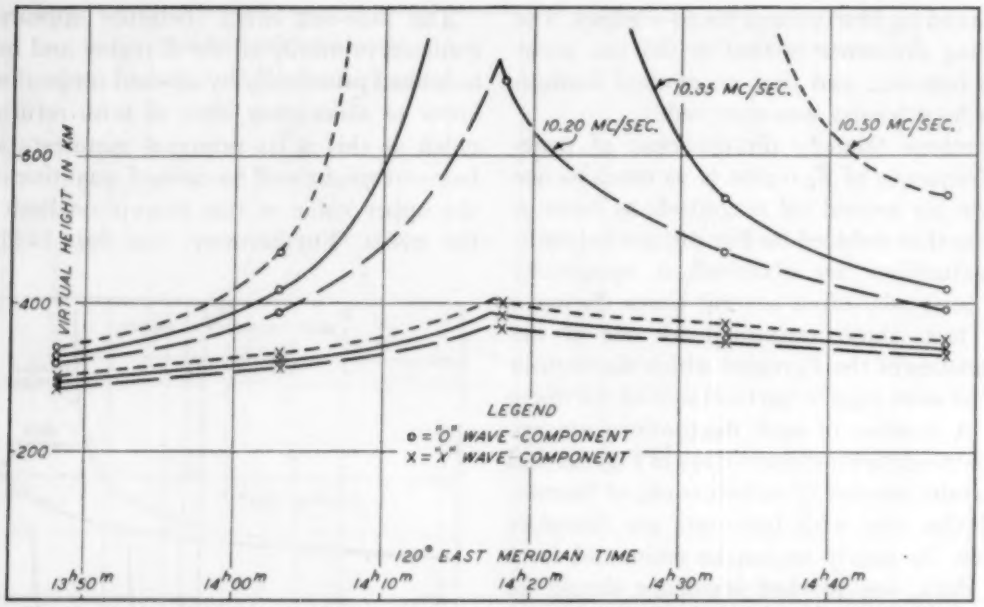

FIG. 12—FIXED FREQUENCY GRAPHS DURING DIP OF PENETRATION FREQUENCY OCCURRING ON SEPTEMBER 17, 1938, DERIVED FROM MULTIFREQUENCY DATA OF FIGURE 9, WATHEROO MAGNETIC OBSERVATORY, WESTERN AUSTRALIA

region of intense absorption (and ionization) during the fade-out with some degree of assurance, namely, below 110 km.

There are certain interesting consequences of this localization. An analysis of geomagnetic effect during a number of fade-outs by McNish[14] shows it to be an augmentation of the diurnal variation of terrestrial magnetism. The necessary and sufficient conditions required by this statement appear to be fulfilled by demonstration that, not only is the magnetic vector of the associated geomagnetic effect always in the same direction as the diurnal variation, but also these vectors agree in direction at locations where the diurnal-variation vector appears anomalous. These arguments show that the geomagnetic effect associated with radio fade-out is not only similar in character to the diurnal variation but must arise in the same atmospheric regions, and therefore must in fact be a part of it. The localization of the effect in the lower ionosphere brings strong evidence to bear on the theories of diurnal variation of geomagnetism. It appears from the present state of the theories that only the Stewart-Schuster "atmospheric-dynamo" theory of diurnal variation is possible under restrictions imposed by these observations.

The positive evidence of selective absorption of particular radiation in definite atmospheric regions permits more definite formulation of ideas concerning layer-formation. This is illustrated in the recent work of Wulf and Deming,[15] who consider photochemical processes involved which are consistent with selective absorption of this nature.

The writer wishes to acknowledge the active interest and assistance of Dr. J. A. Fleming, Director of the Department of Terrestrial Magnetism of the Carnegie Institution of Washington, in the conduct of these investigations and to thank his colleagues at Watheroo Magnetic Observatory for their active assistance in making the observations.

[14] A. G. McNish, Terr. Mag. **42**, 109–122 (1937); Phys. Rev. **52**, 155–160 (1937).

[15] O. R. Wulf and L. S. Deming, Terr. Mag. **43**, 283–297 (1938).

Zeeman Effect of the Forbidden Lines of Potassium

F. A. JENKINS AND E. SEGRÈ
University of California, Berkeley, California

(Received January 30, 1939)

The Zeeman effect of the lines $S-S$ and $S-D$, absorbed by potassium vapor in an electric field of about 2000 volts/cm, is studied. A magnetic field of 27,000 gauss was obtained by using the magnet of the new Berkeley cyclotron. The lines $4S-14S$ to $4S-19S$ show no effect, except for a slight broadening of the last one or two lines. The Zeeman patterns for $4S-12D$ to $4S-15D$, with the magnetic field perpendicular to the electric field and to the direction of observation, are resolved. They agree with the predicted pattern $\frac{0(1)2}{1}$, and show qualitatively the expected intensities.

THE $^2S-^2D$ combinations in the alkali spectra are among the most thoroughly studied of forbidden lines. It has been shown by the Zeeman effect investigations of Segrè and Bakker[1] that the first member of this series, which is absorbed by sufficiently dense alkali vapor, is due to quadrupole radiation. Kuhn,[2] Bakker,[3] Segrè[4] and Amaldi[5] have shown that the high members of this series, as well as of the forbidden series $^2S-^2S$, can be obtained in absorption by applying an electric field to sodium or potassium vapor. The main features of their appearance, and of their variation of intensity with field strength have been at least qualitatively cleared up.[5a]

It is well known that the type of radiation to which a line is due, e.g. quadrupole, magnetic dipole, forced dipole, etc., may be determined by studying its Zeeman effect. In the present case, there is no question that the lines are dipole lines induced by the electric field. However, since relatively few cases of forced dipole lines are known, and since for only two of these cases has the Zeeman effect been studied,[6] it seemed worth while to attempt to obtain the Zeeman effect of these lines in a uniform electric field. Potassium was chosen rather than sodium because the levels are so placed that the $S-D$ series is well separated from the allowed lines $S-P$.

EXPERIMENTAL

The apparatus was similar in many respects to that used in our work on the quadratic Zeeman effect.[7] The principal change was the introduction into the absorption tube of a pair of electrodes for applying the electric field to the potassium vapor. Fig. 1 shows a cross section of the tube. T is a Pyrex tube of 3.0 cm internal diameter and length 110 cm. The electrodes E, E were

FIG. 1. Cross section of absorption tube.

of nonmagnetic stainless steel 46 cm long, 2.5 cm high and 0.5 cm thick. They were held in position, with the inner surfaces 0.5 cm apart, by screwing them at the ends to fiber rings F. To the outside of one of the electrodes was welded a stainless steel "pouch" K, 20 cm long and closed tightly at each end. This held the metallic potassium to be vaporized and avoided the possibility of a short circuit by the fused

[1] E. Segrè and C. J. Bakker, Zeits. f. Physik **72**, 724 (1931).
[2] H. Kuhn, Zeits. f. Physik **61**, 805 (1930).
[3] C. J. Bakker, Proc. Amst. Acad. **35**, 589 (1933).
[4] E. Segrè, Rend. Lincei **19**, 595 (1934).
[5] E. Amaldi, Rend. Lincei **19**, 588 (1934).
[5a] E. Segrè and G. C. Wick, Proc. Amst. Acad. **36**, 3 (1933).
[6] Hg λ3680, $^3P_2-^3P_2$ induced by unordered ionic fields, C. J. Bakker and E. Segrè, Zeits. f. Physik **79**, 655 (1932) and certain singlet and triplet He lines appearing in the Stark effect, J. S. Foster, Proc. Roy. Soc. **A122**, 599 (1929); **A131**, 142 (1931). In the latter work the Zeeman patterns were incompletely resolved.
[7] F. A. Jenkins and E. Segrè, Phys. Rev. **55**, 52 (1939).

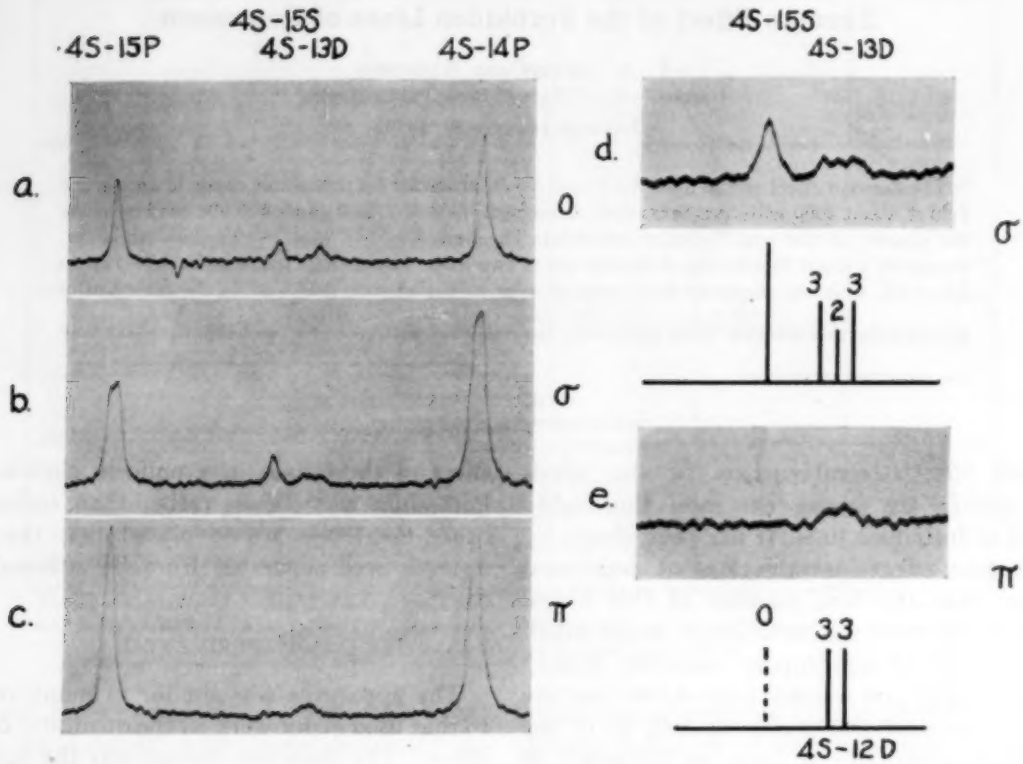

FIG. 2. Microphotometer curves of allowed and forbidden lines. (*a*) Electric field only. Light polarized parallel to electric field. $F=2080$ volts/cm. (*b*) Electric and magnetic fields. $F=2220$, $H=27{,}000$. σ components (polarized perpendicular to H). (*c*) Electric and magnetic fields. $F=2220$, $H=27{,}000$. π components. (*d*) Detail of (*b*), with wider microphotometer slit. The theoretical pattern is shown underneath. (*e*) π components of $4S-12D$, with theoretical pattern.

metal. The electrodes were connected by a pair of thin insulated wires, brought out through the waxed joint at the window, to a rectifier set delivering a constant potential up to 2000 volts. In operation, the tube contained hydrogen at a pressure of 10–15 cm to prevent excessively rapid distillation of potassium to the ends of the heated portion (35 cm long), with the consequent formation of "trees" of metallic potassium between the electrodes.

This tube was placed between the built-up poles[7] of the large cyclotron magnet, giving a field of 27,000 gauss. The hydrogen lamp had a platinized quartz capillary and was operated with a current density of 55 ma/mm^2. Images in the two polarizations were focused through a calcite crystal on the slit of the two-prism Littrow quartz spectrograph, which gave a dispersion of 1.36 A/mm in the region used.

In our work the forbidden lines were somewhat less intense than those obtained by Segrè and by Amaldi. This is due in part to the slightly greater electrode separation in our case. Although this decreased the electric field obtainable without breakdown, it was necessary for reasons of intensity. Furthermore, the length of the absorbing column of vapor was smaller, being limited by the length of the uniform part of the magnetic field. Another important reason was the lower density of potassium vapor we had to use to avoid undue broadening of the lines, and obliteration of the Zeeman patterns.

Plates were taken with a potential between the electrodes somewhat greater than 1000 volts. The actual electric field in the vapor was less than the indicated value of 2000 volts/cm by an indefinite amount, since a current of a few milliamperes flowed continuously between the electrodes. This electric field was perpendicular to the magnetic field and of course to the direction of observation. Fig. 2 shows microphotometer curves of the best plates. Without

the magnetic field, both the $S-S$ and $S-D$ lines appear in the spectrum polarized parallel to the electric field (Fig. 2(*a*)), but only the $S-D$ lines in that polarized perpendicular to it.[3] Below the two curves (*d*) and (*e*) taken with the magnetic field are shown the theoretical patterns, the calculation of which is discussed in the following section.

The lines $S-S$ are, as expected, not split by the magnetic field. The last few lines are, however, perceptibly broadened, especially the last strong one, $4S-19S$. The measured width at half-maximum on the microphotometer curve is 5.3 cm^{-1}, as compared to 2.4 cm^{-1} for this line with the electric field only. We have not been able to account for this broadening, but it seems to be real, and not due to field inhomogeneities, etc.

Taking into account the weakness of the lines $S-D$, which is accentuated by the fact that each is split into five components by the magnetic field, we believe that the agreement with theory is satisfactory. The intensities of the outer σ components are equal, as far as can be judged, to those of the π components, while the central σ component may very well be only $\frac{2}{3}$ as strong. It is undoubtedly somewhat enhanced because of overlapping by the outer components.

Experiments were made with the electric and magnetic fields parallel. In this case a normal triplet is predicted theoretically, as one might infer from the fact that the symmetry of the system is not changed by the addition of the electric field. No successful plates could be obtained in this case, because when the magnetic field is in this direction the electric field which could be maintained without breakdown was much lower than was possible when the magnetic and electric fields were perpendicular. In the latter case the magnetic field assists in preventing breakdown, as no continuous discharge can be maintained perpendicular to it. It would be rather interesting to modify the design of the electrodes so that the electric field would be perpendicular to the magnetic field but parallel to the direction of the light. One would then expect a pattern like that of Fig. 2(*d*) and (*e*) but with the central component absent, and with the intensities of the remaining four components equal.

Discussion

Before taking up the specific case in question we might recall briefly the theory of the production of forbidden lines by an electric field. Let us suppose that we have two levels *a* and *b* which do not combine with each other in a dipole transition, and in addition a number of levels *s* of a third type, which combine with both *a* and *b*. An electric field F produces a perturbation, and under this perturbation the eigenfunction of the state *b*, which is ψ_b^0 for the unperturbed atom, becomes

$$\psi_b = \psi_b^0 + \sum_s \frac{eFz_{bs}}{E_b - E_s}\psi_s^0, \qquad (1)$$

if the field is parallel to the z axis. The perturbation thus mixes up the *b* eigenfunction with those

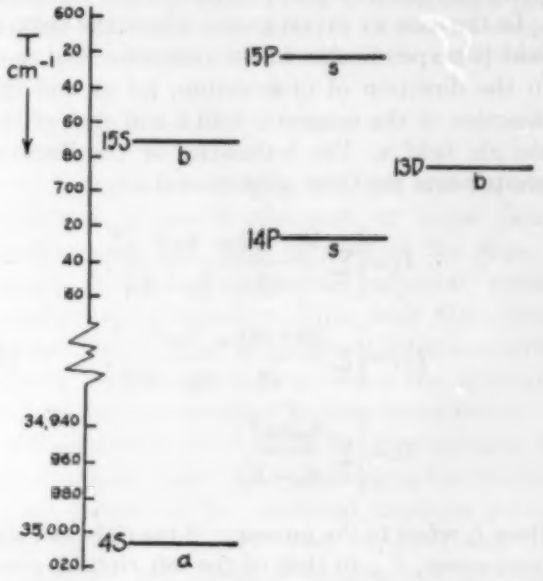

FIG. 3. Energy levels of potassium involved in the forbidden lines of Fig. 2.

of the *s* states, and since the latter combine with *a*, the transition between *a* and the perturbed *b* level also becomes allowed. As shown by Eq. (1), the perturbation is inversely proportional to the difference between the energies E_b and E_s of the *b* and *s* states. It is frequently the case that distance between the *a* and the *s* levels is so great that the perturbation of *a* may be neglected. In our present case the levels lie as shown in Fig. 3, and it is seen that the only

perturbations which count are the perturbation of the D terms by the P terms, for the $S-D$ combinations, and the perturbation of the upper S terms by the P terms, for the $S-P$ combinations. Furthermore, to a sufficient approximation, all P terms but that nearest the perturbed level may be neglected.

If now one adds a magnetic field to the electric field, the Zeeman effect may be easily calculated with certain simplifying assumptions, which are certainly valid in our case. These are that the Zeeman splitting is small compared with the distance between the terms perturbing each other, and that the relative intensities of the electric and magnetic fields are such that the electric shift of the levels is small compared with the magnetic shift. In these calculations the spin may be neglected, since for these high terms the doublet separation practically vanishes.

In the case we investigated, where the electric field is perpendicular to the magnetic field, and to the direction of observation, let us call the direction of the magnetic field z and that of the electric field x. The intensities of the Zeeman components are then proportional to

$$I_1=\left|\sum_s \frac{(x-iy)_{as}}{\sqrt{2}}\frac{x_{sb}F}{E_b-E_a}\right|^2,$$

$$I_{-1}=\left|\sum_s \frac{(x+iy)_{as}}{\sqrt{2}}\frac{x_{sb}F}{E_b-E_a}\right|^2, \qquad (2)$$

$$I_0=\left|\sum_s \frac{z_{as}x_{sb}F}{E_b-E_a}\right|^2.$$

Here I_1 refers to the intensity of the right circular component, I_{-1} to that of the left circular component, and I_0 to that of the component vibrating parallel to the magnetic field. In the y direction one observes one-half of the intensities represented by I_1 and I_{-1} as σ components (polarized perpendicular to the magnetic field) and the whole intensity represented by I_0 as π components.

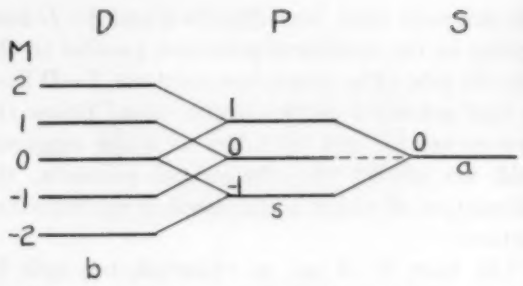

FIG. 4. Diagram showing magnetic levels for computation of intensities according to Eqs. (2).

In the application of Eqs. (2), a diagram such as Fig. 4, showing the individual magnetic levels of S, P and D, is convenient. S is the state $4S$, which combines with the states $M=\pm 1$ of P for σ polarization (solid lines in Fig. 4) and with $M=0$ for π polarization (broken line). Now since the electric field is in the x direction, only those P and D states differing by unity in M can interact (solid lines), and it follows that the S state combines with $M=2$, 0 and -2 of the D state in σ polarization, and with $M=1$ and -1 in π polarization. Thus one obtains the Zeeman type $\frac{0(1)2}{1}$, as illustrated in Fig. 2(d) and (e). For the intensities one substitutes the well-known matrix elements representing $x+iy$ and z in Eqs. (2) obtaining the values 3, 2, 3 for the σ components, and 3, 3 for the π components. It is to be noted that here the sum of the intensities of the σ components differs from that of the π components, in contrast to Zeeman types in the absence of an oriented electric field.

In conclusion, we wish to thank Professor E. O. Lawrence for his cooperation in making the large magnet available, and Dr. L. I. Schiff for valuable suggestions and assistance.

Onset Studies of Positive Point-to-Plane Corona in Air at Atmospheric Pressure

ARTHUR F. KIP
Department of Physics, University of California, Berkeley, California
(Received January 12, 1939)

Positive point-to-plane corona studies in air have been continued with special emphasis on pre-onset region. Oscillographic and photographic studies show two kinds of current pulses occurring below onset voltages. Both types of pulses can be observed by inductive effects on a plate placed near the gap and by the ion currents produced. At lowest voltages for counting action, pulses lasting for about 0.003 second are recorded on the oscillograph and are accompanied by a glow around the point as described by Trichel for steady corona. These correspond to the regular corona process continuing for several thousand bursts after which space charge modification of the field causes extreme likelihood of extinction. At voltages approaching corona onset, streamers are observed which extend far out into the gap and which can propagate only into a space-charge-free gap. The steady corona process is normally initiated by one of these streamers. The mechanism for both bursts and streamers is shown to involve space charge intensification of the field. Streamer propagation and stable burst corona both depend on photoelectric ionization in the gas. Streamer length is found to depend primarily on point size and for very fine needle points no distinction can be made between bursts and streamers. By the use of a shielding screen to cut out the electrostatic pulse produced by a streamer or a group of bursts, it was possible to determine the number of ions produced. This was found to be approximately 5×10^9 ions per cm of visible streamer, and about 2×10^9 ions in an average burst pulse. The time necessary for positive ions produced by a streamer to cross the gap was measured and found to be of the order of 10^{-4} second, and to vary with gap geometry in a way consistent with the minimum time between two consecutive streamers. Considerable photoelectric ionization was found to occur at the plate as much as 2.15 cm ahead of the visible streamers. Streamers occurring just prior to spark breakdown of the gap are associated with the pre-onset streamers. In this case the higher voltage near breakdown gives the high field necessary for streamer propagation despite space charge modification of the field by the stable corona process.

INTRODUCTION

As a result of observations by Loeb, that the positive point-to-plane corona consisted of many individual streamers, an extensive study of positive and negative point coronas has been undertaken in these laboratories. Previous papers by Kip[1] and Trichel[2, 3] in these laboratories have investigated the current-voltage characteristics of positive point corona, the nature of the negative corona, and the essential characteristics of positive point-to-plane corona. The last investigation concerned itself with what was termed the burst corona. Subsequent improvement of technique and facilities have now made it possible to investigate the appearance and nature of the streamers in the two regions in which they occur. It is the purpose of this paper to consider streamer formation and the attendant phenomena.

APPARATUS AND TECHNIQUE

The experiments were carried on in air, with gap geometry as described,[1] using hemispherically-ended wires of 0.5; 1.0; 2.0; and 4.7-mm diameters, made of platinum or brass. Steel needles were also used in some of the experiments. A 25-kv transformer supplied power through a half-wave rectifier and filter condenser. The voltage is stabilized by a saturable reactor stabilizer which provides the accurate voltage control necessary in these experiments.

Observations were made by photographs of the discharge itself and by photographed oscillograph records of the electrical impulses generated by the discharge. The impulses may be studied by two kinds of oscillograph pick-up, one the detection of the electrostatic pulse due to the appearance of charge (+ions) in the gap, and the other the detection of the ion currents collected at the plate. Fig. 1A shows the inductive method of detecting the electrostatic pulse with a metal disk placed in the vicinity of the gap. The disk is connected to the oscillograph and is shielded by a paper box to prevent the collection of ions by the disk. Fig. 1B shows the second method of pick-up where the voltage drop produced across a resistance in series with the plate is observed on the oscillograph.

[1] A. F. Kip, Phys. Rev. **54**, 139 (1938).
[2] G. W. Trichel, Phys. Rev. **54**, 1078 (1938).
[3] G. W. Trichel, Phys. Rev. **55**, 382 (1939).

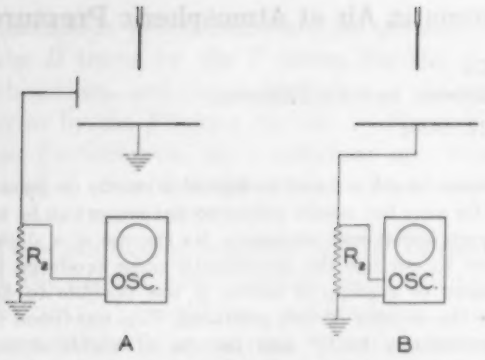

FIG. 1. A, Inductive method for detecting electrostatic pulses from corona with oscillograph. B, Method for detecting ion current and electrostatic pulses from corona with oscillograph.

Actually, this method picks up both the electrostatic signal and the ion current, but by introducing a shielding screen above the plate as shown in Fig. 2, the electrostatic signal may be cut out, so as to observe only the ion current pulse.

The oscillograph used is particularly suited to these experiments by virtue of its two stages of amplification, giving a sensitivity of 0.05 volt/inch on the screen, and by virtue of a single sweep circuit making it possible to observe and photograph separate events which would otherwise be superposed on each other on the oscillograph screen.

The radioactive source used to provide external ionization was an old radon ampule. Intensity of ionization in the region of the gap was regulated by moving the source to various distances from the gap, from a minimum of a few centimeters to over a meter away.

EXPERIMENTAL RESULTS

With the radioactive source in the vicinity of the gap, as the voltage applied to the point is gradually increased, the field in the intense field region immediately surrounding the point eventually becomes great enough for electrons falling into the positive point to multiply as they travel. That is, α, Townsend's coefficient of electron multiplication, becomes large enough for each radioactively-produced electron to produce an avalanche of electrons, the magnitude of the avalanche depending on $\int Edx$ taken over the distance x, where E, the electric field, and therefore α, which depends on E, has a value large enough to produce multiplication. The maximum size of these single avalanches at potentials below the onset of stable corona vary from 10 to 10^4 electrons for various point sizes, and are too small to detect with the limited sensitivity of the oscillograph. As the voltage is increased, with the oscillograph placed in the plate circuit as in Fig. 1B, pulses begin to appear on the oscillograph, lasting up to about 0.003

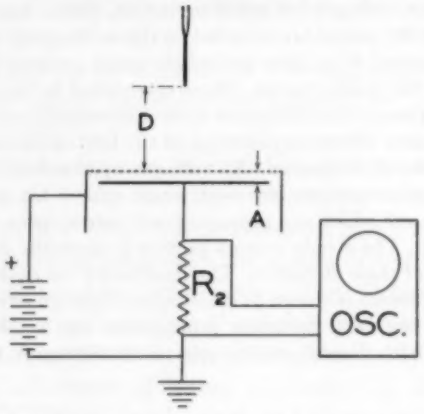

FIG. 2. Shielded plate for detecting ion current pulses with oscillograph.

second, increasing in magnitude with increasing voltage from the smallest observable on the screen up to a size such as is shown in Fig. 3. With these pulses there is associated a glow around the point exactly similar to the glow which occurs in the stable corona process above onset voltages. A photograph of such a glow caused by many groups of bursts is shown in Fig. 4A. These pulses thus correspond to the initiating of self-maintaining corona by the external ionization, but because of the limited voltage applied, after the process has continued for about 0.003 second, accumulated space charge so weakens the field around the point that the process stops. The pulses are thus composed of many ($\sim 10^3$) unresolved separate discharges, partially resolved on the oscillograph by Trichel, and termed by him *bursts*. If the shielding screen is placed above the plate, the irregularities in the pulse disappear and one gets only the smooth pulse due to the collection of positive ions whose duration corresponds to the duration of the group of bursts, as modified by diffusion.

As the voltage is further increased, in addition to the bursts, there appear intense pulses on the oscillograph such as are shown in Fig. 5, where an intense pulse and a group of bursts appear on the same picture. Associated with these large pulses are faint streamers which penetrate far out into the gap and which make an audible noise. These will be termed pre-onset streamers, and a photograph of many of these is shown in Fig. 4B.

Both individual bursts and streamers are characterized by far greater ionization than is possible in an avalanche. Thus both must depend on a mechanism involving the space charge intensification of the electrostatic field. That is, the first avalanche of electrons leaves a positive ion column out from the point with an enhanced field at its tip. Ultraviolet light produced during the electron avalanche has meanwhile produced more electrons out in the gas by photoelectric ionization and these electrons make new avalanches as they fall into the intensified axial field of the extended point. This process repeats until diffusion of the ions, possible branching, and the naturally lower fields far out in the gap cause self-propagation to stop. There is then a time of relaxation necessary before another streamer or burst can propagate from this region, this time being the time necessary to restore the original high fields. Then if negative ions or electrons are present, a new streamer or burst can occur. It is to be noted that while the time of relaxation for streamers is of the order of 0.001 second, the bursts, which require smaller fields, can occur at the rate of 10^6 per second, by spreading laterally over the point surface as shown by Trichel, due to the lower fields necessary, which allows for new bursts despite incomplete clearing of the space charge.

It is important to note that all evidence indicates that the pre-onset streamers can occur *only* into a cleared gap, that is, one in which there are no space charges. In fact it is probable that not only do streamers require a certain starting field at the point, but furthermore they cannot propagate unless the tip of the streamer finds itself in a field which exceeds some minimum value. As soon as either a pre-onset streamer or burst pulse fouls the gap with space charge, the streamers cannot form. Hence after the first streamer, the space charge prevents the development of another streamer until the gap is cleared. However, a streamer may be followed immediately by bursts, since streamer propagation is so rapid as to allow very little lateral spread of the space charge over the point surface, and therefore fields sufficient for the production of bursts initiated by photoelectrons may exist over at least part of the point surface. Thus at slightly higher voltages, the streamer

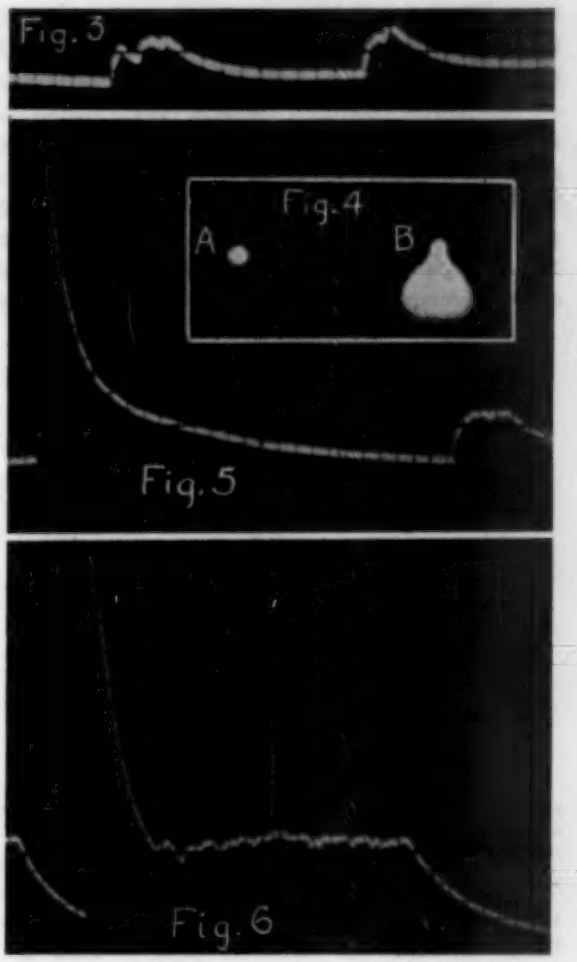

FIG. 3. Pulses of burst corona as shown on oscillograph, using pick-up method 1B. Duration of pulse is 0.003 second.

FIG. 4. A, Glow around point caused by a series of burst pulses. This is similar to the glow in stable corona. B, Picture of many pre-onset streamers. Five-minute exposure at *f*-2, with radioactive source near gap to produce streamers.

FIG. 5. Oscillogram of a streamer and a burst pulse, using pick-up method 1B.

FIG. 6. Oscillogram of streamer with plateau, using pick-up method 1B. Plateau is due to burst corona initiated by and immediately following streamer.

oscillograph may show a plateau as shown in Fig. 6. In this case the streamer is choked off as before, but in spite of the modification of the field around the point by the ions from the streamer, the field is great enough so that these ions can initiate a burst pulse or, if the voltage is high enough, the streamer will initiate stable burst corona. In fact, under most gap geometries, stable corona is always initiated by one of these streamers. An exception to this is the case of very fine needle points, which will be discussed later. These initiating streamers have previously been noted and termed a brush discharge[4, 5] but largely ignored owing primarily to the extremely narrow voltage range in which they can occur, and because they occur only as the initial stage of stable corona.

The variation of streamer length with gap geometry is shown in Fig. 7, where streamer length is plotted against the radius of curvature of the hemispherical points for 3- and 6-cm gaps.

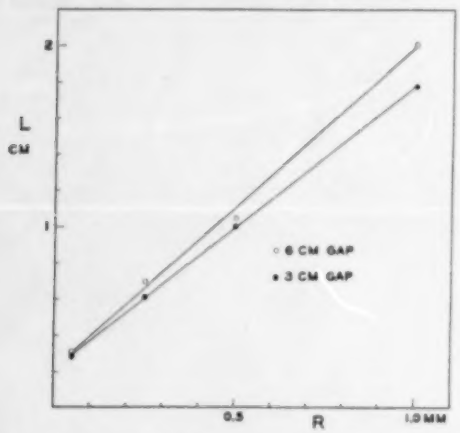

FIG. 7. Length of visible pre-onset streamers plotted against R, the radius of curvature of the point, for 3- and 6-cm gaps.

Since the streamer length depends primarily on the shape of the high field region of the gap, little variation of streamer length with gap distance is to be expected. It is seen that with large radius of curvature where the high fields extend farther into the gap, the streamers are longer.

Observations with a series of needle points of different sizes show that as the size of the point is decreased, streamers become smaller and smaller and finally there is no distinction between bursts and streamers as shown in the oscillograph pictures of Fig. 8. This is more or less to be expected, since the high field region for smaller points becomes extremely short, in which case the streamers become shorter and shorter, until no distinction can be made between bursts and streamers.

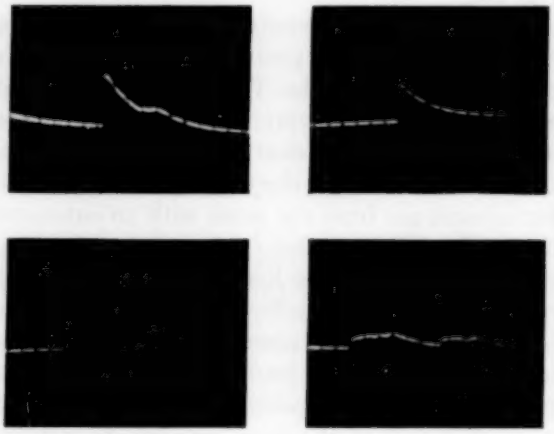

FIG. 8. Oscillogram taken by method 1B, showing decrease in size of streamer pulse with decreasing point size.

Trichel has estimated the number of ions per burst as of the order of 10^7 ions. Using the shielding screen as shown in Fig. 2, it was possible to measure the number of ions produced by either a series of bursts in a burst pulse or by a streamer. A voltage V' was put between the screen and plate such as to draw most of the positive ions through to the plate. Connecting the oscillograph across R_2 in series with the plate, the pulse obtained is caused entirely by the collection of positive ions at the plate. Knowing the sensitivity of the oscillograph, its time scale, and the value of R_2, the number of ions in the pulse can be calculated. This value must be corrected for the fraction of the ions which are collected at the screen. This is done approximately by increasing the gap voltage above onset, where the ratio of steady currents to plate and screen can be measured by a microammeter. This fractional loss to the screen is then corrected for in the calculations. The results of such measurements and calculations show that the number of ions produced is proportional to

[4] M. Toepler, Ann. d. Physik **2**, 560 (1900).
[5] J. Zeleny, Phys. Rev. **3**, 69 (1914); J. Frank. Inst. **218**, 685 (1934).

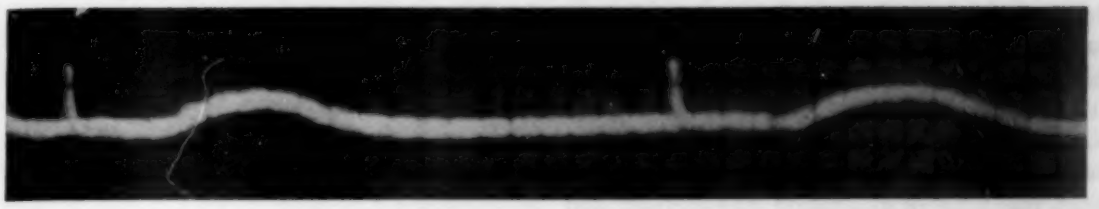

FIG. 9. Oscillogram taken by method 2, with screen moved aside to allow recording of small electrostatic pulse at time of streamer propagation, followed by ion current at plate. Pulses from two streamers are shown.

the length of the streamer, giving approximately 5×10^9 ions per cm of visible streamer. In the normal burst pulse in the same region the number of ions is about 2×10^9. Hence the fouling of the gap by a burst pulse is not very different from that in a streamer.

This last experimental arrangement may be modified to give the time the positive ions formed by the streamer take to cross the gap. Thus if the shielding screen is moved to the side so that a small part of the plate is no longer shielded from the electrostatic pulse, the oscillograph will show not only the pulse due to the ions collected at the plate, but also a small inductive kick will mark the point on the time axis when the streamer occurred. Such an oscillograph picture is shown in Fig. 9 where the time between the inductive pulse and the maximum of the ion pulse is 0.005 second. Fig. 10 shows a plot of this time interval for various points at 3- and 6-cm gap lengths. In such measurements, the distance A and voltage V' are of such magnitudes as to make the time for the positive ion travel through the distance A negligible with respect to the total time interval measured.

Observations gave evidence that sometimes streamers are repeating, that is, apparently streamers sometimes occur in groups of from two to five. This indicated that under some conditions the ionization produced by a streamer is effective in starting a new streamer after at least most of the space charge is removed from the gap. The arrangement in Fig. 2 was found to enhance this self-repetition and to make possible the verification of the mechanism. In this arrangement it is possible to vary the distance A and the voltage V' between screen and plate. Using the 2.0-mm diameter point with the gap distance D at 3.0 cm, and setting the gap voltage V to the streamer region, it was found that the application of a certain range of voltages V', depending on the distance A, would cause series of up to more than 20 streamers to occur, following each other at a nearly uniform frequency. The frequency of the streamers increased as V' was increased, up to a certain maximum frequency when the streamers cease to occur unless a radioactive source is present to start them. The frequency was investigated as a function of V' and A, where A was varied from 2.0 to 11.5 mm.

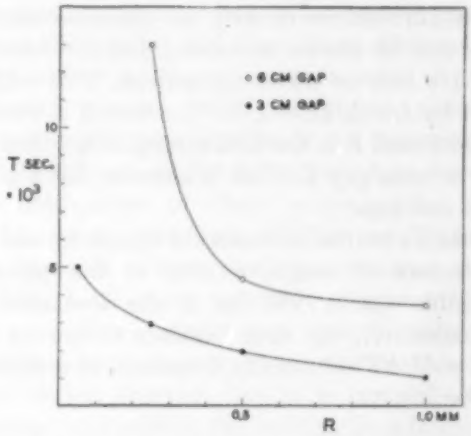

FIG. 10. Time of positive ion transit from streamer to plate vs. R, the radius of curvature of the point. Time measured from oscillograms similar to that shown in Fig. 9.

From the nature of the experimental results, the mechanism of repetition must be explained on the following basis, which necessitates photoelectric ionization at the plate by the ultraviolet light emitted by the streamer. Regardless of whether or not the screen is in place, electrons must be photoelectrically produced at the plate and must attach to O_2 molecules almost immediately, to form negative ions. There are also electrons produced in the gas, as will be shown

below, but in the region A, the number of these is apparently not appreciable as compared to those produced at the plate, and not sufficient to initiate a new streamer. If D is not too great ($\sim$3 cm), and the screen is not present the negative ions so produced are swept into the point before the time of relaxation has elapsed and therefore cannot serve to initiate a new streamer. However, with the screen in place, the values of V' and A are such as to give a lower field in region A than would exist without the screen. Under such conditions the negative ions produced at the plate travel slowly enough to allow the main gap to clear, after which the group of negative ions are able to initiate a new streamer as they fall into the point. As the field in region A is increased, the time for the negative ions to pass through A becomes less, and they reach the point sooner, causing increased frequency of streamers until finally repetition ceases when the negative ions are getting into the point before the time of relaxation has elapsed.

The correctness of such an assumed mechanism may be shown as follows. Let t_1 = time for negative ions to travel through A. This will be given by $t_1 = A/kE = A^2/kV'$, where k is the ion mobility and E is the field strength. t_2 = time for ions to cross gap D. This is constant for a given point and gap.

Then if the time between the streamers and the appearance of negative ions at the plate is negligible (as it will be if the ionization is photoelectric), the time between streamers will be $T = A^2/kV' + t_2$, or the frequency of streamers will be

$$F = \frac{1}{A^2/kV' + t_2}.$$

Figure 11 shows a plot of F *vs.* V'/A^2, where A has been varied from 2.0 to 11.5 mm, and V' from 22.5 to 585 volts. The curve drawn in represents the values of F given by the equation when t_2 is taken as 0.001 second and $k = 1.3$ cm/sec. per volt/cm. Considering the wide range of values for A and V' used, the fit is remarkably good, and leaves little doubt as to the validity of the assumed mechanism. The spread of values is most likely due to the difficulty in assigning the exact value of A in each

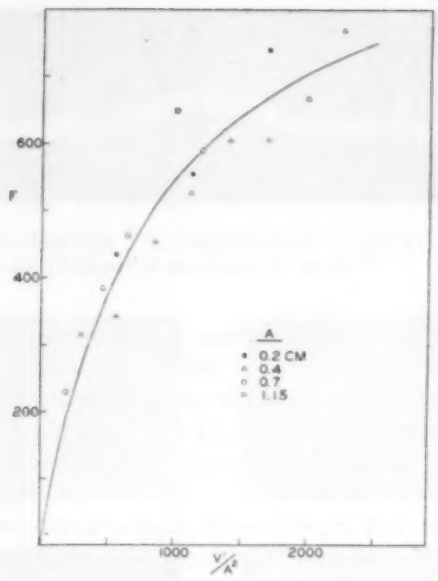

FIG. 11. Frequency of streamer repetition plotted against V'/A^2 for various values of V' and A. Curve drawn in is theoretical value, assuming k, the negative ion mobility = 1.2 cm/sec./volt/cm, and $t_1 = 0.001$ second. 3-cm gap, using 1.0-mm radius point.

case, together with the difficulty in assigning the exact frequency. It is important to note that this gives proof that photoelectric ionization occurs at the plate, in the most extreme case, 2.15 cm beyond the end of the visible streamer.

Verification of this mechanism for larger gap distances becomes increasingly difficult, because with larger gaps there is some chance of repetition without the screen present, since ions formed in the gap begin to take long enough to reach the point for the relaxation time to elapse, and also, the photo-ionization at the plate rapidly becomes weaker as the gap increases, until the process finally stops.

Proof of photo-ionization in the gas (which is hardly necessary in view of the known mechanism of streamer propagation) is obtained if, for the same point, the gap is reduced to 2.0 cm. In this case the visible streamers get completely across to the screen, but do not penetrate and one would expect heavy ionization in the gas in region A. This is shown to be the case by the fact that varying V' no longer changes the frequency of repetition, which means that repetition does not depend on ions formed at the plate, but on those formed throughout region A. However, if zero or reversed voltage is applied between

screen and plate, the ions formed do not get out into the gap and repetition ceases.

The foregoing experiments with repeating streamers provide the explanation of the action of fine needle point streamers. With fine points there is considerable evidence for repetition. Groups of 4, 5 or more streamers are often seen on the oscillograph. This can be explained by the fact that for small points the high field region is more radial and much more concentrated around the point. The field is much weaker around the gap where photo-ionization can occur than for larger points, with the result that the negative ions formed travel much more slowly towards the point, allowing the time of relaxation to pass before they all reach the point, while the streamer space charge projected towards the plate is swept out nearly as fast as before.

Still another way to obtain repeating streamers is to put a high resistance (of the order of 10^9 ohms) in series with the point. With this, when a streamer propagates, the electrons falling into the point lower the point potential instantaneously until the charge leaks through the resistance. The effect of this lowered potential is to increase the time of relaxation and also increase the time taken by the photoelectrically produced negative ions to fall into the point. The effect on this latter time is greater, so that with the series resistance the gap is effectively cleared by the time the negative ions reach the point, giving repetition of the streamers. In the early work of Toepler,[4] the same effect was produced, because the voltage was supplied by an electrostatic generator of limited capacity. Thus Toepler noted that the positive glow discharge was preceded at lower voltages by a brush discharge, which must now be interpreted as a series of repeating pre-onset streamers, brought about by the lowering of the point potential by each streamer. That this is the actual mechanism is shown by the fact that with the high resistance in the point circuit, if the electrostatic pick-up is above the gap and near the point, a negative pulse is seen, instead of the positive pulse which occurs when the pick-up is placed near the gap. This negative pulse gives proof that there is considerable actual lowering of the point potential.

An additional effect of a series resistance in the point circuit is that if the resistance is of the order of 10^8 ohms or more, the streamer length is decreased. A resistance of 2.4×10^9 ohms decreases the length of the streamers by about 25 percent. This is to be expected in view of the mechanism of virtual self-extension of the positive point by succeeding avalanches of electrons leaving behind positive ions. As each avalanche of electrons falls into the point it causes a lowering of the potential of the point, and the consequently lowered fields cause extinction of the streamer before it attains its normal length. If the streamers were not decreased in length it would indicate that streamer propagation was so rapid that there was not time for electrons to reach the point before the streamers stop propagating. This is consistent with the very rapid propagation of electrons up ionized streamer channels observed by Schonland and Collins,[6] Allibone and Meek,[7] and especially Snoddy, Dietrich and Beams.[8]

Since the photographic intensity of the streamers is weak, it has so far been impossible to get pictures of less than about 50 streamers more or less superposed on each other. A single streamer picture would be highly desirable, since it would show whether or not the streamers are forked, as might be expected in view of the mechanism of their propagation. There are, however, two lines of evidence for forked streamers. It is seen that the streamers shown in Fig. 4 all start vertically downward in a narrow column and then spread out. This spreading out indicates at least that the streamers bend rather sharply, and it is certainly more reasonable to explain the bending by a branching of the tracks. Perhaps better evidence for forked tracks comes from the cloud chamber pictures of single pre-onset streamers taken by Gorrill in this laboratory, and those of breakdown streamers (see below) of Bradley and Snoddy,[9] Raether,[10] and Nakaya and Yamasaki,[11]

[6] B. F. J. Schonland and H. Collins, Proc. Roy. Soc. **A143**, 654 (1934).
[7] T. E. Allibone and J. M. Meek, Proc. Roy. Soc. **A166**, 97 (1938).
[8] L. B. Snoddy, J. R. Dietrich and J. W. Beams, Phys. Rev. **52**, 739 (1937).
[9] C. D. Bradley and L. B. Snoddy, Phys. Rev. **47**, 541 (1935).
[10] H. Raether, Zeits. f. Physik **94**, 567 (1935).
[11] U. Nakaya and F. Yamasaki, Proc. Roy. Soc. **148**, 446 (1935).

which show considerable branching, both near their beginning, as suggested by Fig. 4, and also near the end of the track, where 4 or 5 branches may occur. The failure to observe branches visually in such streamers is doubtless because of their feeble intensity.

As has been stated earlier, the pre-onset streamers can occur only in a cleared gap, and therefore cease as soon as stable burst corona sets in. However, at voltages approaching values near those for spark breakdown of the gap, streamers similar in appearance to the pre-onset streamers may appear. In this case the voltage has been so much increased that in spite of the space charge modification of the intense field region of the gap by the stable burst corona process, fields are great enough to allow streamer propagation. For a 0.5-mm diameter point, with a 6-cm gap, pre-onset streamers occur at 5.4 kv. Breakdown streamers appear above 40 kv. These streamers are unaffected by external ionization provided by a radioactive source, since the stable corona provides a continuous source of ionization. The minimum length of these breakdown streamers depends on gap geometry as in the case of the pre-onset streamers, but for a given size of point, the breakdown streamers are much longer than the pre-onset streamers. Thus for a needle point with 0.05-mm radius of curvature the minimum length of the breakdown streamers is approximately twice that of the pre-onset streamers. The length of the breakdown streamers is found to be decreased by a high series resistance, as was the case for onset streamers, presumably for the same reason, as explained above.

In contrast to the pre-onset streamers, whose occurrence is limited to a narrow voltage range, breakdown streamers persist from the voltage at which they begin up to spark breakdown. Under some gap geometries this range may be quite large, and may allow the measurement of the length of streamers as a function of applied voltage. A typical case was studied using the 0.05-mm needle point with a 6-cm gap distance, and eventually spark breakdown occurs. With larger points, the minimum length may be equal to the gap distance and breakdown may occur at once upon the appearance of the breakdown streamers. These streamers are the primary mechanism of spark breakdown in all cases. As soon as the streamers reach the plate cathode with enough intensity to form a cathode spot giving a copious supply of electrons, the discharge becomes unstable, a return stroke occurs, and spark breakdown ensues.

The similarity of pre-onset and breakdown streamers can be shown by the phenomena occurring near the corona point distance, that is, the gap below which spark breakdown occurs without the appearance of stable corona. The variation of this distance as a function of point size was investigated and given previously.[1] At the time these experiments were carried out, it was found that under certain conditions, stable corona could be maintained with gaps less than the corona point distance; namely, if enough resistance was placed in the gap circuit so that spark breakdown would be extinguished by the *IR* drop in the resistance, it often happened that after a spark, stable corona would occur and would continue through a considerable voltage range before breakdown again occurred. Present knowledge of the pre-onset streamers makes this easily understood. At less than the corona point distance, the pre-onset streamers reach completely across the gap with such intensity as to insure the production of a cathode spot and consequent spark breakdown. Since these streamers are the inevitable precursors of stable corona, spark breakdown necessarily takes place. However, if the spark is choked off by a series resistance, the ions in the gap prevent immediate repetition of another streamer, and at the same time allow for the initating of stable corona. Thus both types of streamers are found to produce spark breakdown in the same way, and the short gap phenomena are completely explained.

In conclusion, the author wishes to express his gratitude to Professor Loeb for his hearty support and guidance and valuable assistance in interpretation during the carrying out of these researches.

A Self-Consistent Field for Doubly Ionized Chromium*

ROBERT L. MOONEY†
Department of Physics, Brown University, Providence, Rhode Island

(Received December 10, 1938)

A self-consistent field without exchange has been calculated for doubly ionized chromium in the configuration $(3p)^6$ $(3d)^4$. All integrations were carried out numerically with the aid of a calculating machine. The difference between the final and semi-final approximations to $Z_{n,l}$ is nowhere greater than ± 0.003.

A GLANCE at the periodic table of the elements will show that chromium occurs in the middle of the transition group from scandium to nickel. In the elements of this group the $3d$ sub-shells are not full in the sense of the Pauli exclusion principle. Classically considered this feature may be regarded as due to the fact that the attractive force exerted on a $3d$ electron by the field of the rest of the atom is not sufficiently large to balance or overcome the centrifugal force due to the orbital angular velocity of the electron—with the result that the electron finds a stable position of dynamic equilibrium in the $4s$ shell. It is to be expected that the self-consistent field for chromium will exhibit strongly the kind of "over-stability" in the $3d$ sub-shell that was found by Hartree.[1]

The method of the self-consistent field is so well-known that a detailed description is unnecessary here. It is assumed that the ion is described by a simple product function of one-electron functions of the form $[P_{n,l}(r)/r]\cdot S(\theta, \phi)$. The differential equation satisfied by $P_{n,l}$ is

$$\frac{d^2P_{n,l}}{dr^2}+\left[\frac{2(Z_p)^{(n,l)}}{r}-\epsilon_{n,l}-\frac{l(l+1)}{r^2}\right]P_{n,l}=0. \quad (1)$$

When the wave functions satisfying the appropriate boundary conditions are known, the field due to a particular sub-group (n, l) with $N_{n,l}$ electrons is given by $Z_{n,l}/r^2$, where

$$Z_{n,l}=N_{n,l}\int_r^\infty P^2_{n,l}dr \Big/ \int_0^\infty P^2_{n,l}dr. \quad (2)$$

$(Z_p)^{(n,l)}$ occurring in (1) is defined by

$$(Z_p)^{(n,l)}=C+1+\sum_{n,l} Z_{p_{n,l}}-\frac{1}{N_{n,l}}\cdot Z_{p_{n,l}}, \quad (3)$$

where C is the number of electrons removed from the neutral atom to produce the ion. $Z_{p_{n,l}}$ is obtained by integrating

$$\frac{dZ_{p_{n,l}}}{dr}=\frac{Z_{n,l}-Z_{p_{n,l}}}{r}. \quad (4)$$

Slater[2] has shown that good approximations to the correct radial wave functions can be obtained by an interpolation method utilizing analytic approximations to wave functions already calculated for other atomic systems. This fact suggests that a crude initial field may be obtained by direct interpolation in the case of Cr III between tabulated values of the contributions to $Z_{n,l}$ already determined for Cl^-,[1] K^+,[3] Ca^{++},[4] Cu^+,[1] and Rb^+.[5] This interpolation was done graphically. For a given value of the radius, values of $Z_{n,l}$ as ordinates were plotted as functions of the atomic numbers of the corresponding atoms. The ordinate of the intersection of the curve drawn through the five points (corresponding to the five ions used for the interpolation) with the ordinate erected at the number corresponding to the atomic number of chromium was taken as the trial value of $Z_{n,l}$ for Cr III for that particular value of the radius and sub-shell considered. Subsequent calculations showed that this method is empirically justified for the K and L shells but is unsatisfactory for the M

* Part of a dissertation presented to the faculty of the Graduate School of Brown University in candidacy for the degree of Doctor of Philosophy.
† Now at Georgetown University, Washington, D. C.
[1] D. R. Hartree, Proc. Roy. Soc. **A141**, 281 (1933).
[2] J. C. Slater, Phys. Rev. **32**, 339 (1928).
[3] D. R. Hartree, Proc. Roy. Soc. **143**, 506 (1934).
[4] D. R. Hartree and W. Hartree, Proc. Roy. Soc. **A149**, 210 (1935).
[5] D. R. Hartree, Proc. Camb. Phil. Soc. **24**, 111 (1927).

shell, primarily because of the double ionization of Cr III in contrast with the lower degree of ionization of the ions compared (Ca^{++} excepted). A table of approximate values of $Z_{n,l}$ as calculated by A. Porter[6] was used as a first estimate for the M electrons. (Porter's results are admittedly inaccurate because of the methods he used to determine the energy parameters and the fact that the initial distributions of the core electrons from the $(1s)^2$ to $(2p)^6$ were left unchanged in all subsequent approximations.) In order to integrate (1) it is necessary to choose a trial value of $\epsilon_{n,l}$. Very good approximations to the correct energy parameters are furnished by x-ray data in the cases of the K and L electrons. Linear interpolation between the results for Cu^+ and Ca^{++} yield values of $\epsilon_{n,l}$ satisfactory as first trial values for the M electrons.

Introducing the variable $\eta_{n,l}=-P'_{n,l}/P_{n,l}$, we can write (1) as

$$\eta'_{n,l}=\eta^2_{n,l}-\epsilon_{n,l}-\frac{l(l+1)}{r^2}+\frac{2(Z_p)^{(n,l)}}{r}. \quad (5)$$

It is convenient to integrate (5) inwards from $r=\infty$ to the value of the radius at which the last maximum of $P''_{n,l}$ counted outwards from $r=0$ occurs. At such a point $\eta_{n,l}$ can be compared with $-P'_{n,l}/P_{n,l}$ obtained from the outward integration of (1). The correct value of $\epsilon_{n,l}$ will give a smooth join. When the point of join is selected as above, it turns out that curves for

[6] A. Porter, Mem. Manchester Phil. Soc. **79** (1935).

TABLE I. *Tabulation of the calculated values of* $Z_{n,l}$.

r	$(1s)^2$	$(2s)^2$	$(2p)^6$	$(3s)^2$	$(3p)^6$	$(3d)^4$	r	$(1s)^2$	$(2s)^2$	$(2p)^6$	$(3s)^2$	$(3p)^6$	$(3d)^4$
0.000	2.000	2.000	6.000	2.000	6.000	4.000	.76		.006	.016	1.347[5]	4.231	3.181
.005	1.996	2.000	6.000	2.000	6.000	4.000	.80		.004	.010	1.240[5]	3.954	3.077
.010	1.975	1.998	6.000	2.000	6.000	4.000	.84		.002	.006	1.133	3.673	2.973
.015	1.929	1.994	6.000	1.999	6.000	4.000	.88		.001	.004	1.028	3.394	2.867
.020	1.859	1.988	6.000	1.998	6.000	4.000	.92		.001	.002	.927	3.120[5]	2.762
.025	1.767	1.981	5.999	1.997	6.000	4.000	.96		.000[5]	.001	.831	2.856	2.658
.030	1.660	1.973	5.997	1.996	6.000	4.000	1.00			.001	.741	2.604	2.554
.035	1.540	1.964	5.995	1.995	6.000	4.000	1.04			.000[5]	.657	2.364	2.452
.040	1.415	1.956	5.991	1.994	6.000	4.000	1.08				.580[5]	2.139	2.352
.045	1.288	1.948	5.984	1.993	6.000	4.000	1.12				.510[5]	1.929	2.254
.050	1.165	1.941	5.976	1.992	5.997	4.000	1.16				.447	1.734	2.158
							1.20				.390	1.554	2.065
.06	.928	1.931	5.950	1.990	5.994	4.000	1.24				.339[5]	1.391	1.974
.07	.723	1.925	5.910	1.990	5.988[5]	4.000	1.28				.294	1.234	1.886
.08	.552	1.923	5.852	1.989[5]	5.981	4.000	1.32				.256	1.115	1.801
.09	.415	1.923	5.776	1.989[5]	5.972	4.000	1.36				.221	.993	1.718
.10	.308	1.922	5.680	1.989	5.960	4.000	1.40				.191	.882	1.639
.11	.225	1.919	5.564	1.989	5.947	4.000	1.44				.164	.782	1.561
.12	.163	1.912	5.430	1.987	5.931	4.000	1.5				.130	.652	1.453
.13	.117[5]	1.898	5.277	1.985	5.914	4.000	1.6				.088	.478	1.283
.14	.084	1.878	5.109	1.982	5.896	3.999	1.7				.059	.348[5]	1.130
.15	.059	1.850	4.928	1.978	5.876	3.999	1.8				.040	.251	.992
.16	.042	1.815	4.735	1.972[5]	5.857	3.998	1.9				.027	.179	.869
							2.0				.018	.128	.760
.18	.020	1.723	4.324	1.960	5.818	3.997	2.1				.011	.091	.663
.20	.010	1.607	3.896	1.945	5.782	3.995	2.2				.008	.064	.577
.22	.005	1.473	3.467	1.929	5.750	3.992	2.3				.005	.045[5]	.501
.24	.001	1.329	3.052	1.915	5.725	3.988	2.4				.003	.032	.423
.26	.000[5]	1.182	2.658	1.902	5.707	3.982							
.28		1.038	2.294	1.892	5.695	3.975	2.6				.001	.016	.322
.30		.897	1.964	1.885	5.688	3.966	2.8					.008	.229
.32		.773	1.667	1.880	5.685	3.955	3.0					.004	.175
							3.2					.002	.123
.36		.554	1.179	1.877	5.684[5]	3.927	3.4						.085
.40		.384	.814	1.877	5.677[5]	3.889	3.6						.060
.44		.262	.552	1.872	5.650	3.842	3.8						.042
.48		.167	.368	1.857	5.592[5]	3.785	4.0						.030
.52		.110	.241	1.827	5.498	3.719							
.56		.072	.157	1.780	5.364	3.644	4.4						.015
.60		.044	.100	1.717[5]	5.193	3.562	4.8						.007
.64		.028	.064	1.640	4.988	3.473	5.2						.004
.68		.017	.040	1.550	4.755	3.380	5.6						.002
.72		.010	.025	1.452	4.501	3.282	6.0						.001

which values of $\eta_{n,l}$ and $-P'_{n,l}/P_{n,l}$ at the point of join are plotted as functions of $\epsilon_{n,l}$ closely approximate straight lines over a surprisingly large range of values of $\epsilon_{n,l}$ as long as $Z_{n,l}$ is left unchanged. The solution of (1) is completed by integrating

$$\log_e P_{n,l}\Big]_{r_1}^{\infty} = -\int_{r_1}^{\infty} \eta_{n,l}\, dr, \qquad (6)$$

where r_1 is the value of the radius at which the join is made.

In integrating (4) and in normalizing $P_{n,l}$, a method of mechanical quadrature based upon the interpolation formulae of Stirling and Bessel and perfected by Milne[7] proved to be quite satisfactory. Eq. (5) is best solved by the Runge-Kutta method,[7] which has an inherent error smaller than that characteristic of Milne's method. A modification of Milne's method for first-order equations can be applied to second-order equations in which the first derivative is absent.[8] The formulae used in both the Milne method and the Runge-Kutta method involved ordinates instead of differences. If at most only two figures are involved in taking differences, it is perhaps advisable to use difference methods, as has been done by Hartree. Even though the calculations at each step in going from one interval to the next in the ordinate methods are more complicated than in the difference methods, whenever a calculating machine is available, it seems strongly advisable to use ordinates. A larger number of significant figures can usually be carried throughout the entire integration using ordinates instead of differences.

Tabulated values of $Z_{n,l}$ were used as bases for further approximations. A strict iterative process does not in every case lead to the fastest rate of convergence to self-consistency; and, indeed, in the case of the 3*d* electrons such a process actually led to a divergence from a self-consistent distribution. In the present calculations the following facts were empirically determined. It was found that the actually calculated values of $Z_{n,l}$ offered the best estimates for a new approximation for the (1*s*),

[7] J. B. Scarborough, *Numerical Mathematical Analysis* (Johns Hopkins Press, Baltimore, 1930).
[8] Bull. Nat. Research Council, No. 92 (1935).

TABLE II. *Values of the unnormalized wave functions $P_{n,l}$. Values of the normalization constants appear at the bottom of the table.*

r	$(1s)^2$	$(2s)^2$	$(2p)^6$	$(3s)^2$	$(3p)^6$	$(3d)^4$
0.000	0.000	0.000	0.000	0.000	0.000	0.000
.005	.443	.442[5]	.023[5]			
.010	.786	.781	.089	.781	.049	.001
.015	1.046	1.031	.188	1.030	.188	.003
.020	1.237[5]	1.204	.316	1.201	.315	.007
.025	1.373	1.312	.465	1.306	.465	.013
.030	1.463	1.364	.633	1.354[5]	.631	.021
.035	1.516	1.370	.813[5]	1.355	.810	.033
.040	1.539	1.336	1.004	1.316	.999	.047
.045	1.538	1.269	1.201	1.243	1.193	.065
.050	1.518	1.175	1.402	1.142	1.390	.086
.06	1.439	.925	1.806	.877	1.783	.138
.07	1.327	.620	2.203	.556	2.162	.204
.08	1.199	.284	2.580	.205	2.515	.285
.09	1.067	−0.064	2.931	−0.155	2.835	.379
.10	.938	−0.410	3.250	−0.509	3.115[5]	.487
.11	.817	−0.745	3.536	−0.847	3.353	.607
.12	.706	−1.060	3.787	−1.160	3.552	.739
.13	.606	−1.352	4.002	−1.443	3.702	.882
.14	.517	−1.617	4.183	−1.692	3.807	1.036
.15	.439	−1.854	4.330	−1.905	3.870	1.198
.16	.372	−2.063	4.446	−2.081	3.891	1.369
.18	.263	−2.396	4.501	−2.325	3.821	1.733
.20	.184	−2.626	4.637	−2.432	3.617	2.119
.22	.127	−2.765	4.600	−2.417	3.300	2.522[5]
.24	.086	−2.828	4.501	−2.297	2.892	2.937
.26	.057	−2.829	4.351	−2.090	2.412	3.357
.28	.036	−2.780	4.165	−1.813	1.878	3.778
.30	.020	−2.693[5]	3.954	−1.483	1.306	4.197
.32	.007[5]	−2.579[5]	3.726	−1.113	.711	4.609[5]
.36	.000	−2.300[5]	3.251	−0.306	−0.506	5.403
.40		−1.993	2.781	0.528	−1.697	6.141
.44		−1.689	2.343	1.329	−2.810	6.809
.48		−1.407	1.949	2.061	−3.811	7.402
.52		−1.155	1.604	2.701	−4.684	7.915
.56		−0.938	1.309	3.240	−5.421	8.351
.60		−0.755	1.060[5]	3.675	−6.024	8.713[5]
.64		−0.600	0.854	4.011	−6.498[5]	9.007
.68		−0.478	.684	4.255	−6.855	9.237
.72		−0.377	.545	4.417	−7.105	9.411
.76		−0.296	.433	4.507[5]	−7.262	9.536
.80		−0.231	.343	4.536	−7.337	9.617
.84		−0.180	.270	4.514	−7.342	9.660
.88		−0.139	.213	4.449	−7.290	9.671
.92		−0.108	.167	4.350	−7.189	9.654
.96		−0.084	.131	4.225	−7.049	9.613
1.00		−0.064	.103	4.079	−6.877	9.553
1.04		−0.050	.080	3.919	−6.681	9.475
1.08		−0.038	.063	3.748	−6.466	9.383
1.12		−0.029	.049	3.571	−6.237	9.279[5]
1.16			.038	3.391	−5.999	9.166
1.20				3.211	−5.755	9.044
1.24				3.029	−5.481	8.915
1.28				2.852	−5.228	8.780
1.32				2.680	−4.981	8.641
1.36				2.513	−4.740	8.498
1.40				2.352	−4.512	8.351[5]
1.44				2.198	−4.264	8.203
1.50				1.970	−3.871[5]	7.977
1.60				1.645	−3.414[5]	7.594
1.70				1.363[5]	−2.922	7.210
1.90				.922	−2.156	6.451
2.0				.733	−1.789	6.081[5]
2.1				.613	−1.563	5.722
2.2				.497	−1.321	5.373
2.3				.403	−1.117[5]	5.036
2.4				.325	−0.943	4.744
2.6				.210	−0.636	4.103
2.8				.135	−0.443	3.554
3.0				.108	−0.309	3.059
3.2				.084	−0.258	2.625
3.4					−0.214	2.232
3.6					−0.178	1.897
3.8					−0.148	1.600
4.0					−0.122	1.340
4.4					−0.083	.932[5]
4.8						.645
5.2						.441
5.6						.299
6.0						.201
$\int_0^\infty P^2_{n,l}\,dr$	0.1871	2.1877	5.9898	15.3101	46.095	142.115

$(2s)$, and $(2p)$ groups. For the $(3s)$ and $(3p)$ groups best rates of convergence were obtained by adding to the results of the preceding approximation two-thirds of the difference between the results of the preceding and immediate approximations to obtain an estimated table for the immediately following calculations. In the case of the $(3d)$ electrons, only one-half the difference between successive approximations was added in the above manner to obtain the best results.

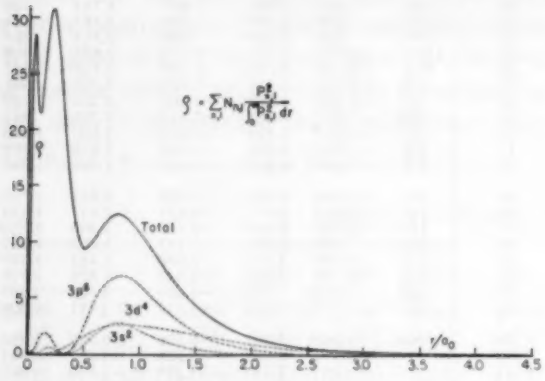

FIG. 1. Radial charge distributions for individual sub-shells and total charge distribution.

In all, three approximations were made for the $(1s)$, $(2s)$ and $(2p)$ sub-groups, and seven for the outer electrons; the distributions of the inner groups were left unchanged from the results of the third approximation for those sub-shells.

RESULTS

Table I gives a complete tabulation of the finally calculated values of $Z_{n,l}$. Nowhere does the difference between the calculated results and the results of the immediately preceding approximation differ by more than ± 0.003. A tabulation of the unnormalized wave functions, $P_{n,l}$, is given in Table II with the normalization constants given below the table. $P_{n,l}$ was calculated throughout to at least five significant figures, and it is probable that the values of $P_{n,l}$ are everywhere correct to at least two units in the third decimal place. The energy parameters (in atomic units) which characterize the self-consistent field are given in Table III. The radial charge distributions for the individual sub-shells (from $(3s)$ to $(3d)$) are plotted along with the total radial charge distribution (the full-line curve) in Fig. 1. A greater accuracy than is customary in self-consistent field calculations has been aimed at here, since, as has been pointed out by Hartree[9] the exchange corrections can be rather accurately estimated from accurate solutions of the self-consistent field without exchange with the aid of Fock's equations.

TABLE III. *Energy parameters in atomic units which characterize the self-consistent field.*

$\epsilon_{n,l}$	442.11	50.845	44.242	6.972	4.946[a]	1.797
x-ray	441.1		42.6			

The author wishes to thank Professor R. B. Lindsay for proposing this problem and Dr. A. O. Williams of the University of Maine for his suggestions on numerical integration methods. Part of this work was made possible by a stipend from Brown University.

[9] D. R. Hartree and W. Hartree, Proc. Roy. Soc. **A157**, 490 (1936).

High Pressure Arcs in Common Gases in Free Convection

C. G. SUITS
General Electric Company, Schenectady, New York

(Received January 30, 1939)

An oscillographic method is described for measuring the electric gradient E (volts cm^{-1}), current density I (amp. cm^{-2}), total voltage e (volts) as a function of current i in the discharge. The method is applied to arcs in the 0–10-ampere range under conditions of free convection in N_2, A, and He in the 1–50-atmosphere pressure range, and to air, CO_2, and steam at atmospheric pressure. The exponent n and B in $E=Bi^{-n}$ are determined for these cases. The range of n is $0.54<n<0.73$, and some dependence on pressure is observed. The exponent m in $E=B_0p^m$ is measured for N_2, H_2, He, and A, and is found to be 0.31, 0.32, 0.20, and 0.16, respectively, with some dependence on current. The method is applied to arcs between electrodes of a number of common metals in air.

INTRODUCTION

THERE exists nowhere in the literature a comprehensive set of measurements of the important electrical quantities in the positive column of the arc in common gases. This information must be reckoned as fundamental to the understanding of the mechanism and to the development of the theory. For the purpose of this study we consider the following measurables: E—electric gradient (volts cm^{-1}); I—current density (amp. cm^{-2}); i—arc current (amp.); in the region of the positive column as described below. By the method of measurement the total arc voltage e is also recorded, but since e is determined partly by electrode properties and phenomena, it is of secondary importance for the present purpose.

EXPERIMENTAL METHOD

Previous measurements of arcs at atmospheric and higher pressure[1] have indicated that the pressure range up to 100 atmospheres was sufficiently great to develop prominent changes in the electrical constants of the arc and that in this pressure range some new measurement methods would have to be developed, especially for E. In an arc in N_2 (at one atmosphere, 10 amperes, and 10 mm), $e=73$ volts, while E is only 21 volts cm^{-1}. Thus the 7-mm portion of this arc which represents the positive column accounts for only 20 percent of the total arc voltage. In view of the fact that the spread in e under the best measurement conditions is 10 percent, the difficulty of determining E as a difference in arc voltage for a change in arc length is apparent.

A very satisfactory solution of this problem was found in a vibrating electrode. It is the change of voltage Δe resulting from a change in arc length Δl at constant current from which the gradient E is calculated, as $E=\Delta e/\Delta l$. Comprehensive experiments were undertaken to discover how rapidly the change in arc length can take place without altering Δe. It was found that for arc lengths in the 10-mm range and for Δl of one- or two-mm Δe is independent of the frequency at which the arc length is changed for frequencies at least as high as 30 per second. More recent measurements under a variety of experimental conditions confirm this conclusion. The interpretation of this experimental fact is that the steady state in the thermal and electrical process is established in a time short compared to the period of the vibrating electrode. This equilibrium time, or thermal time constant, is known from numerous experiments[2,3] and is approximately 0.001 second in arcs in air at atmospheric pressure.

Measurement of gradient by means of the vibrating electrode is accomplished as follows. The vibrating mechanism is driven by a synchronous motor at 30 vibrations per second. The resulting 30-cycle component of voltage is selected by a 30-cycle band-pass filter and amplifier system and applied to a galvanometer of the oscillograph. This filter has a time constant of about one cycle at 30 cycles, so that its response to gradient changes is very rapid.

[1] C. G. Suits, J. App. Phys. **10**, 203 (1939).

[2] C. G. Suits, Gen. Elec. Rev. **39**, 194 (1936).

[3] H. Witte, Zeits. f. Physik **88**, 415 (1934).

The procedure of selecting only the 30-cycle component in the arc voltage permits a great improvement in the accuracy of measuring E, since it suppresses much of the random variation in arc voltage.

Very little appears in the literature on the causes of the random voltage variations (r.v.v.) which characterize the high current, high pressure arc with nonthermionic cathodes. It is known that in air at a pressure of one atmosphere (1) the arc voltage at constant current shows a random variation around a mean value for all electrode materials at some values of current and electrode diameter; (2) the r.v.v. is entirely absent in the 1–10-ampere range if electrode dimensions are so chosen that the cathode becomes incandescent for pure carbon, cored carbon, tungsten, and possibly some other electrode materials in air, nitrogen, hydrogen, argon, helium, and mercury; (3) the r.v.v. is absent in mercury vapor in the 1–30-atmosphere range for oxide-coated cathodes in the 0.5-ampere range; and (4) of the nonthermionic metallic electrodes, the r.v.v. is a minimum with polished copper.

TABLE I. *Arc gradient E as function of length l.*

E (v cm^{-1})	125	71	60	54	53	53	53
l (mm)	0	1	2	3	4	6	8

As a result of investigation, pure carbon electrodes were chosen as the best from the standpoint of r.v.v. in the subsequent experiments in the 50-atmosphere pressure range. It was found necessary to adjust the electrode diameter from 1.5 mm at one atmosphere to 6 mm at 30 atmospheres for best results in nitrogen. Above 30 atmospheres no electrode condition was found which would eliminate r.v.v. in the 10-ampere current range. Precise measurements of arc electrical properties, therefore, do not extend much above this pressure. By the vibrating electrode method which has been described, and by the use of pure carbon electrodes of a size adjusted to the pressure range, the measurement of E can be carried out to a satisfactory degree of accuracy.

It appears that the only high pressure arcs free from r.v.v. are those which have stable thermionic cathode emission capable of accommodating the cathode current densities imposed by gas pressure, and that above 30 atmospheres (in N_2) there is no thermionic cathode material which can provide sufficient emission in the 10-ampere range.

There remains the question of the dependence of gradient on arc length. This is shown by the data of Table I, which were taken for an arc in air with a maximum amplitude in electrode vibration of 4.6 mm. The gradient of 125 v/cm at zero arc length means that this is the total voltage change divided by 0.46 cm when the vibrating electrode just failed to short-circuit the arc. In this region the apparent gradient would be higher if the amplitude of vibration were smaller. The characteristic feature shown by Table I, however, is that in air (and in most common gases) the gradient is constant when the arc length exceeds approximately 3 mm. Observations of the diameter also show that the arc column assumes a constant maximum cross section when the length is greater than 3 mm. This region of constant diameter, constant gradient is analogous to the positive column in a

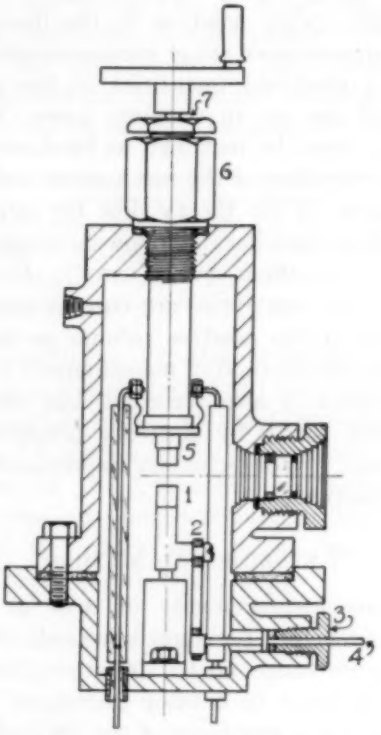

FIG. 1. Arc chamber with vibrating electrode.

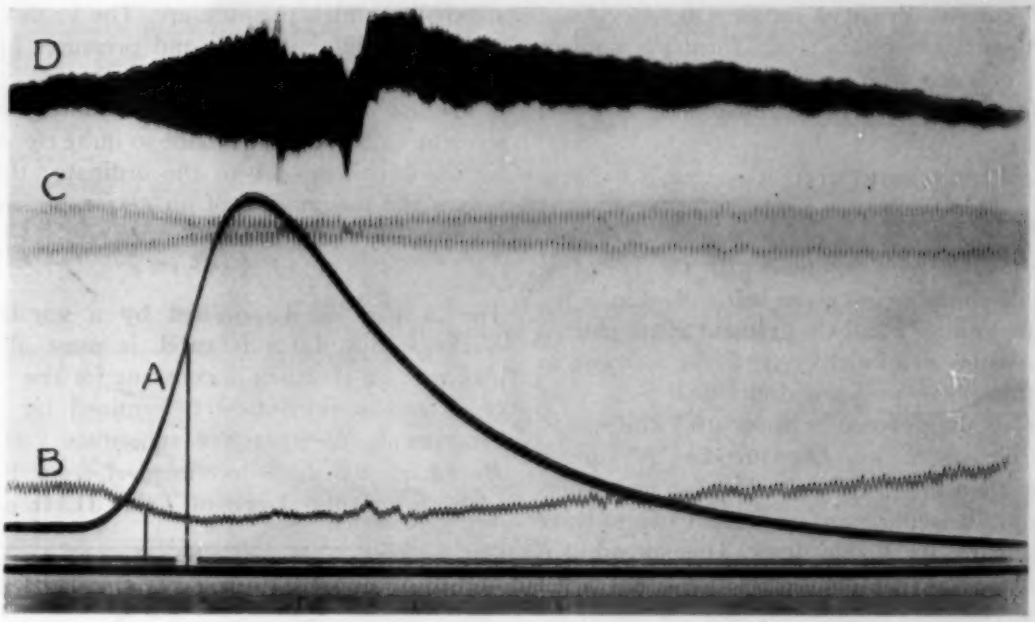

FIG. 2. Oscillographic record of an arc in nitrogen at one atmosphere pressure in the vibrating electrode chamber. A, arc current. B, total arc voltage. C, gradient in positive column. D, diameter (proportional to width of trace) of the arc column midway between electrodes.

low pressure discharge, and for convenience will be referred to as the positive column here. The measurements reported below were made at a mean arc length of 10 mm in all gases, and they are therefore properly interpreted as the gradient in the positive column of the high pressure arc in the above sense.

The diameter of the arc column is the next important quantity in the high pressure arc. In the present experiment it is measured photographically by forming an image of the arc on the film with a lens mounted on the oscillograph. This image is taken through a slit system which selects a section through the arc perpendicular to the axis and midway between the electrodes. To minimize photographic errors the exposure is adjusted at the maximum current to give a density of approximately one on the film with a set of neutral density filters and by adjustment of lens aperture. Errors due to a *variation* of exposure within a given record are discussed below.

The method therefore measures on a single record the arc voltage e, gradient E, and oscillographic diameter D as a function of current and yields the approximate luminosity.

An arc chamber with a vibrating electrode is shown in Fig. 1. Two observation windows are provided, and the strength of structure is sufficient for use up to 200 atmospheres pressure. The lower electrode, 1, can be vibrated through a total amplitude adjustable from zero to 5 mm by means of an arm, 2, and eccentric operated through the bushing, 3, by shaft, 4. The upper electrode, 5, is adjustable vertically through a range of 20 mm by a worm and pin arrangement, which can be operated externally at the highest pressures by rotating the shaft, 7, in the bushing, 6. Starting the arc is accomplished by bringing the electrodes in contact. This design of chamber has been very satisfactory for this pressure range.

An oscillographic record of the arc in nitrogen at a pressure of one atmosphere in the vibrating electrode chamber is shown in Fig. 2. Trace A is the arc current, B the total arc voltage, C the gradient in the positive column, and D the diameter (proportional to the width of the trace) of the arc column at a point midway between the electrodes. Thus a single oscillogram records the chief electrical measurables as a function of current for a given experimental condition.

The current density, lumen efficiency, and brightness data of this study form the subject matter of a separate paper. We now proceed to consider the gradient measurements.

Experimental Results

E and *e* for nitrogen

The chief results obtained with the vibrating electrode chamber are given below. In Fig. 3 the total arc voltage e and the gradient E are plotted for the same set of eight records for nitrogen at one atmosphere pressure. Individual points are shown for the purpose of illustrating the spread in the measurements. The spread in E is much greater than in e, although the absolute deflections on the oscillograms were from two to three times greater for E than for e. This spread in E must, therefore, represent a real variation in the gradient, possibly because the mid-portion of the arc column is most sensitive to convection forces. Within the spread of the measurements the log E − log i relationship is linear; hence

$$E=Bi^{-n}, \tag{1}$$

where $B=84$, $n=0.6$, for nitrogen at p=one atmosphere.

In fact the gradient data for all of the gases studied (with the possible exception of air), over the entire pressure range at which accurate measurements can be made, fit an equation of the form (1), which can therefore be regarded as a general equation for the gradient of the steady-state high pressure arc. The values of B and n for different gases and pressures appear below.

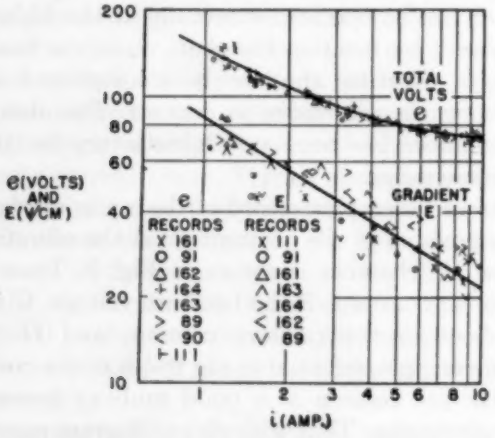

Fig. 3. Total arc voltage e(volts) and electric gradient E(v/cm) for an arc between pure carbon electrodes in N_2 at one atmosphere (arc length one cm).

The log e − log i relation is definitely not a straight line, but can be made so quite closely by adding a constant A to the ordinate; this involves the assumption of an $e-i$ expression of the form

$$e=A+B/i^n. \tag{2}$$

The A can be determined by a number of methods, but if (2) is valid, it must allow a choice of an A which is constant for the values of B and n previously determined by direct experiment. We therefore substitute values of $B=84$, $n=0.6$, and determine A from Fig. 3, with the results shown in Table II. It can be seen that for currents in the 2–10-ampere range A is constant within ±4 percent. We conclude that

$$e=51+84/i^{0.6}$$

is a satisfactory approximate expression for the total arc voltage of the one atmosphere nitrogen arc of length 1 cm.

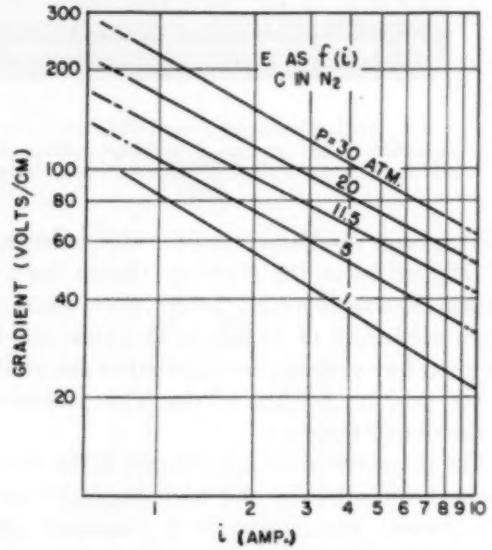

Fig. 4. Gradient as a function of arc current for nitrogen at various pressures (carbon electrodes).

An alternative method of determining the constants of an equation of the form of (2) is to plot log $(e+A)$ and log i, adjusting the value of A to obtain the best straight line.[4, 5] The n is

[4] C. G. Suits, Phys. Rev. **46**, 252 (1934).
[5] W. B. Nottingham, Phys. Rev. **28**, 764 (1926).

then calculated for the selected value of A. For the present case a value of 0.9 ± 0.2 is obtained by this method. This value should be compared to the direct experimental value of $n=0.6$. The example points out the fallacy of interpreting n in terms of gradient from $\log(e+A)-\log i$ plots, since the method fundamentally lacks sufficient accuracy for this purpose.

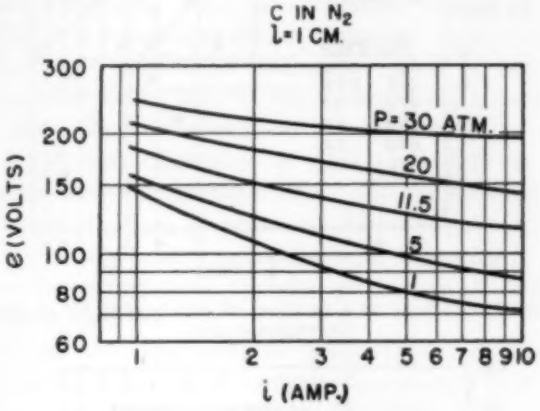

FIG. 5. Arc voltage as a function of arc current for nitrogen at various pressures (carbon electrodes).

The $\log E-\log i$ characteristics for nitrogen at 1, 5, 11.5, 20, and 30 atmospheres are given in Fig. 4; the values of n (Eq. (1)) for these pressures are shown by Table III. Although n shows an extreme range of 0.51 to 0.60, an average value of $n=0.55$ would be consistent with the results over the whole range of pressure. The family of curves for $e-i$ for the pressure range up to 30 atmospheres is shown as Fig. 5.

E for helium and argon

By the method outlined above, the gradient in steady-state arcs between pure carbon electrodes has been determined for He, A and H_2. Fig. 6 shows the $\log E-\log i$ curve for He between 1 and 48 atmospheres. The dotted portions of the

TABLE II. *Values of* $A=e-84/i^{0.6}$.

e	145	107	84	77	74	73
i	1	2	4	6	8	10
A	61	52	48	49	50	52

TABLE III. *Values of n for nitrogen, 1–30 atmos. pressure.*

p (atmos.)	1	5	11.5	20	30
n	0.60	0.53	0.51	0.52	0.54

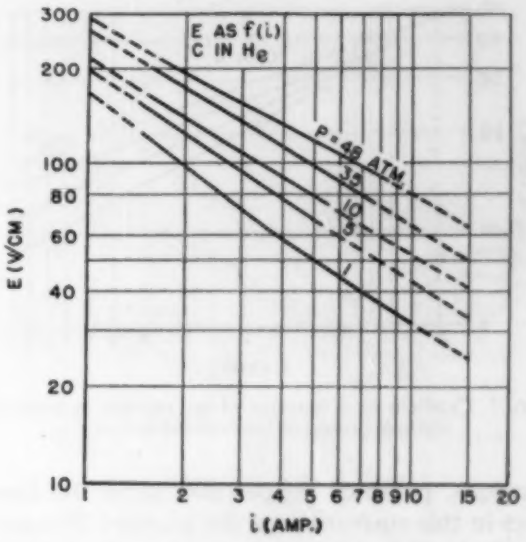

FIG. 6. Gradient as a function of arc current in helium at various pressures (carbon electrodes).

curves represent extrapolations beyond the best experimental points. The arc in He is stable and reproducible and resembles the N_2 arc in many respects. The gradient in He is somewhat higher than in N_2; the difference becomes less at higher pressure. The exponent n (Eq. (1)) is given in Table IV over this pressure range.

Similar data for argon are given by Fig. 7 and Table V. The arc in argon is characterized by a low gradient and a very small change of E with p, particularly at low current.

Because the hydrogen arc shows some unusual features not found in the case of N_2, He and A, these results are being reported in a separate paper. In a summary of results at the end of the present paper, however, the gradient for the normal arc state of hydrogen is included.

Arc gradient for metallic electrodes in air

The gradient data above apply to cases of pure carbon electrodes in gases of 98 percent purity, that is, to metal-vapor-free arcs in which the thermal ionization of the gas provides the electron density required for current conduction. One may expect the above results to be correct for arcs between metallic electrodes in cases in which, because of high thermal conductivity and low vapor pressure, the metal vapor concentration is low. Favorable electrode materials in this respect are tungsten, molybdenum, clean (for

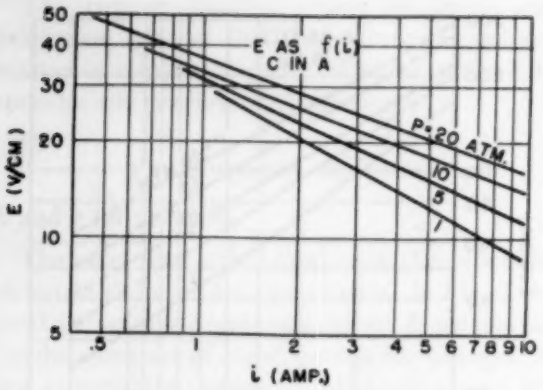

FIG. 7. Gradient as a function of arc current in argon at various pressures (carbon electrodes).

example, polished) copper and silver. In these arcs in this current range the gradient E cannot be distinguished from pure carbon. In the case of other metals the effect of the metal vapor is such that it lowers the gradient by an amount which is greater than the uncertainty of measurement.

The spread in the measurements is large, however, because of the random voltage variation and other causes. When the data are taken in air, the absence or presence of the oxide and the condition of the surface influence the results. This is illustrated in the case of copper by Fig. 8 where gradient E (measured with a vibrating electrode) is plotted as a function of current. Three surface treatments were used, as indicated. The gradient is consistently lower for electrodes which are heavily coated with oxide, higher for freshly turned surfaces, highest for electrodes with polished surfaces. Also the effect is most pronounced at high currents. It is not immediately evident from this result that discrete states for the Cu arc, characterized by relatively small voltage differences, could be identified as reported by White[6] and Fry.[7]

TABLE IV. *Values of the exponent n in Eq. (1) for helium.*

p (atmos.)	1	5	10	35	48
n	0.72	0.66	0.61	0.61	0.56

TABLE V. *Values of the exponent n in Eq. (1) for argon.*

p (atmos.)	1	5	10	20
n	0.53	0.45	0.38	0.35

TABLE VI. *Exponent n of the gradient equation for various gases.*

Gas	Hg	A	N_2	Air	CO_2	He	H_2O	H_2
n	0.26	0.54	0.60	0.60	0.60	0.73	0.59	0.70

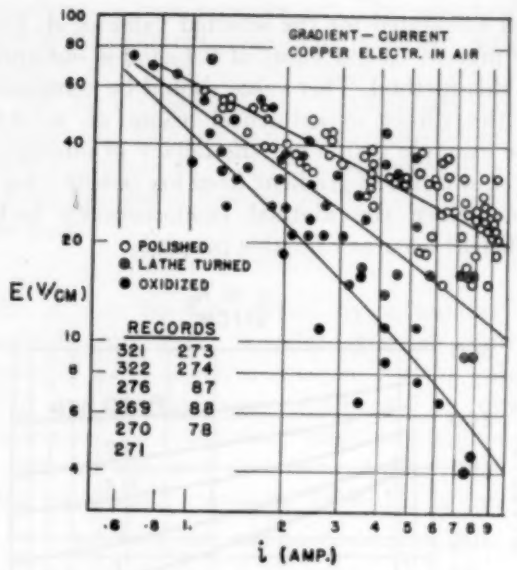

FIG. 8. Gradient as a function of arc current for copper electrodes in air.

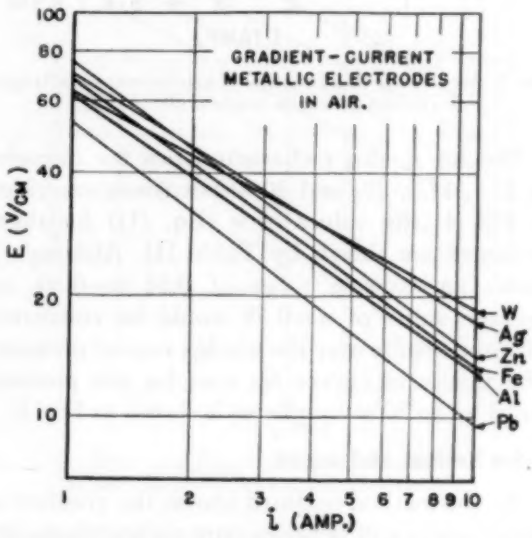

FIG. 9. Gradient as a function of arc voltage for various metallic electrodes in air.

Curves for a number of additional metals are shown in Fig. 9. At 10 amperes one might form three groups on the basis of gradient. In the first group, characterized by high gradient, are W,

[6] A. B. White, Phys. Rev. **53**, 935 (1938).
[7] A. S. Fry, Phys. Rev. **51**, 63 (1937).

Ag, Cu and C. In the second group one can place Zn, Fe and Al; and, finally, the lowest gradient grouping would include Pb.

Comparison of Gradient Data for Various Gases

The plot of Fig. 10 shows the $\log E - \log I$ data for the gases He, N_2 and A, discussed above, together with the H_2 data and some additional measurements on steam and CO_2, and Elenbaas'[8] results for mercury vapor at one atmosphere. In Table VI the values of n for arcs in these gases are given.

A detailed discussion of this gas effect together with the pressure effect will be deferred to another paper, in which it is shown that[9] the changes in gradient correlate with the conduction-convection heat transfer properties of the gaseous medium.

From the approximate proportionality between $\log E$ and $\log i$ we have determined m in the relation

$$E \sim p^m$$

as an average value for the range $1 < p < 30$, for N_2, He, and A. Comprehensive pressure data are not available for H_2, but from a single measurement at $p = 0.014$ atmos. and the H_2 one atmosphere data, an approximate value of m has been calculated.

These results are given in Table VII.

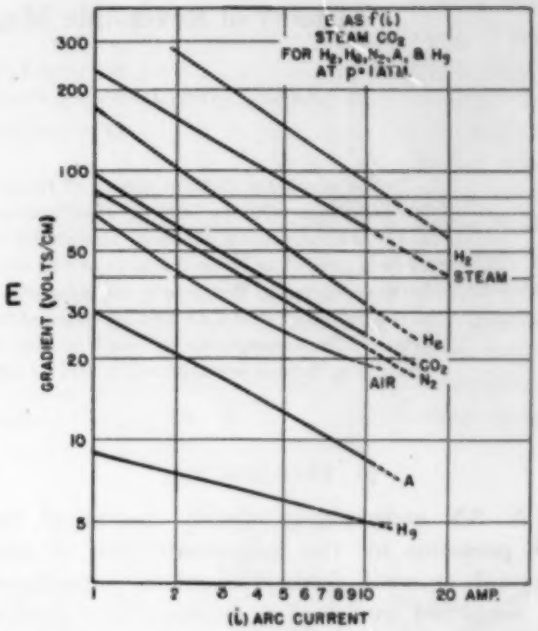

Fig. 10. Gradient as a function of arc current for various gases.

Table VII. *Exponent m in the gradient-pressure relation.*

N_2 i	N_2 m	H_2	He i	He m	A i	A m
1	0.29	$m = 0.32$	1	0.15	1	0.06
2.5	.30	(approx.)	3	.20	2.5	.12
5	.31		5	.20	5	.21
10	.32		15	.24	10	.27
Av. = .31			Av. = 0.20		Av. = 0.16	

[8] W. Elenbaas, Physica **2**, 787 (1935).
[9] C. G. Suits and H. Poritsky, Phys. Rev. **52**, 136 (1937).

Theory of Reversible Magnetization in Ferromagnetics

WILLIAM FULLER BROWN, JR.
Palmer Physical Laboratory, Princeton University, Princeton, New Jersey
(Received December 27, 1938)

In the statistical domain theory of Heisenberg and others it is assumed that the domains have constant volumes, but that their magnetic moments change from one direction to another as the field or stress is changed. This model is highly artificial, for the actual process is believed to be a growth of some domains at the expense of others by displacement of the boundary between them. In this article the equations of the statistical theory are derived without use of the simplified model, by an adaptation of Kondorsky's analysis of the boundary displacement process. The assumptions necessary for this derivation are discussed critically, and the effect of modifying them is investigated in several special cases.

§1. INTRODUCTION

IN AN endeavor to obtain theoretical expressions for the magnetostriction of iron crystals in weak fields, Heisenberg[1] introduced a simplified model of a ferromagnetic crystal that has been used with surprising success in calculating a number of properties of crystals and of polycrystalline specimens.[2–6] In this model it is assumed that the domains are all of the same size; as the field is increased the domain volumes remain constant, but the magnetization of individual domains changes from one direction of easy magnetization to another, so that the magnetization of the specimen increases. The relative numbers of domains magnetized in the various possible directions are calculated by statistical methods. To justify such methods it is argued[6] that the internal forces that really determine the microscopic state of affairs vary irregularly from point to point, and may therefore be considered random. But before the derivation can be completed it is necessary to become much more specific in the definition of "randomness;" and the definition that has to be adopted is difficult to interpret in terms of any physical picture of internal forces.

This model, despite its success, must be regarded as a makeshift. There is strong evidence[7–9] that changes in magnetization, whether reversible or irreversible, occur by a progressive reorientation of electron spins in the boundary region between domains, describable on a larger scale as a growth of favorably oriented domains at the expense of their less favorably oriented neighbors by displacement of the boundary between them. It is therefore the volumes that change and the domain magnetizations that remain constant. Heisenberg himself pointed this out in introducing the simplified model. His expectation that it might nevertheless lead to approximately correct results has been amply justified; its chief shortcoming is not any lack of agreement between theory and experiment, but rather that the artificiality of the model makes it difficult to interpret the assumptions of the theory in terms of a more realistic model, or to modify the theory by substituting less drastic assumptions in regard to the mode of behavior of the internal forces.

A mathematical analysis of the boundary displacement process was carried out by Bloch[7] and by Becker[10] in a few especially simple cases. It has recently been extended by Kondorsky,[11] who has obtained a formula for the re-

[1] W. Heisenberg, Zeits. f. Physik **69**, 287 (1931).
[2] R. Gans and J. v. Harlem, Ann. d. Physik **15**, 516 (1932); **16**, 162 (1933).
[3] R. M. Bozorth, Phys. Rev. **42**, 882 (1932).
[4] R. H. Fowler, *Statistical Mechanics*, second edition (Macmillan Co., 1936), p. 520.
[5] N. Akulov and E. Kondorsky, Zeits. f. Physik **78**, 801 (1932); **85**, 661 (1933).
[6] W. F. Brown, Phys. Rev. **52**, 325 (1937); **53**, 482 (1938); **54**, 279 (1938).
[7] F. Bloch, Zeits. f. Physik **74**, 295 (1932).
[8] K. J. Sixtus and L. Tonks, Phys. Rev. **37**, 930 (1931); **39**, 357 (1932); **42**, 419 (1932); **43**, 70 and 931 (1933); K. J. Sixtus, Phys. Rev. **48**, 425 (1935); W. Döring, Zeits. f. Physik **108**, 137 (1938).
[9] F. Bitter, *Introduction to Ferromagnetism* (McGraw-Hill Book Co., 1937), p. 194 ff.; W. C. Elmore, Phys. Rev. **51**, 982 (1937); **53**, 757 (1938).
[10] R. Becker, Physik. Zeits. **33**, 905 (1932).
[11] E. Kondorsky, Physik. Zeits. Sowjetunion **11**, 597 (1937); Comptes rendus Acad. Sci. U.R.S.S. **18**, 325 (1938); **19**, 397, 401 (1938); Phys. Rev. **53**, 319, 1022 (1938).

versible susceptibility of iron crystals. This formula involves the relative volumes v_i oriented in the various possible directions i; when the field is in direction [111] or when only orientations nearest the axis of the specimen occur, the symmetry of the problem makes it possible to determine the v_i's at once as functions of the magnetization, but in general this is not the case. Kondorsky therefore evaluates the v_i's by the use of formulas borrowed from the statistical theory; these formulas give the relative *numbers of domains*, n_i, oriented in the various possible directions i in the simplified model of this theory.

Now the statistical theory itself, as has been shown by the writer,[6] is capable of yielding formulas for the reversible susceptibility, and the formulas in some cases give excellent agreement with experiment. If, therefore, the formulas of this theory must be used in the end, it seems preferable to use them from the beginning, rather than mixing the two models. But if this final step can be avoided and Kondorsky's theory made complete in itself, his analysis is to be preferred because of its more realistic approach. This can be done: in fact it is possible, by introducing certain assumptions, to derive the equations of the "statistical" theory by an analysis similar to Kondorsky's, without any use of the simplified model or of statistical methods. The assumptions made in this derivation can be clearly stated in terms of the boundary motion process and the internal and external forces controlling it. By making slightly different assumptions, modified formulas may be derived in several simple cases. The two theories thus become one, and the Heisenberg model with its objectionable artificiality may be discarded without sacrifice of any of its essential results.

§2. Boundary Displacement Theory: A Review

In the boundary displacement theory it is assumed that the position of the boundary surface S_{ij}, between two domains whose magnetic moments are oriented in directions i and j, is determined by an equilibrium between external and internal forces. The external forces (field components and stresses)* have a direct effect on the boundary position only insofar as they cause the external free energy density u_i on the i side of the boundary to differ from the value u_j on the j side. Thus if only fields are present, $u_i=-\mathbf{H}\cdot\mathbf{J}_i$ and $u_j=-\mathbf{H}\cdot\mathbf{J}_j$, where $\mathbf{J}_i$ and $\mathbf{J}_j$ are the vector magnetizations on the two sides; a change of field is effective in displacing the boundary only if it affects the difference $u_j-u_i=\mathbf{H}\cdot(\mathbf{J}_i-\mathbf{J}_j)$. If the boundary S_{ij} is supposed to undergo a virtual displacement, such that at each point P the surface is displaced normally through a distance $\delta x_{ij}(P)$ from side i toward side j, the increase in free energy due to external forces is

$$\int_{S_{ij}}(u_i-u_j)\delta x_{ij}dS;$$

so that the surface S_{ij} may be regarded as subject to a force $-u_i$ per unit area pushing on it from the i side, and a force $-u_j$ per unit area pushing on it from the j side. Since the effect on the boundary depends only on the values of the

* The "external" field **H** and the "external" stresses are the field and stresses that would be produced by the same magnetizing currents and applied forces in a specimen macroscopically indistinguishable from the actual specimen, but homogeneous instead of being made up of domains. The actual field and stresses at an interior point P would not be affected appreciably if all the matter at a distance greater than r were to be replaced by homogeneous matter, provided r is large compared with the dimensions of the domains. The deviations of the actual field and stresses from the value for the homogeneous specimen are therefore determined by the state of affairs near P, and may appropriately be termed "internal" fields and stresses. The internal field and stresses as thus defined result from the inhomogeneous character of the material about P; that is, from the domain structure itself, from inherent distortions, and from impurities. The field under discussion is one that is continuous throughout the interior of a domain: the atomic structure of the material and the nature of the elementary magnets are involved only indirectly, through such constants as J_s, λ_{100}, C. The internal field and induction therefore differ, and the question rises whether **H** or **B**, and whether stresses or strains, should be used as the independent variables. The answer depends on whether the simplifying assumptions to be made are a better approximation as applied to the one set of quantities or to the other. It is evident for example that, if the internal stresses are constant, the internal strains must vary as the domains change in size, because of magnetostriction. The use of field rather than induction as independent variable appears to lead to reasonable results, probably because the former is more nearly uniform for elongated domains, and the internal part is therefore a smaller part of the whole and more nearly continuous across the boundaries. The use of stresses and the use of strains as independent variables lead to slightly different results that usually lie on opposite sides of the correct one (see reference 6).

u_i's and not on the way in which the fields and stresses are manipulated in order to attain these values, it is legitimate to regard the u_i's as the independent variables, whether or not there are actually enough independently variable field and stress components to produce arbitrary variations in the u_i's. (In iron crystals, with only six directions of easy magnetization, arbitrary variations of the u_i's can actually be produced by varying the three field components and three components of tension.)

The internal forces include internal stresses and internal fields. To some extent these are inherent in the material and unaffected by the magnetization process. This is true for instance of internal stresses resulting from permanent distortion of local regions, and of magnetic forces due to small regions of permanent magnetic saturation in a definite direction, resulting from high local stresses. To a large extent, however, the internal forces acting at any point of a boundary may be expected to depend not only on the state of the material at that point when the boundary reaches it, but also on conditions at other points. For instance, magnetic forces on one boundary due to Poisson distributions of magnetic charge on other boundaries will vary with the positions of the other boundaries; again, the stresses at and near a boundary will be altered when a neighboring boundary is displaced, because of the magnetostrictive change in dimensions of the regions through which the second boundary has passed. Thus a boundary S_{ij} may be displaced even though u_i and u_j remain constant, because changes in other u_k's may displace other boundaries and this in turn may alter the *internal* forces on S_{ij}.

These indirect effects seem too hopelessly complicated to analyze, and the usual procedure has been to avoid the difficulty by assuming that the permanent, local part of the internal forces is much larger. In many cases to which one would like to apply the theory, for instance in annealed specimens, this is certainly not true. On the other hand, the importance of magnetic forces between neighboring boundaries is decreased by the tendency of boundaries to assume shapes for which the Poisson densities vanish.[7, 12]

[12] L. Landau and E. Lifshitz, Physik. Zeits. Sowjetunion **8**, 153 (1935).

Perhaps by arguments of this sort it would be possible to justify the neglect of indirect effects. At any rate, the results obtained by assuming them negligible seem to apply even in some cases (annealed polycrystalline nickel is an example[6]) in which the assumption is not strictly justified. In the remainder of the analysis, this assumption will be made.

The free energy associated with these local, permanent internal forces is of two kinds: (1) Energy associated with the region on each side of the boundary, but whose amount w per unit volume is different on the two sides, so that a displacement of the boundary S_{ij} produces a change in total energy of the form

$$\int_{S_{ij}} [w_i(x, y, z) - w_j(x, y, z)] \delta x_{ij} dS.$$

An example of this is the energy associated with permanent internal stresses, and arising from the fact that a reorientation of the magnetization vector is accompanied by a magnetostrictive change of dimensions of the affected region, and therefore involves work against the permanent internal stress in that region. In an iron crystal this energy, for a domain oriented along the positive or negative cubic axis Ox_i, is of amount $w_i = -\lambda_{100}\sigma_i(x, y, z)$ per unit volume, where λ_{100} is the magnetrostriction of a crystal magnetized to saturation along such an axis, and the quantity written for brevity as σ_i is the local tension along the axis in question minus the mean tension along the other two axes.[10] (2) Energy associated with the boundary layer between domains, but whose amount per unit area of the boundary varies with the position of the boundary, so that a displacement of the boundary S_{ij} produces a change in energy of the form

$$\delta \int_{S_{ij}} \epsilon(x, y, z) dS.$$

Here ϵ represents the boundary energy per unit area of the boundary, and depends on the local conditions (stresses, for instance) in the boundary layer. An example is the boundary energy discussed by Bloch,[7] which results from the joint action of exchange forces and anisotropy

(spin-orbit) forces. This energy is given by

$$\epsilon \leqq (J'C)^{\frac{1}{2}}/a^2, \tag{1}$$

where a is the lattice constant, J' is the exchange integral, and C is the anisotropy energy per atom. Internal stress distorts the lattice locally and therefore alters the values of these quantities. Kondorsky has added to C a magnetostrictive term, designed to take account of the fact that in the boundary region the magnetostriction has a value different from that corresponding to magnetic saturation. If the variation of ϵ with position of the boundary is due chiefly to variation of this magnetostrictive term, the magnitude of this variation is according to Kondorsky

$$\partial\epsilon/\partial x_{ij} = \tfrac{1}{2}\lambda'\delta\partial\sigma/\partial x_{ij}, \tag{2}$$

where λ' is the saturation magnetostriction minus the boundary value, δ is the thickness of the boundary layer, and σ is the internal stress.

In a virtual displacement of the boundary, the total change of free energy is

$$\delta W = \int_{S_{ij}} \{(u_i - u_j) + (w_i - w_j) + \partial\epsilon/\partial x_{ij} + \epsilon[(1/r_1) + (1/r_2)]\}\delta x_{ij} dS. \tag{3}$$

The last term, in which r_1 and r_2 are the principal radii of curvature of the surface, takes account of the variation of the boundary area as the boundary progresses: $\delta dS = [(1/r_1) + (1/r_2)]\delta x_{ij} dS$. It may be regarded as a sort of surface tension, tending to contract the boundary. It plays a role in determining the size of the domains,[12-14] but its inclusion in the present analysis would seriously complicate the equations. It can be safely omitted if the linear dimensions of the domains are large compared with the distances over which ϵ changes by large fractions of itself, that is if a domain contains many maxima and minima of ϵ, for then $\partial\epsilon/\partial x_{ij} \gg \epsilon/r_1$ or ϵ/r_2. Even if this is not true, there is some justification for omitting the surface tension term in the fact that a boundary of type ij will be concave toward i in some parts and toward j in others, so that the average curvature should be small. This argument breaks down when domains of one type have become so small as to be completely surrounded by others. Nevertheless this term will be omitted in the remainder of the analysis, on the assumption that it has been taken sufficiently into account by postulating the existence of domains of a certain average size.

The condition for equilibrium is that in a virtual displacement δW shall be zero, or

$$[w_i(x, y, z) - w_j(x, y, z)] + \partial\epsilon(x, y, z)/\partial x_{ij} = u_j - u_i. \tag{4}$$

The locus of points satisfying this equation defines an equilibrium position of the boundary for given values of the u's. In order that the equilibrium be stable it is necessary in addition that

$$\partial[(w_i - w_j) + \partial\epsilon/\partial x_{ij}]/\partial x_{ij} > 0. \tag{5}$$

As long as this condition is satisfied the boundary proceeds reversibly as the u's are varied. When the boundary reaches a point at which the left member of (5) changes sign, the equilibrium becomes unstable, and the boundary proceeds irreversibly until it either reaches a new position of stable equilibrium, or reaches another boundary and fuses with it (annulling it, if it is one of opposite type). Throughout the reversible part of this process, the change of position of the boundary produced by a change δu_i, δu_j in the external conditions is given by

$$\{\partial[(w_i - w_j) + \partial\epsilon/\partial x_{ij}]/\partial x_{ij}\}\delta x_{ij} = \delta(u_j - u_i),$$

or

$$\delta x_{ij} = k_{ij}\delta(u_j - u_i), \tag{6}$$

where

$$k_{ij} = \{\partial[(w_i - w_j) + \partial\epsilon/\partial x_{ij}]/\partial x_{ij}\}^{-1} > 0. \tag{7}$$

The total increase of volume of domains of type i at the expense of domains of type j, in unit total volume, is

$$\delta v_{ij} = \int_{S_{ij}} k_{ij}\delta(u_j - u_i) dS = \bar{k}_{ij} S_{ij} \delta(u_j - u_i) = p_{ij}\delta(u_j - u_i), \tag{8}$$

where S_{ij} is the total area of boundaries of type ij in unit volume of the specimen, and $\bar{k}_{ij}$ is the mean value of k_{ij}.

To carry the analysis further it is necessary to make some assumption in regard to the mode of variation of $\bar{k}_{ij}$ and of S_{ij} as the boundaries

[12] J. Frenkel and J. Dorfman, Nature **126**, 274 (1930).
[14] W. Döring, Zeits. f. Physik **108**, 137 (1938).

move. Kondorsky assumes: (1) that the quantities $\bar{k}_{ij}$ remain constant; (2) that if there is no tendency for particular types of domain to be grouped together, S_{ij} is proportional to the product v_iv_j.

The constancy of the $\bar{k}_{ij}$'s is assured if there is negligible correlation between the mean reciprocals of the normal gradients of internal force, averaged over surfaces of equal force, and the corresponding values of the force. (By "internal force" is meant the quantity $(w_i-w_j)+\partial\epsilon/\partial x_{ij}$.) The assumption therefore is roughly equivalent to the assumption that the space rate of variation of internal force does not depend in any regular manner on the magnitude of the force itself. This is a reasonable assumption when the internal forces vary irregularly from point to point and force maxima occur in all ranges of force values. Irreversible displacements carry the boundaries to positions where the force gradients are different, and therefore should make the assumption more rather than less justifiable.

For the assumption $S_{ij}\propto v_iv_j$ Kondorsky offers no justification. It can be defended to some extent by the following argument. It must be assumed first that the S_{ij}'s are single-valued functions of the v_i's. The total surface area S_i, bounding domains of type i in unit volume, is made up of portions $S_{ij}(j\neq i)$ in contact with domains of the various types j. If there is no tendency for domains of one type to be grouped with domains of a particular other type,[15] it is reasonable to suppose that these portions S_{ij} are proportional to the corresponding volumes v_j; then S_{ij}/v_iv_j is the same for all j's. By a similar argument it is the same for all i's. Let $S_{ij}/v_iv_j=a$: then

$$S_i=\sum_{j\neq i}S_{ij}=av_i\sum_{j\neq i}v_j=av_i(1-v_i).$$

If it is now assumed that the surface bounding domains of a particular type remains unchanged if the corresponding volume remains unchanged, it follows that a is a constant. This assumption is somewhat arbitrary, but may be partially defended if the internal forces and hence the shapes of the boundaries are irregular; for then a change in which some domains of type i grow larger and others smaller, so that the changes in volume compensate, may be expected to produce no significant systematic change in the shape of the aggregate of domains of type i, and hence in the bounding area.

If the assumptions just stated are made, Eq. (8) becomes

$$\delta v_{ij}=a\bar{k}_{ij}v_iv_j\delta(u_j-u_i)=A_{ij}v_iv_j\delta(u_j-u_i), \quad (9)$$

where the A_{ij}'s are constants; and hence

$$\delta v_i=\sum_{j\neq i}\delta v_{ij}=\sum_{j\neq i}A_{ij}v_iv_j\delta(u_j-u_i). \quad (10)$$

This equation is implied, though not explicitly stated, in Kondorsky's work. The assumptions on which it is based may be summarized as follows.

(1) The position of the boundary between domains of two types is determined by an equilibrium between external and internal forces.

(2) External forces are directly effective only insofar as they alter the free energy per unit volume in one or the other of the two regions separated by the boundary.

(3) The internal forces are preponderantly ones that depend only on conditions in or near the boundary; interactions over distances of the order of magnitude of the domain dimensions may be disregarded.

(4) The tendency of boundary forces to decrease the boundary area, having once been taken into account by postulating the existence of domains, may be neglected in studying the detailed motion of domain boundaries.

[15] The "grouping" excluded here (but to be investigated in § 4) means a situation in which some parts of the crystal contain only domains of two particular types, other parts no domains of these two types. Thus an iron crystal may consist of three types of region, in each of which the magnetization is parallel or antiparallel to a single one of the positive cubic axes; such a region in turn then consists of parallel and antiparallel domains. Even if grouping does not occur in this extreme form, there is probably a tendency toward it because of the fact (already noted) that the boundaries tend to assume shapes for which the Poisson densities vanish. This requires that the domains be elongated in the direction of their magnetizations; the areas between oppositely oriented domains must then exceed the areas between domains oriented at right angles to each other. For this reason it may seem more reasonable to assume not that $S_{ij}:S_{ik}=v_j:v_k$, but that $S_{ij}:S_{ik}=c_{ij}v_j:c_{ik}v_k$, where the c_{ij}'s are constant weighting factors. The further assumption that S_{ij} depends only on v_i and v_j leads to Kondorsky's equation $S_{ij}=a_{ij}v_iv_j$, with different proportionality constants for different types of boundary. Eq. (9) is unaffected except that the A_{ij}'s have a slightly different meaning, and the physical interpretation of Eq. (13) is no longer contained in as simple a statement as (10a).

(5) There is no correlation between the mean reciprocals of the internal force gradients normal to surfaces of equal force, and the corresponding force values.

(6) The total area of all the boundaries of a given type in unit volume is a single-valued function of the relative volumes occupied by the various types of domain.

(7) There is no tendency of domains of one type to become grouped with domains of any particular other type. (The alternative assumption will be considered in §4.)

(8) When (7) is true, domains of any given type are in contact with domains of the other types over areas proportional to the relative volumes occupied by the various types.

(9) In a change in which the volume occupied by domains of a given type is unaltered, the combined surface area of these domains is also unaltered.

Stated this fully, the assumptions that must be made are dismayingly many. The last seven, however, are merely more precise expressions of the general assumption that the internal forces governing the boundary displacement process are local in origin, permanent in nature, and irregular in their spatial variation.

Kondorsky actually considers only the effect of a magnetic field ($u_i = -\mathbf{H}\cdot\mathbf{J}_i$) and writes not Eq. (10), but the equation for the reversible susceptibility derivable from it ($\delta J = \sum_i J_i \delta v_i$). He also supposes that there are only two values of the A_{ij}'s, one for boundaries between oppositely oriented domains and one for all other boundaries. Moreover he considers chiefly the case in which oppositely oriented domains are grouped together, so that Eq. (10) has to be modified somewhat. Nevertheless Eq. (10) is essentially due to Kondorsky.

§3. Completion of the Theory

The derivation of the equations of the "statistical" theory from Eq. (10) requires only one additional assumption; this will be stated first in a form that seems, but is not, trivial:

(10a) The reversible properties of a specimen are properties that it would be possible for a reversible specimen to have.

This means that a reversible specimen could have the properties described by Eq. (10), with the same A_{ij}'s, without violating thermodynamics. But for such a specimen the v_i's would be single-valued functions of the u_j's and the δv_i's would be their differentials, hence $\delta v_i/v_i = \delta(\log v_i)$ would be a perfect differential, and

$$\partial(A_{ij}v_j)/\partial u_k = \partial(A_{ik}v_k)/\partial u_j; \tag{11}$$

whence, since

$$\partial v_j/\partial u_k = A_{jk}v_jv_k = \partial v_k/\partial u_j, \tag{12}$$

$$A_{ij} = A_{ik} = \cdots = A. \tag{13}$$

Thus assumption (10a) implies that:

(10b) The mean reciprocals of the gradients of internal force normal to the boundary are the same for all types of boundary.

If it is preferred, (10b) may be taken as the assumption and (10a) regarded as a corollary. There seems no doubt, if Kondorsky's description of internal forces is correct, that (10b) is an oversimplification. Nevertheless it leads to interesting results.

If condition (13) is satisfied, Eq. (12) shows that there is a function $\phi(u_1, u_2, \cdots)$ such that $v_i = \partial\phi/\partial u_i$, and satisfying

$$\partial^2\phi/\partial u_i\partial u_j = A(\partial\phi/\partial u_i)(\partial\phi/\partial u_j) \tag{14}$$

for every i, $j \neq i$. The solution of this is

$$e^{-A\phi} = \sum_i f_i(u_i). \tag{15}$$

The functions f_i are determined by the condition $\sum_i \partial\phi/\partial u_i = 1$, whence $f_i = \exp\,[-A(u_i - c_i)]$, where the c_i's are arbitrary constants, and

$$\phi = -(1/A)\log\sum_i e^{-A(u_i - c_i)}, \tag{16}$$

$$v_i = e^{-A(u_i - c_i)}/\sum_j e^{-A(u_j - c_j)}. \tag{17}$$

For a reversible specimen in which no directions are especially favored by the shape of the specimen, the v_i's are equal when all the u_j's are zero; the c_i's may then be set equal to zero, and (17) becomes the formula for the n_i's of the statistical theory. In the present theory, therefore, this formula corresponds to complete reversibility and implies equivalence of the different types of boundary.

For a specimen capable of irreversible changes, the integrated Eq. (17) still describes the behavior in reversible changes. The c_i's will be zero only in the initial reversible change from

the demagnetized, unstressed state. In a reversible change from any other state, the c_i's will have values determined by the initial state. An irreversible change takes the specimen from one set of c_i's to another.

This may be illustrated by considering a specimen subject to a field H of variable magnitude but fixed direction; in this case $u_i = -J_s h_i H$, where J_s is the saturation magnetization and h_i is the cosine of the angle between magnetization and field for domains of type i. It will be assumed (this is admittedly an oversimplification) that the v_i's are single-valued functions of the magnetization J, and that these functions are the same as if the specimen were reversible. For a reversible specimen the functional relations may be written parametrically in the form $v_i = z^{h_i}/\sum_i z^{h_i}$, $J/J_s = \sum_i h_i z^{h_i}/\sum_i z^{h_i}$ ($z = \exp(AJ_sH)$). If the more general equations are to give the same relations, the c_i's must be given by $c_i = ch_i$, where c is a constant in reversible changes and varies in irreversible changes; then for the actual specimen $z = \exp(AJ_sH - c)$. Thus

$$J/J_s = \sum_i h_i e^{\eta h_i}/\sum_i e^{\eta h_i} = f(\eta), \qquad (18)$$

where

$$\eta = AJ_sH - c. \qquad (19)$$

The curve for a completely reversible specimen ($c = 0$) is that given by the statistical theory, and passes through the origin (Fig. 1, curve 1). The initial reversible change of magnetization follows this curve from the origin; thus the initial susceptibility is the same as in the statistical theory. A reversible change from any initial point P, P' follows a curve obtained by displacing 1 to the left or right until it passes through the point in question (Fig. 1, curves 2 and 3). The reversible susceptibility is the slope of this curve; it evidently depends only on J, and is given as in the statistical theory by the parametric equations $J = J_s f(\eta)$, $\chi_r = AJ_s^2 f'(\eta)$. Irreversible changes take the specimen from one such curve to another (Fig. 1, curve 4).

If the v_i's are not assumed to be single-valued functions of the magnetization, it no longer follows that the reversible susceptibility is determined by the magnetization alone. Experimentally, it appears that such a functional relation between reversible susceptibility and magnetization holds approximately, but not exactly.[16]

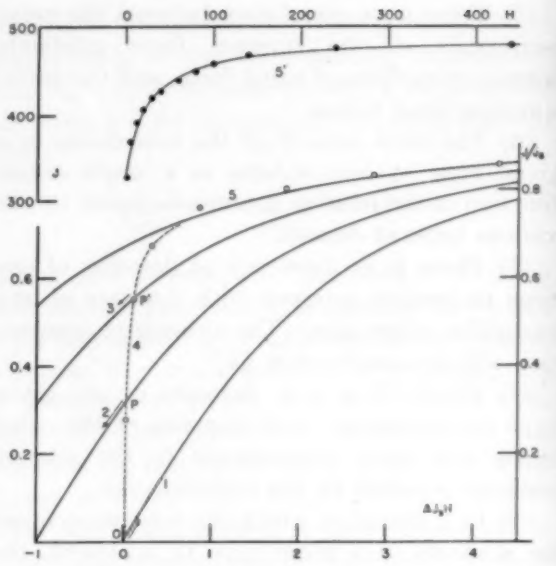

FIG. 1. Magnetization curves of specimen with polycrystalline domains. 1, theoretical curve of reversible specimen ($H_0 = 0$). 2 and 3, theoretical curves for reversible changes from initial states P and P' ($AJ_sH_0 = 1$ and 2, respectively). Small reversible changes occur as indicated by the arrows at O, P and P'. 4, qualitative representation of the irreversible ascending magnetization curve. 5, a possible theoretical curve for high fields. 5′, theoretical J *vs.* H curve calculated with values of H_0, J_s and A given in the text; solid circles are experimental values on the normal magnetization curve of a nickel ellipsoid at room temperature. The solid circles and curve 5′ of the upper figure, plotted on a different scale and extended to lower fields, give the open circles and curve 5 ($AJ_sH_0 = 3.00$) of the lower figure.

For a polycrystalline specimen in which the domains are larger than the crystals, the direction of magnetization of each domain is a direction that minimizes its total free energy. This energy is due partly to the external field, partly to crystalline anisotropy forces (which cancel to some extent but not completely if the crystal axes are oriented at random), and partly to internal fields and stresses. All but the first of these are taken account of as internal forces, and therefore in the statistical theory such domains were treated as "isotropic," in the sense that every direction is a direction of easy magnetization, and the sums over directions of easy magnetization were replaced by integrals over the unit sphere. The corresponding limiting case in the present

[16] R. Gans, Physik. Zeits. **12**, 1053 (1911); Ann. d. Physik **61**, 379 (1920).

theory would be one in which a domain may be magnetized in any direction, and may absorb a portion of an adjacent domain without undergoing any change of its direction of magnetization. The first of these conditions is satisfied if the domains are polycrystalline, but the second is not; for if the boundary moves, the crystalline forces and internal stresses in the absorbed region may be expected to change the direction of magnetization of the absorbing domain. Rotation of the magnetization vector should occur simultaneously with boundary displacement. The "isotropic domain" formulas are therefore a trifle difficult to justify in the present theory, although some of the best agreement between theory and experiment has been obtained with these very formulas, applied to polycrystalline nickel.[6] It is clear, however, that these formulas result from either of two simplified theories: one in which boundary displacement is allowed, without change in the directions of domain magnetizations, and one in which changes in these directions are allowed, without displacement of the boundaries. If the actual process is a combination of these, the formulas that follow equally well from either alone should hold at least approximately when they are combined.

In this limiting case, Eq. (18) becomes

$$J=J_s(\coth\eta-1/\eta)=J_sL(\eta), \qquad (18')$$

where

$$\eta=AJ_s(H+H_0). \qquad (19')$$

Here c has been written $-AJ_sH_0$. The initial susceptibility is

$$\chi_0=AJ_s^2L'(0)=\tfrac{1}{3}AJ_s^2, \qquad (20)$$

and the reversible susceptibility is $AJ_s^2L'(\eta)$. The experimental verification of the formula for the reversible susceptibility (originally proposed by Gans),[16] and of its dependence on J alone, has already been discussed.[6] Additional confirmation of the theory may be obtained from the magnetization curve at high fields, where the magnetization process is practically reversible and should therefore follow a curve like 5, given by Eq. (18') with a positive value of H_0 and with $A=3\chi_0/J_s^2$. The points in the upper part of Fig. 1 are experimental values obtained at 19.4°C by Kirkham[17] on the ellipsoid he used for magnetostriction measurements.[18] The theoretical curve 5' has been calculated with $J_s=487$ gauss, obtained by extrapolation of the J *vs.* $1/H$ curve at high fields ($L(\eta)\doteq 1-1/\eta$, $H\gg H_0$), and with the following values of the other constants, chosen to fit the curve to the data as well as possible: $H_0=21.1$ oersteds, and $\chi_0=23.2$ or $1/A=3.52\times10^3$ erg cm^{-3}.

A physical interpretation of H_0 must await a more complete analysis of irreversible processes. The initial susceptibility is not known for this specimen, but a rough check of $1/A$, which should be of the order of magnitude of the free energy density associated with the internal forces, may be made if these are assumed to be chiefly internal stresses of magnetostrictive origin. The energy density should then be of the order of magnitude of $\lambda_\infty^2E_\infty$, where λ_∞ is the saturation magnetostriction and E_∞ the saturation value of Young's modulus.[19] Since[18, 20] $\lambda_\infty=3.99\times10^{-5}$ and $E_\infty=2.22\times10^{12}$ dynes/cm^2, this gives $1/A=3.54\times10^3$. The numerical agreement is, of course, fortuitous; the agreement in order of magnitude, however, is significant. An experimental determination of the initial and reversible susceptibility of this specimen is being undertaken in this laboratory.

§4. Modifications of the Theory

The assumptions on which the formulas of the statistical theory are based have now been stated clearly. If any of these assumptions are modified, the theory must be modified accordingly. Several such modifications will now be considered.

(a) Inequality of the A_{ij}'s; grouping of domains

If the condition (13) is not satisfied, the reversible properties of the specimen are not ones that a reversible specimen could possess, and the equations describing these properties are not integrable. Nevertheless they are still useful. The case that will be considered is the one treated by Kondorsky: an iron crystal with two values of the A_{ij}'s, a value A for oppositely magnetized domains and a value B for domains magnetized at right angles to each other. Let u_i, v_i refer to the positive cubic axes and $\bar{u}_i, \bar{v}_i$ to the corresponding

[17] Unpublished data.

[18] D. Kirkham, Phys. Rev. **52**, 1162 (1937).

[19] M. Kersten, Zeits. f. Physik **12**, 665 (1931).

[20] S. Siegel and S. L. Quimby, Phys. Rev. **50**, 1165 (1936).

negative axes. If the crystal is subjected to a field of variable magnitude H in a fixed direction (l_1, l_2, l_3), u_i and $\bar{u}_i$ becomes $-HJ_s l_i$ and $+HJ_s l_i$, respectively, and Eq. (10) becomes

$$\delta x_i/\delta H=\beta(l_i y_i \sum_{j\neq i} x_j - x_i \sum_{j\neq i} l_j y_j), \tag{21}$$

$$\delta y_i/\delta H=\alpha l_i(x_i^2-y_i^2) +\beta(l_i x_i \sum_{j\neq i} x_j - y_i \sum_{j\neq i} l_j y_j), \tag{22}$$

where $x_i=v_i+\bar{v}_i$, $y_i=v_i-\bar{v}_i$, $\alpha=AJ_s$, $\beta=BJ_s$. From (22), if j is the ratio of the magnetization J in the field direction to its saturation value J_s,

$$\delta j/\delta H=\sum_i l_i \delta y_i/\delta H =\alpha\sum_i l_i^2(x_i^2-y_i^2) +\beta\sum_i \sum_{j>i} \{(l_i^2+l_j^2)x_i x_j - 2l_i l_j y_i y_j\}. \tag{23}$$

If, as is supposed by Kondorsky, oppositely oriented domains are grouped together in the crystal, the relation $S_{ij}=av_i v_j$ must be replaced by the relations[21]

$$S_{i,\,i-}=av_i\bar{v}_i/(v_i+\bar{v}_i), \tag{24}$$

$$S_{i,\,j}=bv_i v_j, \quad S_{i,\,j-}=bv_i\bar{v}_j, \text{ etc.} \tag{25}$$

The α-term in (22) must therefore be divided by x_i; (23) then becomes Kondorsky's formula for reversible susceptibility.

To complete the calculation in the more complicated cases, Kondorsky substituted in this formula the values of the v_i's and $\bar{v}_i$'s (as functions of j) given by the statistical theory. It is clear from §3 that this is inconsistent with the assumption $A\neq B$. This inconsistency may be avoided by assuming merely that the v_i's and $\bar{v}_i$'s are single-valued functions of j, and that these functions are the same as if the specimen behaved reversibly for changes of H alone. The x_i's and y_i's are then to be obtained as functions of j by eliminating δH from (21), (22) and (23) and integrating. For H along [100] or [110], the integration leads to the following results: Without grouping,

$$\begin{aligned}
&[100] \quad j^2=x^2-(1/9)[\tfrac{3}{2}(1-x)]^{2\alpha/\beta},\\
&\qquad \delta j/\delta H=(\alpha/9)[\tfrac{3}{2}(1-x)]^{2\alpha/\beta}+\beta x(1-x);\\
&[110] \quad j^2=2x^2-(2/9)[3(1-2x)]^{(\alpha+\beta)/\beta},\\
&\qquad \delta j/\delta H=(\alpha/9)[3(1-2x)]^{(\alpha+\beta)/\beta}\\
&\qquad\qquad +\beta\{x(1-2x)\\
&\qquad\qquad +(1/9)[3(1-2x)]^{(\alpha+\beta)/\beta}\}.
\end{aligned} \tag{26}$$

With grouping,

$$\begin{aligned}
&[100] \quad j^2=x^2-(1/9)[(1-x)/2x]^{2\alpha/\beta},\\
&\qquad \delta j/\delta H=(\alpha/9x)[(1-x)/2x]^{2\alpha/\beta}\\
&\qquad\qquad +\beta x(1-x);\\
&[110] \quad j^2=2x^2-\tfrac{2}{3}(1-2x)[(1-2x)/x]^{2\alpha/\beta},\\
&\qquad \delta j/\delta H=\tfrac{1}{3}\alpha[(1-2x)/x]^{(2\alpha/\beta)+1}\\
&\qquad\qquad +\beta(1-2x)\{x+\tfrac{1}{3}[(1-2x)/x]^{2\alpha/\beta}\}.
\end{aligned} \tag{27}$$

The parameter $x=v_1+\bar{v}_1$ runs from $\frac{1}{3}$ to 1 in case [100], from $\frac{1}{3}$ to $\frac{1}{2}$ in case [110]. The case $\mathbf{H}\|[111]$ was solved by Kondorsky without use of the statistical theory.

Kondorsky gives reasons for supposing that $\alpha\ll\beta$. In this case, both (26) and (27) become

$$\begin{aligned}
&[100] \quad j^2=x^2-\tfrac{1}{9}, \quad \delta j/\delta H=\beta x(1-x);\\
&[110] \quad j^2=2x^2-\tfrac{2}{3}(1-2x), \qquad \delta j/\delta H=\beta(x+\tfrac{1}{3})(1-2x).
\end{aligned} \tag{28}$$

The statement that $\alpha\ll\beta$ implies not that boundaries between oppositely oriented domains do not move, but that they move irreversibly. Since this irreversible process proceeds rapidly, it may be a better approximation to evaluate the v_i's by assuming that the 180° reversals are completed before the volume oriented perpendicular to the field has changed appreciably.[22] This gives

$$\begin{aligned}
&[100] \quad \delta j/\delta H=2\beta/9, \quad (0\leq j\leq\tfrac{1}{3}),\\
&\qquad\qquad =\beta j(1-j), \quad (\tfrac{1}{3}\leq j\leq 1);\\
&[110] \quad \delta j/\delta H=(2\beta/9)(1-9j^2/4),\\
&\qquad\qquad (0\leq j\leq\tfrac{1}{3}\sqrt{2}),\\
&\qquad\qquad =\beta j(1/\sqrt{2}-j), \quad (\tfrac{1}{3}\sqrt{2}\leq j\leq 1/\sqrt{2}).
\end{aligned} \tag{29}$$

[21] Equation (24) follows from the fact that the previous analysis holds throughout the region $v_i+\bar{v}_i$, in which boundaries of type i, $i-$ exist, if S_{ij} is replaced by $S_{i,\,i-}/(v_i+\bar{v}_i)$ and if v_i, v_j are replaced by $v_i/(v_i+\bar{v}_i)$, $\bar{v}_i/(v_i+\bar{v}_i)$. To obtain Eq. (25), it must be assumed that the total area S_{ij}' separating domains of types i and $i-$ from domains of types j and $j-$ is made up of portions $S_{i,\,j}$, $S_{i,\,j-}$, $S_{i-,\,j}$, $S_{i-,\,j-}$ whose ratios are given by $S_{i,\,j}/S_{i,\,j-}=v_j/\bar{v}_j$, etc. Then $S_{i,\,j}=S_{ij}'v_i v_j/[(v_i+\bar{v}_i)(v_j+\bar{v}_j)]$, $S_{i,\,j-}=S_{ij}'v_i\bar{v}_j/[(v_i+\bar{v}_i)(v_j+\bar{v}_j)]$, etc. By the previous analysis, $S_{ij}'=b(v_i+\bar{v}_i)(v_j+\bar{v}_j)$; (25) follows at once.

[22] N. Akulov, Zeits. f. Physik **69**, 78 (1931).

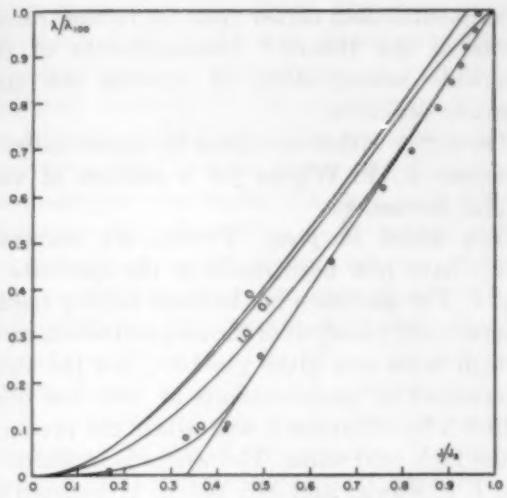

FIG. 2. Magnetostriction of iron crystal magnetized in [100] direction. Curves have been calculated theoretically by formulas (26) and (30); the number next to each curve is the corresponding value of α/β. Curve 1 coincides with Heisenberg's, curve ∞ with Akulov's. Circles are Webster's experimental values.

The curves obtained by either method agree with Kondorsky's and differ from those of the statistical theory ($\alpha=\beta$ in (26)) in that the [100] curve rises initially to a maximum equal to 9/8 the value for $j=0$. Measurements of the reversible susceptibility of crystals should therefore show whether the relation $\alpha\ll\beta$ holds.

None of these formulas are applicable to the specimens measured by Williams.[23] The initial susceptibilities in directions [100], [110], [111] for these specimens were in the ratios 6 : 3 : 2, a fact that can be explained only by assuming that every domain is magnetized along one of the [100] directions nearest the specimen axis. If this assumption is made, the observed ratios can be explained by assuming either no grouping and $\alpha=\beta$ (statistical theory)[6] or grouping and $\alpha\gg\beta$.[11] Kondorsky, accepting the grouping hypothesis, explains the large α in this case as measuring an *irreversible* initial susceptibility. Until measurements of the reversible susceptibility have been made, no conclusion seems possible. The two sets of assumptions give identical curves for reversible susceptibility as a function of j.

The magnetostriction may be calculated as a function of magnetization for the [100] and [110] cases considered before, from the equations for j as a function of x together with[1, 22]

$$\lambda/\lambda_{100}=\tfrac{3}{2}x-\tfrac{1}{2}. \tag{30}$$

For $\alpha=\beta$, with no grouping, this gives Heisenberg's[1] curves; for $\alpha\gg\beta$ it gives Akulov's,[22] which are also obtained if the 180° inversions are assumed to be completed first by an irreversible process. These and several other cases are plotted in Fig. 2, together with Webster's[24] experimental values (with $J_s=1750$, $\lambda_{100}=19.5\times10^{-6}$, the values used by Heisenberg). The curve $\alpha=10\beta$ follows the experimental data more closely than either Heisenberg's or Akulov's, but the data are not sufficiently precise to make this of much significance.

Data on reversible susceptibility, taken if possible on crystals with a large enough demagnetizing factor to insure distribution of the domain magnetizations among all possible directions, are highly desirable. The reversible susceptibility curves for $\alpha\ll\beta$, $\alpha=\beta$, and $\alpha\gg\beta$ differ much more than the magnetostriction curves.

(b) More general relations

Assumption (10a) seems a thoroughly reasonable one, even if (10b) does not hold. The fact that one of these necessitates the other is a result of the previous assumptions, some of which are much more arbitrary than (10a). In particular, assumptions (5) to (9), leading to the relation $p_{ij}=A_{ij}v_iv_j$, are open to question. If these are abandoned and (10a) is retained, (10b) no longer follows, but Eq. (8) now gives

$$\delta v_i=\sum_{j\neq i}p_{ij}\delta(u_j-u_i), \tag{31}$$

where the p_{ij}'s are functions of the u_i's, with $p_{ji}=p_{ij}$. Hence $\partial v_i/\partial u_j=\partial v_j/\partial u_i$, and there is a function ϕ such that $\partial\phi/\partial u_i=v_i$. This function is arbitrary except for the one condition $\sum_i\partial\phi/\partial u_i=1$. If $\phi=-(1/A)\log\psi$ and $u_i=-(1/A)\log\xi_i$, where A is any convenient constant of the proper dimensions, this becomes $\sum_i\xi_i\partial\psi/\partial\xi_i=\psi$, showing that ψ is a homogeneous function of degree 1 in the ξ_i's. Thus

$$v_i=-(1/A\psi)\partial\psi/\partial u_i, \tag{32}$$

[23] H. J. Williams, Phys. Rev. **52**, 1004 (1937).

[24] W. L. Webster, Proc. Roy. Soc. **A109**, 570 (1925).

where ψ is a homogeneous function of degree 1 in the quantities e^{-Au_i}. The result obtained in §3 corresponds, with proper choice of A, to the case of a *linear* function.

These examples illustrate the greater flexibility of the present theory as compared with the statistical model.

§5. Conclusion

It has been shown that the equations previously obtained by means of an artificial model may also be obtained by a detailed analysis of the process of reversible boundary displacement. The necessary assumptions have been stated explicitly, and it is now possible to investigate the effect of modifications in these assumptions. The agreement with experiment is surprisingly good in view of the large number of assumptions that must be made in order to make the mathematics manageable.

Although more theoretical work will be necessary in the future, it may be fairly asserted that the immediate need is for more and better experimental data rather than for further refinements of the theory.[25] Measurements of the reversible susceptibility of crystals are particularly desirable.

The writer wishes to express his appreciation to Professor E. P. Wigner for a number of very helpful discussions.

Note added in proof: Preliminary measurements have now been made on the specimen of Fig. 1. The specimen has become slightly harder magnetically; analysis of the magnetization curve at high fields now gives $\chi_0 = 19.7$, and the value determined by measurements at very low fields is 20.3. The difference is well within the precision of the high field value. The writer is indebted to Mr. J. L. Fowler and Mr. W. M. Woodward for assistance in these measurements, and to Professor S. L. Quimby of Columbia University for the loan of the specimen.

[25] There is need, however, for further theoretical study of *irreversible* boundary displacement. Some progress in this direction has been made by W. Döring, reference 14, and by E. Kondorsky, Physik. Zeits. Sowjetunion **11**, 597 (1937); Comptes rendus Acad. Sci. U.R.S.S. **20**, 117 (1938).

MARCH 15, 1939 PHYSICAL REVIEW VOLUME 55

The Noncubic Growth of Single Crystals of Silver by Condensation from Vapor

J. H. Howey
*Georgia School of Technology, Atlanta, Georgia**

(Received January 16, 1939)

The condensation of silver vapor upon solidified, spherical drops of silver has been found to produce straight, thin, single-crystal needles of silver under certain conditions. The formation of the drops and the subsequent growth of the needles was a continuous process accomplished by condensing the vapor in vacuum upon an iron surface as that surface was cooling from above the melting point of silver to an equilibrium temperature just below the melting point. The shape and crystalline orientation of the needles indicate that they are the result of a nucleus growing by condensation much more rapidly in a certain ⟨110⟩ direction than in other directions, including other ⟨110⟩ directions.

IT is known that certain metals such as copper sometimes crystallize in the form of filaments or dendrites although the solid form of the metal possesses cubic symmetry.[1] The growth of small single-crystal silver needles or spikes by condensation in vacuum as here described is of interest because it furnishes an additional test for any theory that may be advanced to explain the filamentary growth of cubic crystals.

The procedure by which the crystals here described were grown may be made clear by reference to Fig. 1 which shows a part of the

* The work here reported was done at Sloane Physics Laboratory, Yale University, New Haven, Connecticut.

[1] A photograph showing evidence of dendritic growth in a single crystal of copper is given by A. B. Greninger, Am. Inst. Min. and Met. Eng., Tech. Pub. 596 (1935).

evaporating furnace. About one gram of commercial fine silver (D) was placed on a layer of alundum grain in the bottom of a cylindrical alundum crucible (C). It was found impossible to grow the spikes unless the crucible and sand had been used several times and it was also necessary to repulverize the sand each time to eliminate the effect of a slight sintering. The importance of having loose sand was probably due to the fact that the rate of evaporation depended upon the presence of the sand. Partially evaporated drops of silver left on the sand were always found to be covered over more or less with a coating of the sand. An iron cap (B) fitted into the top of the crucible. The heating element of the vacuum furnace consisted of a $\frac{5}{8}$-inch tube (A) formed from molybdenum sheet 0.005 inch thick. The tube was split along its length as shown so that the heating current (150 amp. a.c.) passed up through one-half of the tube and down through the other. The water-cooled current-leads (E) served for mechanical support and extended out through the furnace walls (not shown) for external connections.

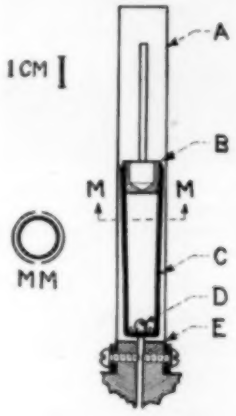

FIG. 1. Diagram of crucible.

After the assembly and evacuation of the furnace the heating current was turned on, heating the iron cap of the crucible to about 1200°C while the silver in the lower end of the crucible near the current-leads remained relatively cold. After this preliminary bake-out of the cap, which lasted about seven minutes, the crucible was raised by an external control until the top of the crucible was above the top of the heating element, without interrupting the heating current. In this final position the bottom of the crucible became hot enough that the entire charge of silver would evaporate in about 25 minutes. The sequence of events was such that the silver started to evaporate before the cap had fallen to its equilibrium temperature and the first silver to condense on the iron cap condensed as liquid in little spherical droplets. The final equilibrium temperature was not known exactly, but it was probably from 25 to 75 degrees centigrade below the melting point of silver. By adjusting both the heating current and the final position of the crucible, the vapor pressure of the silver and the temperature of the cap on which the silver was condensing could be varied independently.

The concentration and nature of impurities is not known. The pressure in the furnace, outside of the crucible, at the time of deposit was about 2×10^{-5} mm of mercury as measured on an ionization gauge calibrated for air. In most of the work, a high speed Apiezon oil diffusion pump was used without any cold trap for vapors other than metal walls cooled with tap water. Some of the work was done with a mercury diffusion pump and a large liquid-air trap next to the furnace and similar results were obtained with both pumping arrangements.

If the vapor pressure of the silver were relatively low, the drops condensing on the iron cap developed octohedral facets as they grew after solidification. The orientation of these facets as determined by the reflection of light showed that each solidified drop was a single crystal and often-times adjacent drops over a considerable area would exhibit a common crystalline orientation. If the vapor pressure was relatively high, the solidified droplets retained a roughly spherical form as they grew into larger globules, and rounded warts and sometimes spikes would grow out from the rounded surface of the globule. A photograph of such a deposit on the flat bottom face of an iron cap is shown in Fig. 2, A. The actual size of the globules and spikes may be judged by comparison with the diameter of the cap which was about one cm. Judging from the rate of deposit, the vapor pressure which was suitable for the growth of the spikes was such that the mean free path of the atoms was small compared to the dimensions of the crucible.

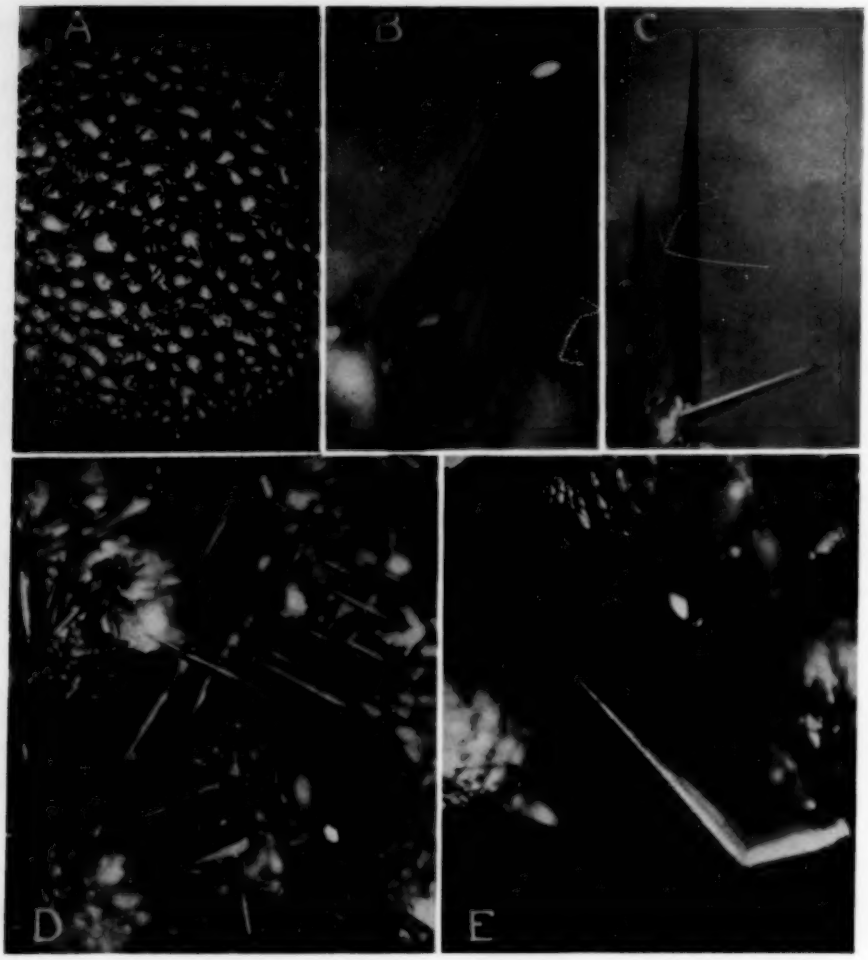

FIG. 2. A, general appearance of globules and spikes of condensed silver. B and C, magnified view of spikes. D, spikes growing from a single globule are crystallographically related. E, spike showing abrupt change in direction of growth.

Also the directions of growth and the shapes of the spikes show no appreciable evidence of a directional effect due to the upstreaming vapor.

Figure 2, B and C show some of the spikes under higher magnification. The actual length of the longer spikes in these photographs is about 1.5 mm. In view of the single-crystal nature of the spikes being so much emphasized by their linear perfection, it is surprising that the sides are so smoothly rounded. Fig. 2, D shows the profusion with which the spikes grew in some cases and also shows that the directions of spikes coming from a single globule are crystallographically related. The diameter of the underlying globules visible in the background was approximately one mm. About five percent of the spikes have abrupt changes of direction similar to the one shown in Fig. 2, E. It is rather obvious from the appearance of the bend in this case that the whole spike must be a single crystal or a pair of twins with the directions of growth before and after the bend crystallographically related in either case. Abrupt changes in direction both more and less than 90° have been observed but no forking or branching has been found.

The conditions which control the nature of the filamentary growths appear to be rather critical. In fact, attempts to grow spikes of any description were only about 30 percent successful even when the conditions of deposit were duplicated as closely as possible with the apparatus used. More than 100 runs made with slight intentional

variations in the conditions of deposit were uniformly unsuccessful, as far as the production of any spikes was concerned.

X-ray diffraction photographs taken of two different spikes showed that those spikes were single crystals with the ⟨110⟩ direction parallel to the spike axis. Additional evidence of this same crystalline orientation has been found by observing the angles between the linear portions of spikes showing abrupt bends and between pairs of spikes growing from the same globule. Seventeen angles between the prolongation of the original axis and the new direction were measured giving the following values in degrees: 38, 50, 52, 58, 59, 62, 63, 65, 67, 69, 69, 75, 80, 107, 112, 114, 139. Ten angles between pairs of spikes growing from a common nucleus were measured giving the following values in degrees: 52, 59, 60, 65, 68.5, 71, 100.5, 105, 107, 114. The possible error of these values is as much as 10° for some of the angles. The possible angles between two ⟨110⟩ directions in a single crystal are 60° and 90°. If twinning occurs as a rotation of the crystal axes through 180° about an axis of form ⟨111⟩, angles of 70.5° and 33.5° are also possible between two ⟨110⟩ directions in adjacent twins: Of the 27 observed angles, 18 are consistent with an assumed possible angle of 60°, 25 are consistent with assumed possible angles of either 60° or 70.5° and the remaining three are consistent with an assumed possible angle of 33.5°.

The ⟨110⟩ direction in a silver crystal is a direction in which there are linear rows of atoms piled one against the next with a minimum of distance between centers. The fact that such a direction is the direction for most rapid growth by condensation and the absence of branching lend support to the idea that the filamentary growth might be due to the existence in a silver atom of a unique direction along which the available interatomic binding forces were greater than in any other. According to this idea, a nucleus of a spike would start as a row of atoms having a stronger field of force at the end than along the sides. Spikes made up of parallel strings of atoms would grow more rapidly at the end due partly to re-evaporation from the sides and partly to the motion of condensing atoms around on the surface of the solid phase. If one of the six equivalent directions of form ⟨110⟩ in the ideal face-centered cubic crystal becomes distinguishable from the others, the crystal structure can no longer be cubic. However the actual crystal structure can perhaps be most simply described as a slightly distorted cubic structure. The elliptical cross section of some of the spikes, such as the one shown in Fig. 2, B, is suggestive of a secondary preferred direction.

The possibility that the interatomic forces in a crystal such as silver might be greater in some one direction than in any other has been discussed by Bitter.[2] There is a possible connection between the phenomenon observed here and some observations of others. Greninger[1] found that adjacent mosaic blocks in a single crystal of copper which was solidified from the melt most frequently had a common ⟨110⟩ direction. That might be taken to mean that the atoms have a strong tendency to maintain a certain ⟨110⟩ direction intact throughout a considerable volume. Andrade and Martindale[3] have found evidence by means of polarized light that very small fibrous crystal grains which were obtained under certain conditions were uniaxial. These workers considered this uniaxial property to be due to the small cross section of the fibrous grains, but it might also be explained on the basis of an inherent uniaxial distribution of the interatomic forces.

The above explanation of the filamentary growth of the silver crystals is made as a suggestion. Definite conclusions cannot be drawn without further study of the structure of the spikes, and of the conditions necessary for their growth. In spite of the unfinished state of the investigation it is thought that the observations here reported may be of sufficient interest to justify publication. The author would welcome any independent investigations of the same subject that might be undertaken, particularly since the work has been indefinitely interrupted.

[2] F. Bitter, Phys. Rev. **42**, 731 (1933).
[3] E. A. da C. Andrade and J. G. Martindale, Nature **134**, 321 (1933).

LETTERS TO THE EDITOR

Prompt publication of brief reports of important discoveries in physics may be secured by addressing them to this department. Closing dates for this department are, for the first issue of the month, the eighteenth of the preceding month, for the second issue, the third of the month. Because of the late closing dates for the section no proof can be shown to authors. The Board of Editors does not hold itself responsible for the opinions expressed by the correspondents.

Communications should not in general exceed 600 words in length.

The Doppler Effect and Field Distribution in the Hailer Canal-Ray Tube

Recently C. Hailer[1] has made a systematic study of various forms of discharge tubes in the endeavor to find one that would give a more intense beam of positive ions. Twelve different arrangements of the electrodes were tried, and in some cases thermionic emission from a hot cathode was also employed. The tube shown in Fig. 1 was found by

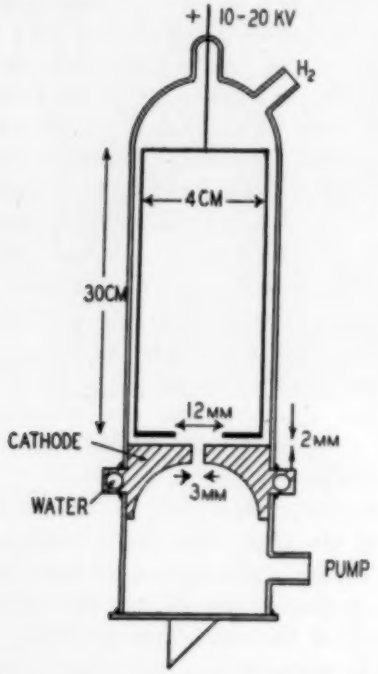

FIG. 1. Hailer canal-ray tube used in observations.

him to be much superior to the others; with this tube he obtained, for example, a positive ion current of one milliampere with 17 milliamperes in the main discharge. He ascribes the increased efficiency to a concentration of the ions in the center of the tube and to an increase in the field just before the cathode.

In this paper observations of the luminous canal-ray bundle in this tube are reported. The luminosity was much more intense than with the ordinary discharge tube. Doppler effect photographs were made, as it was thought possible that the concentration of the field over a short space in front of the cathode might give a homogeneous velocity.[2, 3] This was found not to be the case. The intensity distribution in the displaced wave-lengths showed no appreciable difference from that observed in Doppler effect photographs with an ordinary discharge tube. With 16,000 volts across the tube, most of the radiation in hydrogen, as shown by the Doppler effect at H_β and H_γ is emitted by hydrogen atoms which have been accelerated by potentials that vary from 150 to 5000 volts. It is well known that the intensity in the Balmer series lines from the atoms in motion is very small for velocities above that corresponding to 3000 volts, although some intensity is emitted from atoms with energies up to 50,000 volts or more.[4]

The field distribution near the cathode was measured by observing the Stark effect at H_β and H_γ at right angles to the rays. With 16,000 volts applied to the tube displacements of 6.15A were found on photographs at H_γ. The intensity was so great that the splitting up of the lines could be easily observed visually. The field distribution as computed is shown in Fig. 2, curve A. For comparison the field distribution observed by Krefft in an ordinary discharge tube is shown in curve B. In curve A the total potential was 16,000 volts, while in Krefft's tube the potential was 47,000 volts. For comparison his curve B is plotted with ordinates reduced in the ratio of the applied potentials. There is thus a concentration of the field intensity in the neighborhood of the cathode as suspected by

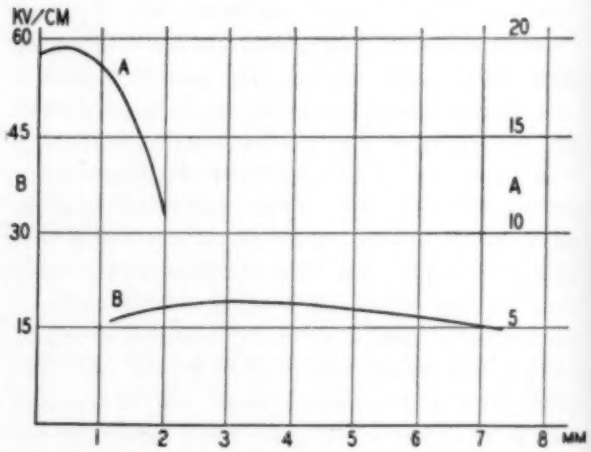

FIG. 2. Field distribution at various distances in front of cathode. A with Hailer tube showing concentration near cathode. B, Krefft's observations with ordinary tube. Ordinates adjusted in ratio of the total potential on tube.

Hailer. The total potential drop in the two millimeter space as computed from the Stark effect was however only 3000 volts, when the applied potential was 16,000 volts. This is approximately what would be expected from the theoretical electrostatic field with the opening used. Since the larger part of the potential drop occurs inside the hollow anode we would expect to find ions of a great range of velocities, and thus explain the large spread in velocities observed in the Doppler effect photographs.

C. W. SHERWIN
A. J. DEMPSTER

Ryerson Physical Laboratory,
University of Chicago,
Chicago, Illinois,
February 24, 1939.

[1] C. Hailer, Wiss. Veroffentlichungen der Siemens-Werke **17**, 115 (1938).
[2] H. F. Batho and A. J. Dempster, Astrophys. J. **75**, 34 (1932).
[3] H. E. Ives and G. R. Stilwell, J. Opt. Soc. Am. **28**, 215 (1938).
[4] H. Krefft, Ann. d. Physik **75**, 75, 513 (1924).

Are There Multiple Charged Primary Particles in Cosmic Radiation?

William P. Jesse and Piara S. Gill have recently reported[1] a considerable latitude effect for very large cosmic-ray bursts (about 30 percent) the existence of which raises most interesting questions as to the manner of its origin. If, as suggested by their note, the burst frequency is a function of geomagnetic, and not of geographic, latitude, the implication is that this latitude effect results from the action of the earth's magnetic field on charged primary particles, essentially in the same manner as for the total radiation. It seems, however, quite certain that the energy involved in a large burst is at least of the order 10^{11} ev, or greater, so that, if the whole energy of such a burst is carried initially by a single primary particle, that primary cannot be an electron or a proton. This follows because the allowed cone for either is already completely open at all latitudes for energies about 7×10^{10} ev, and hence there cannot be any latitude effect for protons or electrons of energy 10^{11} ev. This suggests the very interesting possibility[2] that the primary particles responsible for the latitude effect of large bursts might carry a multiple of the electron's charge and presumably have large mass. For instance, stripped nuclei of atomic weight 11 to 13, even 16, and number 5 or 7, even 8, (e.g., boron, carbon, or even oxygen) of energy around 10^{11} ev would show a latitude effect of 30 percent (which would be very sensitive to a change of charge but rather independent of mass).

Doubtless there are still other alternatives that we wish to mention briefly. One, suggested by recent developments in nuclear physics, is that the energy of the burst is not the original energy of the primary particle. In this case the primaries might well be electrons of energy around 2×10^{10} ev. The problem would then arise as to why such energies give rise to bursts. Another, rather unlikely, alternative is that the observed latitude effect is not related to geomagnetism at all, but has to do, for instance, with atmospheric phenomena such as the bulging of the atmosphere at the equatorial belt as a consequence of the earth's rotation. Although this alternative is practically ruled out by the magnitude of the observed effect, the burst frequency should be, in this case, a function of geographic and not of geomagnetic latitude, which could be easily tested by comparing the measurements taken at two stations at the same geographic but different geomagnetic latitudes.

M. S. VALLARTA

Massachusetts Institute of Technology,
Cambridge, Massachusetts,
February 27, 1939.

[1] W. P. Jesse and P. S. Gill, Phys. Rev. **55**, 414 (1939).
[2] The possibility of a latitude effect for bursts, and the implication brought out here, were already discussed by Lemaitre and the writer at the Zurich Congress on cosmic-rays and nuclear physics, July, 1936.

NH Bands in the Night Sky Spectrum

In J. Gauzit's[1] recent list of ultraviolet radiations in the night sky spectrum there are two bands which are of particular interest when compared with a large number of observations made by me on the high pressure afterglow in nitrogen. These bands are λ3374 and λ3361, and Gauzit assigns to them the intensities four and two, respectively, on a list on which the strongest band has an intensity of five. On many of my afterglow spectra, a strong head appears on the short wave-length side of the strong second-positive band λ3371. This band has a wave-length of about λ3360 and a direct comparison with some old electrical discharge spectra on which both the 3240 and 3360 NH bands are present shows definitely that we are observing the NH band at λ3360 on our afterglow plates. The λ3240 band has not yet been detected in the afterglow, and no band of this wave-length appears on Gauzit's list. In view of these observations we propose to identify the λ3374 and λ3361 bands in the light of the night sky as the two Q branches of the (0, 0) and (1, 1) bands of NH at λ3360 and λ3370. This identification would be a sound one even if heavier exposures fail to reveal the NH band in the light of the night sky on my plates, since the λ3240 NH band requires more energy for its excitation than do λ3360 and λ3370, and there are a number of observations in which λ3240 is absent even though λ3360 appears with great intensity. These points have been adequately discussed by R. W. B. Pearse.[2]

The above identification is supported by the added observation that the λ3360 band increases in intensity as the relative intensity of the auroral ultraviolet line of nitrogen, λ3466.3, increases. This result indicates that a direct combination between atomic nitrogen and hydrogen takes place in the high pressure afterglow. Thus, the presence of NH bands in the light of the night sky, together with this observation, is added evidence for the existence of atomic nitrogen in the upper atmosphere.

JOSEPH KAPLAN

University of California,
Los Angeles, California,
February 16, 1939.

[1] J. Gauzit, Ann. D'Astrophysique, 1re Année, 334 (1938).
[2] R. W. B. Pearse, Proc. Roy. Soc. **A143**, 112 (1933).

The Spectroscopic and Free Electron Values of e/m

In a recent letter[1] on the present status of the value of e/m a conclusion is reached that the spectroscopic and free electron methods yield values of e/m which differ by only 0.0006×10^7 abs. e.m.u. or just the average deviation to be expected from the assigned probable errors. This conclusion is reached by including the writer's[2] x-ray refraction value of e/m with the spectroscopic results. The classification of the x-ray refraction value as a spectroscopic result was made by the writer[2] in discussing bound and free electron values of e/m and this has been followed in the above letter.[1] This value of $e/m=1.7601\pm0.0003$ is not only much higher than any of the spectroscopic but also has the smallest probable error of any values in this group. The high weight thus accorded this value has the effect of raising the general average of the spectroscopic results into approximate agreement with the free electron values.

The x-ray refraction measurement, however, is in reality a free electron result and should not be averaged with the spectroscopic results. The refracting electron is bound to a particular atom during the entire process of refraction, but the frequency of the forced vibration is so much greater than the natural frequency of the electron that it acts almost completely as a free electron. The x-ray refraction process is thus entirely different from that involved when one evaluates e/m spectroscopically by atomic energy level transitions.

If we use the recalculated[1] values and divide them into two groups, the results are given in Table I.

TABLE I.

Spectroscopic Results	
Separation of He and H lines	$1.7601_8\pm0.0008$[3]
" " $H\alpha$ and $D\alpha$ "	$1.7581_4\pm0.0004$[4]
" " " " " "	$1.7579_3\pm0.0004$[5]
" " " " " "	1.7592 ±0.0005[6]
Zeeman effect	1.7569 ±0.0007[7]
Weighted average	$1.7583_1\pm0.0002_8$
Free Electron Results	
Direct velocity measurement	1.7610 ±0.0010[8]
" " "	1.7588 ±0.0009[9]
Magnetic deflection	1.7597 ±0.0004[10]
Crossed fields	1.7581 ±0.0013[11]
X-ray refraction	1.7601 ±0.0003[2]
Weighted average	$1.7598_8\pm0.0001_7$

The discrepancy between the free electron and the spectroscopic values is 3.5 times the sum of the probable errors and statistically there is less than one chance in 10^9 of the free electron value being as low as the spectroscopic. The ratio of the external to internal consistency for the spectroscopic results is 1.24 and for the free electron 0.77. Both of these indicate a reasonable estimate of probable errors, and consistency of results in each group. By considering the two weighted averages, the situation is found to be just as serious as that which led Birge[12] in 1929 to retain two values of e/m.

In seeking a cause for the discrepancy, one is impressed by the consistency (0.77) of the free electron results which are obtained from four entirely different experimental and theoretical methods. The spectroscopic result obtained by means of Houston's new method of analysis[13] is higher than is obtained by the usual spectroscopic method of analysis, but is still considerably lower than seems consistent with the free electron value. The Zeeman effect gives a very low value. The need for further experimental work on the value of e/m and a critical analysis of the theories involved is apparent.

As long as we have no direct evidence for rejecting one or the other of these results, the value of e/m that should be recommended for use in calculation is the average of the two results. In such a case the probable error should be sufficient to include both spectroscopic and free electron results. This value of e/m is

$$e/m=(1.7591\pm0.0008)\times10^7 \text{ abs. e.m.u.}$$

J. A. BEARDEN

Johns Hopkins University,
Baltimore, Maryland,
February 25, 1939.

[1] R. T. Birge, Phys. Rev. **54**, 972 (1938).
[2] J. A. Bearden, Phys. Rev. **54**, 698 (1938).
[3] W. V. Houston, Phys. Rev. **30**, 609 (1927).
[4] C. D. Shane and F. H. Spedding, Phys. Rev. **47**, 33 (1935).
[5] R. C. Williams, Phys. Rev. **54**, 568 (1938).
[6] W. V Houston, see reference 1.
[7] L. E. Kinsler and W. V. Houston, Phys. Rev. **46**, 533 (1934).
[8] C. T. Perry and E. L. Chaffee, Phys. Rev. **36**, 904 (1930).
[9] F. Kirchner, Ann. d. Physik **12**, 503 (1932).
[10] F. G. Dunnington, Phys. Rev. **52**, 475 (1937).
[11] A. E. Shaw, Phys. Rev. **54**, 193 (1938). Shaw's published value 1.7571 was calculated on the basis of international units. The present value is recalculated using absolute units.
[12] R. T. Birge, Rev. Mod. Phys. **1**, 1 (1929).
[13] W. V. Houston, Phys. Rev. **51**, 446 (1937).

The Actinium Series of Radioactive Elements and Their Influence on Geological Age Measurements

A. O. Nier has just published the results of his excellent investigations of the isotopic composition of uranium[1] and radiogenic leads[2] of different geologic origin.

His results completely and finally disprove the evidence, based on chemical atomic weight determinations, against the actino-uranium theory and the necessity of correcting geologic age measurement for the actinium series. They fully support the conclusions drawn in the author's paper,[3] presented before the Geochemistry Symposium at the Rochester Meeting of the American Chemical Society (September, 1937), that the reliability and accuracy of orthodox chemical atomic weight determination is substantially below those based on mass-spectrographic measurements and is insufficient to show the spread in atomic weights of leads expected from theory. In particular the "puzzling" Bedford crystalline lead proved to be in full accord with the predictions of theory.

Only two discrepancies, stressed by Nier, need be discussed here: The *first* is the extremely old (age 1.5–2.10^9a) Manitoba uraninite lead, which shows an AcD : RaG ratio far above our theoretical curve. However, this possibility was envisaged in our 1933 paper[4] in the following paragraph:

"Data on the oldest obtainable uranium leads from minerals unaltered as far as possible are especially desirable, to test the applicability of the actinium D: radium G ratio formula beyond a billion years. (The Manitoba uraninite, for instance, discovered by H. V. Ellsworth, with a lead/uranium = 0.27 should prove worth while.) They might also be interesting in another respect: In case the experimental curve should deviate in that range from our theoretical it might indicate the existence of a second actinouranium isotope (still a possibility as we mentioned in paper 1), not yet in equilibrium with our present isotope. The Rutherford-Soddy disintegration theory allows one to calculate in a simple way the ratio of actinium D to radium G for different possible cases; it would be, however, premature to discuss these points at the present time."

Assumption of the genetic scheme:

$$\mathrm{AcU}^{239} \xrightarrow{\alpha,\ \beta,\ \beta} \mathrm{AcU}_7^{235} = 7.10^5 a$$

with a half-life value of the order of 10^8 years for AcU^{239} and a reasonable concentration in uranium during the early history of the earth's crust would account for the observed facts, i.e., the present absence of AcU^{239} and an excessively high Pb^{207} : Pb^{206} ratio in very old minerals.

The *second* discrepancy is between the activity ratio, R, of Nier = 4.6 percent and the directly determined values of 4.0–4.1 percent (Grosse (1932) = 4.0, E. Gleditsch and Foyn (1934) = 4, Francis and Da Tchang (1934) = 4.1) from the Pa : U ratio. However, the magnitude of this disagreement, i.e., $\leq$10 percent of the actual value, is not discomforting if one remembers that in a number of careful investigations previous to 1932 a much greater spread (B. B. Boltwood (1908) 8 percent; O. Hahn and L. Meitner (1919) 3 percent; G. Kirsch (1920) 4.2 percent; W. G. Guy and A. S. Russell (1923) 3.1 percent; A. S. Russell and W. P. Widdowson (1923) 2.9 percent; A. Piccard and E. Kessler (1923) 5 percent) was observed.

Although in a number of cases the errors were due to incomplete separation of protoactinium, we are reasonably sure this was not the case in our own $Pa - ZrP_2O_7$ precipitations, which were checked for quantitative separation. Errors may have also been introduced by the different corrections required, such as range of particles or thickness of film. In our own measurement inaccuracies *may have* been introduced by inadequate correction for the self-absorption of α-particles in the ZrP_2O_7 film. It is perhaps significant that the results in Mme. Curie's laboratory average 4.0 percent for the tantalum method and 4.2 percent for the ZrP_2O_7-method. Further careful determinations will be required to decide the best value, but we believe no fundamental disagreement with Nier's value exists.

If Nier's value is correct it follows that the AcU^{235}-content of uranium equals 0.7_1 percent by weight and the weight of protoactinium associated in any uranium mineral with 1 g of Ra is increased to 0.9_3 g.

ARISTID V. GROSSE

Department of Chemistry,
University of Chicago,
Chicago, Illinois,
February 20, 1939.

[1] A. O. Nier, Phys. Rev. **55**, 150 (1939).
[2] A. O. Nier, Phys. Rev. **55**, 153 (1939).
[3] A. V. Grosse, see Abstracts of Rochester or 94th Meeting of the American Chemical Society, page 23.
[4] A. V. Grosse, J. Phys. Chem. **38**, 487 (1934).

On the Mass of the Mesotron

Since we published[1] the results of mass determination of the mesotron, the existence of which had theoretically been foreseen by Yukawa, we have been continuing the same experiments with the Wilson cloud chamber.

During last September we obtained a photograph shown in Fig. 1. A lead bar 5 cm thick was mounted in the middle

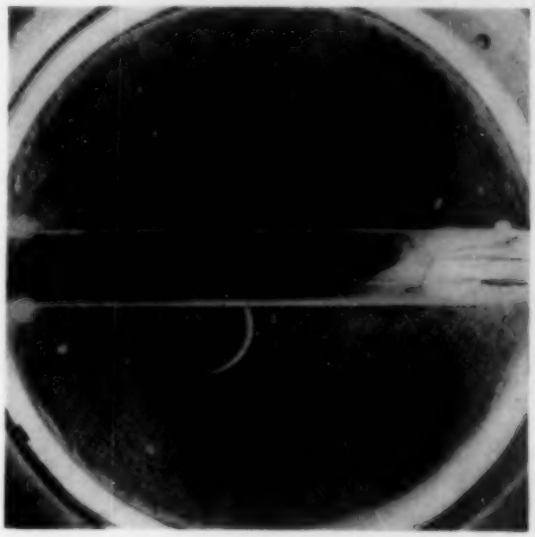

FIG. 1. Wilson track of a mesotron. $H = 12{,}600$ oersteds. $H\rho = 3.88 \times 10^4$ oersted·cm. Observed range = 6.15 cm.

of the chamber 40 cm in diameter, which is filled with air and alcohol vapor, and placed in a magnetic field of about 12,600 oersteds. The operation of the chamber was controlled by two Geiger-Müller tube counters mounted immediately above the chamber. The distance between the counters was about 15 cm. Above the counters was placed a lead block 20 cm thick.

A negatively charged particle of $H\rho = (3.88 \pm 0.08) \times 10^4$ oersted-cm seems to have been created within the lead bar by a certain non-ionizing agent and was brought to rest in the gas of the chamber, the observed range being 6.15 cm. By taking into account the pressure of the gas, which was between 1.23 and 1.30 atmospheres at 25°C, and a possible inclination of the track with respect to the plane of the chamber, we estimate its range in air of 15°C and 760 mm to lie between 7.3 and 8.1 cm. According to the range-energy curve for the proton given by Livingston and Bethe[2] we calculate the mass of the particle by using the above values of $H\rho$ and range and obtain

$$M_m = (170 \pm 9)m, \qquad (1)$$

where m is the mass of the electron.

At the end of the range the photograph shows no sign of an electronic track, which would prove the disintegration of the mesotron.

We have recently re-examined the old photograph mentioned in our preceding paper[1] and obtained the following values. A positively charged particle of $H\rho = (7.4 \pm 0.1)$

$\times 10^5$ oersted·cm passes through a lead bar 3.5 cm thick at an angle of about 47°, the length of the path inside lead thus being 4.8 cm. After traversing the lead bar, $H\rho$ becomes $(5.0\pm0.1)\times10^5$ oersted·cm.

On assuming the mass of the particle, we can calculate its initial and final energies and thus find the loss of energy due to collisions within lead. On the other hand this energy loss can be calculated theoretically, for example, according to Bloch's formula,[3] if we use the assumed mass and the initial energy. The mass of the particle can be adjusted in such a way as to bring both values of the energy loss to agreement. In this manner we formerly obtained with the old data of preliminary measurements

$$M_m=(180\sim260)m. \tag{2}$$

In these calculations we assumed for Bloch's formula the maximum energy W transferred in a direct collision from the particle to a free electron to be $2mv^2$ according to the nonrelativistic theory, where v is the velocity of the particle. In our case, however, we ought instead to have used a relativistic value

$$W=\frac{2mM_m(1+\eta)E}{m^2+2mM_m\eta+M_m^2}, \tag{3}$$

as was given by Bhabha,[4] where E is the initial energy of the particle, $\eta=(1-v^2/c^2)^{\frac{1}{2}}$, and c is the velocity of light. If we do this and use the above data of the new measurements, we obtain

$$M_m=(180\pm20)m, \tag{4}$$

which is in better agreement with the value (1).

A more detailed paper will be published in the Scientific Papers of this Institute.

Y. NISHINA
M. TAKEUCHI
T. ICHIMIYA

Cosmic-Ray Sub-Committee of Japan Society for the Promotion of Scientific Research,
Institute of Physical and Chemical Research,
Tokyo, Japan,
January 31, 1939.

[1] Y. Nishina, M. Takeuchi and T. Ichimiya, Phys. Rev. **52**, 1198 (1937).
[2] M. S. Livingston and H. A. Bethe, Rev. Mod. Phys. **9**, 268 (1937).
[3] Cf. W. Heitler, *The Quantum Theory of Radiation* (Oxford, 1936), formula (1), p. 218.
[4] H. J. Bhabha, Proc. Roy. Soc. **A164**, 255 (1938).

The γ-Rays of Radium E

At the Chicago meeting of the American Physical Society, Professor Jauncey[1] put forward an interesting interpretation of the results of experiments of Gray and Hinds[2] on the so-called γ-rays of radium E. He believes that these rays may be due to what he terms internal scattering, a process in which a β-ray in escaping from the disintegrating atom dislodges an orbital electron, and thus gives rise to characteristic x-radiations, the γ-rays of radium E.

I have no doubt that this process takes place but to a much smaller extent than imagined by Jauncey. As a result of internal scattering, x-rays characteristic of an atom of atomic number 83 would be emitted and would consist of K, L and M radiations. The M radiation would not enter the measuring instrument under the conditions of our experiment. The L radiation would correspond to what are called the soft γ-rays of radium D. The absorption of these soft γ-rays in aluminum has been found by us. In Fig. 1, three curves are shown. Curve A gives the absorption of the γ-rays of radium E in aluminum. Curve B has been obtained on the assumption that 20 percent of the initial ionization is due to L radiation of atomic number 83. When this is allowed for and subtracted from the ionization intensities in curve A, we get the ionization due to remaining radiation, or curve B.

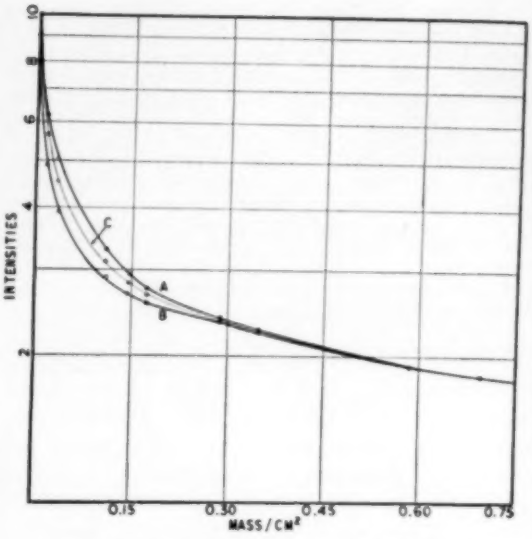

FIG. 1. Absorption of γ-rays of radium E in aluminum.

The slope of any such absorption curve should continually decrease but this is not true in the case of curve B, for it will be seen that the slope increases at about 0.30 g/cm². Consequently L radiation provides less than 20 percent of the initial ionization. Curve C has been obtained by assuming that 10 percent of the initial ionization is due to L radiation. I would say that not more than 10 percent can be due to L radiation. As far as K radiation is concerned it can also be shown that only a small fraction of the harder radiation can be characteristic of an atom of atomic number 83.

Evidently our results have not been interpreted correctly. We believe the spectrum of the γ-rays to be a continuous one. The absorption curve of these rays can be approximately given by a number of exponential terms. We found a fairly close fit by using five, and no special significance was attached to the wave-lengths deduced from these terms. They do give one, however, a very good idea of the type of radiation present and indicate that radium E emits a large number of slow β-rays.

This is shown by the curves in Fig. 2. Curve A gives the variation in intensity of the x-rays produced in aluminum as the mass of the absorbing material is increased. The intensity is a maximum at about 0.05 g/cm² and is 50 percent at about 0.006 g/cm². It is convenient to think of

the β-rays of radium E as consisting of two types; one slow and one fast. A curve similar to curve B which is somewhat arbitrarily drawn, would show the production of x-rays by the fast β-rays, and curve C, the difference between curves A and B, would show the production of x-rays by the slow β-rays. Evidence in support of this method of interpreting the results has since been obtained here by B. W. Sargent in the course of some careful experiments on the absorption in aluminum of the β-rays of radium E and uranium X.

It is our intention to publish a complete description of the experiments which have led us to adopt the view, held

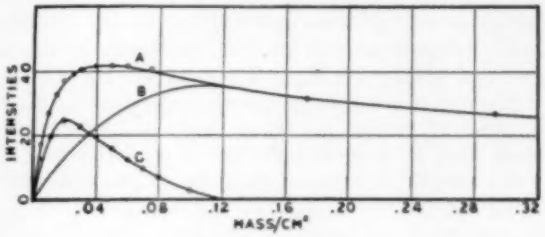

FIG. 2. Production of x-rays in aluminum.

by one of us for many years, that the γ-rays of radium E are, in the main, formed by some of the β-rays as they escape from the nuclei emitting them.

J. A. GRAY

Queen's University,
Kingston, Ontario, Canada,
February 28, 1939.

[1] Jauncey, Phys. Rev. **55**, 237 (1939).
[2] Gray and Hinds, Can. J. Research **16**, 75 (1938).

Low Energy Neutrons from the Deuteron-Deuteron Reaction

In an expansion chamber study of the reaction

$$D+D \rightarrow He^3+n$$

Bonner[1] discovered that the neutrons were not of a single energy. Besides the previously established group of energy 2.50 Mev, a second group of about 1/10 the intensity of the first group and of 1.08 Mev energy was found. Baldinger and his associates,[2] by using an ionization chamber, obtained results in agreement with Bonner's work.

The existence of this low energy group of neutrons suggests that the He^3 nucleus formed simultaneously in the above reaction may be left excited to a level of 1.89 Mev, and a gamma-ray of this energy would be expected when the He^3 falls to its normal state. A search for such a gamma-ray was made by Ruhlig,[3] who found no evidence for it and concluded that not more than one gamma-ray was emitted for every 200 neutrons; this limiting value is in agreement with the work of Kallmann and Kuhn,[4] who studied the deuteron-deuteron reaction by using coincidence counters.

An excited state in He^3 suggests a similar excited level in H^3, but a study of the H^3 and H^1 recoils produced in the above reaction gives no evidence for such a state.[5, 6] The existence of an excited state in either He^3 or H^3 is not in agreement with present nuclear theory, as Share[7] and Schiff[8] have emphasized.

The fact that neutrons also suffer inelastic collisions with heavy nuclei would give rise to neutrons of low intensity spread over a relatively wide range of low energies.[9]

In view of these facts we have made a closer study of the neutrons from the d–d reaction, obtaining 100-kv deuterons with apparatus previously described.[10] The cloud chamber was filled with hydrogen and alcohol vapor and placed about 13 cm from D_3PO_4 target in an aluminum cup, which was substituted for the brass previously used. The low stopping power of the gas in the cloud chamber made it possible to determine whether the low energy neutron spectrum fell to a minimum on the low energy side. Neutrons of energy greater than about two Mev produced recoil protons which passed completely across the chamber.

All proton recoils within 25° of the forward direction which originated in the light beam and within four cm of the chamber wall were tabulated, and 172 such tracks were observed. Of this number, those that remained within the chamber were measured for length and recoil angle. The energies of the low energy neutrons were calculated, and the results are shown in Fig. 1.

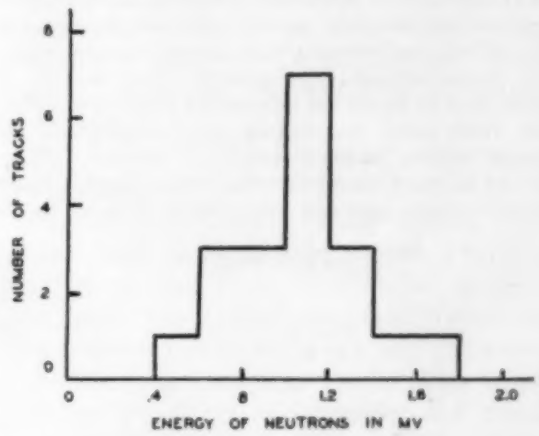

FIG. 1. Low energy neutron spectrum in the deuteron-deuteron reaction.

The stopping power (0.40–0.43) of the gas varies rather rapidly with temperature and with range at low energies; this variation and some uncertainty in determination of recoil angles serve to widen the neutron spectrum found.

The intensity of the low energy group of recoil protons is about $\frac{1}{3}$ that of the high energy group. However, the collision cross section for neutrons of the low energy group, according to the Wigner formula,[11] is approximately twice as great, so that the ratio of the intensities of the two neutron groups is about $\frac{1}{6}$. This neutron group is well defined and of such intensity that it can hardly be ascribed to a group arising from inelastic collisions. The observed energy of 1.1 Mev is in good agreement with Bonner's earlier value.

In order to make certain that the low energy neutrons do not come from some other reaction, photographs were made when deuterons bombarded a target of $H^1_3PO_4$. No recoils of any kind were observed.

It would therefore appear that the expected gamma-ray has been overlooked or that other considerations are necessary to explain the low energy neutrons.

We are grateful to Professor H. A. Wilson for his interest and advice and to Dr. T. W. Bonner for many suggestions.

EMMETT HUDSPETH
HENRY DUNLAP

The Rice Institute,
Houston, Texas,
February 20, 1939.

[1] T. W. Bonner, Phys. Rev. **53**, 711 (1938).
[2] Baldinger, Huber and Staub, Helv. Phys. Acta **11**, 245 (1938).
[3] A. J. Ruhlig, Phys. Rev. **54**, 308 (1938).
[4] H. Kallmann and E. Kuhn, Naturwiss. **26**, 106 (1938).
[5] E. Hudspeth and T. W. Bonner, Phys. Rev. **54**, 308 (1938).
[6] F. E. Myers and L. M. Langer, Phys. Rev. **54**, 90 (1938).
[7] S. Share, Phys. Rev. **53**, 875 (1938).
[8] L. I. Schiff, Phys. Rev. **54**, 92 (1938).
[9] M. S. Livingston and H. A. Bethe, Rev. Mod. Phys. **9**, 158 (1937).
[10] T. W. Bonner, Phys. Rev. **52**, 685 (1937).
[11] H. A. Bethe and R. F. Bacher, Rev. Mod. Phys. **8**, 117 (1936).

Note on the Stopping Power of Hydrogen at Very Low Energies

An experiment has been reported recently[1] on the binding energy of the deuteron, as obtained from low pressure ($H^2_2-H^2_1O$) cloud-chamber observations of proton tracks from photoelectrically disintegrated deuterium. It is desired here to record the information which this experiment yields about the stopping power of hydrogen for (protons of) very low energies.

It can be readily shown that the *average* stopping power of a mixture of n gases at a total pressure P (in cm Hg) is

$$S=\sum_1^n(p_i/76)S_i, \tag{1}$$

$$P=\sum_1^n p_i, \tag{2}$$

where S_i is the *average* stopping power of the ith gas at STP, and where p_i is the partial pressure of the ith gas. By "average" stopping power of a gas, we mean the average value of the stopping power over the path (in the gas) of a charged particle of a given initial energy. For convenience we refer these stopping powers to that of standard air, taken to be unity.

In the experiment mentioned above, $n=2$. Let $i=1$, 2 refer to deuterium and to heavy-water vapor, respectively; then $p_1=P-p_2$. Also, $S_2=S_1+s$, where s is the average stopping power of $\frac{1}{2}O_2$. Thus Eqs. (1) and (2) yield

$$S_1=(76S-p_2s)/P, \tag{3}$$

which is, of course, numerically equal to the average *atomic* stopping power of deuterium relative to the average (atomic) stopping power of air. The experiment mentioned above used $P\leqq 8.0$ cm Hg and $p_2\geqq 2.7$ cm Hg. Fifteen proton tracks (mean of the initial energies being 0.22 Mev) were observed, having an average length of 2.9 cm; these protons have a range of 0.228 cm in air;[2] therefore, $S=0.228/2.9=0.079$. Substituting in Eq. (3), we thus find

$$S_1\geqq 0.35, \tag{4}$$

if we take $s=1.2$.

This value 0.35 for S_1 for (proton) energies $\leqslant$0.22 Mev appears rather high; but in view of the fact that the stopping power of hydrogen increases[3] from 0.20 at about 3 Mev to 0.25 at about 0.6 Mev, it is probably not much higher than would have been expected. This experimentally determined value of S_1, through the (integral) relation between the energy and range of a particle and the stopping power of the gases through which the particle passes, constitutes a *bound* on the variation of the stopping power of hydrogen with energy for (proton) energies $\leqslant$0.22 Mev.

F. T. ROGERS, JR.

The Rice Institute,
Houston, Texas,
February 2, 1939.

[1] F. T. Rogers, Jr., and M. M. Rogers, Phys. Rev. **55**, 263 (1939).
[2] H. A. Bethe, Phys. Rev. **53**, 313 (1938).
[3] M. S. Livingston and H. A. Bethe, Rev. Mod. Phys. **9**, 245 (1937)

Proceedings of the American Physical Society

Minutes of the Washington, D. C. Meeting, December 27–29, 1938

THE 40th Annual Meeting (the 225th regular meeting) of the American Physical Society was held at Washington, D. C., on Tuesday, Wednesday and Thursday, December 27, 28 and 29, 1938. All sessions of the meeting were held at the National Bureau of Standards. The presiding officers were Dr. Lyman J. Briggs, President of the Society, Dean John T. Tate, Vice President, Dr. H. L. Curtis, Dr. Karl K. Darrow, Dr. W. E. Forsythe, Professor Dayton C. Miller, Dr. F. L. Mohler and Professor G. W. Stewart. There were four hundred and fifteen registrations at the meeting.

On Wednesday afternoon, December 28, at two-thirty o'clock Dr. Lyman J. Briggs of the National Bureau of Standards, President of the American Physical Society delivered an address "The National Standard of Measurements" which was followed by an inspection of the standards in the laboratories.

Dr. Briggs presided at the speakers' table on the evening of December 28 at the joint dinner with the American Association of Physics Teachers held at the Wardman Park Hotel. He called upon the newly elected President of the Physical Society, Dean John T. Tate, to speak. There was also present at the speakers' table Professor C. Drummond Ellis of the University of London who spoke briefly. The other speakers were Dr. Harvey Fletcher and Dean F. K. Richtmyer. There were two hundred and eighty-six members and their guests at the dinner.

Annual Business Meeting. The regular annual Business Meeting of the American Physical Society was held on Wednesday afternoon, December 28, 1938 at two o'clock, President Briggs presiding. The President had appointed Messrs. William H. Crew and Karl K. Darrow to canvass the ballots for the officers of the Society. They reported the following elections:

President, John T. Tate; *Vice President*, John Zeleny; *Secretary*, W. L. Severinghaus; *Treasurer*, George B. Pegram; *Members of the Council*, four year term, E. U. Condon and A. J. Dempster; *Members of the Board of Editors*, three year term, Walker Bleakney, Gregory Breit and D. M. Dennison.

The Secretary reported that during the year there had been 202 who accepted election to membership. The deaths of fifteen members were reported, thirty-nine members resigned and five were dropped. The membership as of December 24, 1938 was as follows: Honorary Members, 5; Fellows, 754; Members, 2497; total membership, 3256.

The Treasurer presented a summary of the financial condition of the Society. It was impossible to present a final report for the year at the Annual Meeting because the fiscal year ends on December 31st. The Treasurer's financial report will be audited, printed and distributed to the members.

The Managing Editor made a brief report on the general status of the publications of the Society and stated that a detailed and audited financial report for 1938 would be printed and distributed.

The Annual Business Meeting adjourned at two-twenty P.M.

Meeting of the Council. At the meeting of the Council held on Monday afternoon, December 26, 1938 two candidates were elected to fellowship, thirty-one candidates were transferred from membership to fellowship and sixty-three candidates were elected to membership. *Elected to fellowship:* D. D. Montgomery and Arnold Nordsieck. *Transferred from membership to fellowship:* W. E. Albertson, J. G. Albright, Alexander Allen, Luis Alvarez, John Bardeen, E. L. Bowles, William F. Brown, Jr., R. C. Colwell, Albert S. Coolidge, Palmer H. Craig, Maurice Ewing, W. A. Fowler, G. G. Harvey, Leland J. Haworth, Joseph E. Henderson, J. Barton Hoag, Willis E. Lamb, Jr., John J. Livingood, A. H. Nielsen, A. O. C. Nier, Melba Phillips, J. R. Richardson, Robert Serber, Robert S. Shankland, William Shockley, William R. Smythe, A. F. C. Stevenson, R. L. Thornton, J. G. Trump, L. C. Van Atta and Karl S. Van Dyke. *Elected to membership:* Fadel G. Antippa, William J. Archibald,

Otto J. Baltzer, Mary Banning, Sidney Borowitz, Alexander V. Bushkovitch, Arnold F. Clark, William A. Cole, Gyfford D. Collins, George C. Comstock, A. M. Crooker, Ulrich Dehlinger, Alexis A. B. Dember, Jacobus S. de Wet, William G. Driscoll, A. G. F. Duncan, Clarence A. DuPont, Raymond Ellickson, Bruce Eytinge, Enrico Fermi, Charles B. Green, Carl M. Herget, George C. Higgins, Paul Huber, Richard F. Humphreys, H. Inuzuka, Warren C. Jones, A. Kastler, Nikolai Kemmer, Akio Kobayasi, John D. Kraus, G. J. Kynch, Ernest W. Landen, Eugene Lankford, Jr., S. T. Ma, George E. MacWood, John Marshall, Jr., A. Victor Masket, Robert J. Maurer, Ralph L. McCreary, Henry C. Meadow, Karl W. Meissner, Burton J. Moyer, Maurice E. Nahmias, Kenneth A. Norton, Joseph T. O'Callahan, Herbert M. Parker, Peter Preiswerk, Arnold Raines, Hans H. Renner, Robert G. Sachs, Guenter Schwartz, W. Wallace Sellers, Jr., Erle I. Shobert, II, G. M. Shrum, Charles F. Squire, Joseph B. Stucky, Jr., James K. Thornton, Louis Slotin, Thomas N. White, Jr., Charles M. Wilson, Robert G. Wilson and Syozi Yasimoto.

The regular scientific program of the Society consisted of seventy-nine contributed papers of which one, number 55, was read by title. The abstracts of the contributed papers are given in the following pages. An Author Index will be found at the end.

W. L. SEVERINGHAUS, *Secretary*

ABSTRACTS

1. The Far Infra-Red Pure Rotation Spectrum and the Molecular Structure of Heavy Water Vapor. N. FUSON,* H. M. RANDALL, AND D. M. DENNISON, *University of Michigan*.—An investigation has been made of the spectrum of heavy water vapor (D_2O) in the region from 23mu to 135mu. The instrument used was a recording spectrograph of large aperture.[1] The gratings were of the echelette type, higher order spectral impurity being removed by a combination of filters, *restrahlen* plates, and shutters. Absorption maxima could be located with an accuracy of about 0.05 cm^{-1} over most of the range. Lines 0.5 cm^{-1} apart could be partially resolved, higher resolution and dispersion being unproductive since the true width of the absorption lines is large. A feature of the spectrograph was that a completely evacuated radiation path could be obtained, thus eliminating the intense absorptions of the atmospheric water vapor which overlie this entire region. From this research over 200 pure rotation frequencies have been obtained together with rough intensity estimates. Using an analysis similar to that already used for ordinary water vapor,[2] the rotational energy levels for the ground state of D_2O have been evaluated through quantum number $j=8$. Corrections have been made for centrifugal stretching of the molecule. Cross-identification of the calculated transitions with the observed rotational transition frequencies has been made with some degree of success.

* Now at Rutgers University.
[1] H. M. Randall, Rev. Mod. Phys. **10**, 72 (1938).
[2] H. M. Randall, D. M. Dennison, N. Ginsberg, L. R. Weber, Phys. Rev. **52**, 160 (1937).

2. A Thermal-Gravitational Method for the Separation of Gases and Isotopes. A. KEITH BREWER AND ARTHUR BRAMLEY, *Bureau of Chemistry and Soils, Washington, D. C.*—Methods for separating gases by thermal diffusion[1] have been improved by making the process accumulative. Clusius and Dickel[2] accomplished this by using a long vertical tube with a hot wire down the center. A thermal-syphoning action carries the light gas to the top of the tube and the heavy to the bottom. The writers have modified this procedure by using two large concentric cylindrical members, one being heated and the other cooled. In a glass apparatus consisting of a heated inner and a cooled outer tube, one and two cm in diameter, respectively, and one meter in length, a 350° temperature difference separated He and Br so that no Br could be detected at the top of the tube after 15 minutes. Under similar conditions a 50–50 CH_4-NH_3 mixture underwent a 25 percent enrichment in NH_3 at the bottom of the tube. If l denotes the cylinder length, r the radius of the outer tube, and the d the difference in radii, then to a first approximation, the rate of separation varies as rd and the purity of l/d.

[1] Chapman and Dootson, Phil. Mag. **33**, 248 (1917).
[2] Clusius and Dickel, Naturwiss. **33**, 546 (1938).

3. The Distribution of Ozone in the Stratosphere. W. W. COBLENTZ AND R. STAIR, *National Bureau of Standards*.—Measurements of the spectral quality of ultraviolet solar radiation, with a photoelectric cell and filter radiometer, made in September and early October, 1938, at Flagstaff, Arizona (elevation 7300 ft.), showed that during a well-defined cyclonic disturbance the barometric "low" preceded, by five to six hours, the well-known attendant increase in concentration of ozone, indicating a possible method of studying air circulation in the stratosphere. A decrease of 0.2 in. (five mm) in barometric pressure produced an increase of perhaps eight to ten percent in the amount of atmospheric ozone. In four balloon ascensions, made in Washington, D. C., in June, 1938, the photoelectric cell and filter radiometeorograph attained heights ranging from 83,000 to 88,000 ft. (25 to 27 km), penetrating about 60 to 70 percent of the atmospheric ozone, which became perceptible at a height of about 12 km (as observed in 1937)

and was fairly uniformly distributed through a height of 18 to 27 km, with a wide maximum between 20 and 27 km. At the highest elevations the ultraviolet intensity was about five times the value observed at sea level.

4. Energy Transformations in Novae. Ross Gunn, *Naval Research Laboratory, Washington, D. C.*—Common novae, at maximum, radiate 10×10^{37} ergs/sec. or about 25,000 times more than the sun, whereas so-called "super" novae radiate about 2×10^{41} ergs/sec. The original stars of both types exhibit no unusual characteristics. Nova Pictoris (1925.39) is a common nova which has been observed to develop from a single dwarf F5 type of star into three components of estimated mass A–0.86⊙; B–0.34⊙; C–0.30⊙. Components B and C are now observed to be receding from A with a velocity of 540 km/sec. and are several parsecs from it. The energy necessary to separate the components and provide the present observed velocity is 4×10^{48} ergs. Moreover this energy was provided in a time less than 3.7 years. The average rate of energy conversion, therefore, exceeds 3.3×10^{40} ergs/sec. and this approximates the luminosity of "super" novae. Consequently the rates of energy conversion in common and "super" novae are of the same order of magnitude. This suggests that the observed differences arise from the different distribution of the transformed energy rather than from a cataclysm of a different order. The difference in the gravitational potential energy of the original and final configurations fails to account for any part of the present observed kinetic energy. Therefore, one concludes that unconsidered sources of energy are immediately available in a star and that a massive body may be ejected from it. These processes have an important bearing on the author's interpretation of the origin of the solar system.

5. Radioactive Content of the Atmosphere as Affected by the Presence of Condensation Nuclei. G. R. Wait, *Department of Terrestrial Magnetism, Carnegie Institution of Washington.*—The rate of ion-production inside a closed chamber with extremely thin walls, installed in a closed room, is found to diminish when large quantities of condensation nuclei are introduced into the air. It was at first assumed that this diminution was due to some of the nuclei falling to the floor, carrying radioactive matter collected by them out of range of the instrument. This assumption was, however, not supported by results from simultaneous measurements of the concentrations of small and large ions. According to theory, the product of the two ion-concentrations is proportional to the rate of the production of small ions (when the small ions are not numerous). This product, when a large quantity of condensation nuclei was introduced into the air, decreased in the same proportion as the ionization inside the thin-walled chamber, thus establishing the authenticity of the ionization measurements. These results imply that the radioactive matter in the atmosphere is either diminished in amount or that it becomes less effective in the production of small ions, when condensation nuclei are present in the air.

6. Concentration of the Chlorine Isotopes by Centrifuging.* C. Skarstrom, H. E. Carr, and J. W. Beams, *University of Virginia.*—The evaporative centrifuging method of Mulliken has been used to concentrate the isotopes of Cl in carbon tetrachloride. The centrifuge used consisted of a 20-lb. chrome molybdenum steel tube 12" long, 4" outside diameter by ¼" wall thickness, capped at both ends. The rotor was hung in a vacuum chamber by a small hollow shaft (hypodermic needle tubing gauge 14) which passed through oil-sealed vacuum glands, and to which was attached an air-supported air turbine located above the vacuum chamber. In operation the rotor was initially charged with 105 cc of CCl_4 and accelerated to 1000 r.p.s. The spinning tube was then evacuated through the hollow shaft. The CCl_4 evaporated at the periphery and was collected at the rate of ¼ cc of liquid per min. in separate fractions in dry ice traps in series with the pump. Repetition of this process has reduced 3150 cc of liquid to a set of fractions of various isotopic compositions, the heaviest of which (16 cc of liquid) has a density 0.1 percent above that of ordinary CCl_4. Analysis of this fraction in a mass spectrometer shows the ratio of Cl_{35} : Cl_{37} has been decreased five percent below that in ordinary CCl_4.

* Supported by a grant from the Research Corporation.

7. Impulse Breakdown in Long Discharge Tubes. J. R. Dietrich* and L. B. Snoddy, *University of Virginia.*—A study of the progressive breakdown in a discharge tube (14.2 cm diameter, 1200 cm long) produced by a positive potential impulse applied between an electrode in one end of the tube and a grounded concentric shield (two meters diameter) has been continued.[1, 2] The output end of the tube is insulated. Maximum current and average speed of potential propagation at constant pressure (0.145 mm dry. air) increase from 5.0 amp. and 13.6×10^8 cm/sec. at 19.4 kv to 134 amp. and 41×10^8 cm/sec. at 125 kv. The total charge from current-time oscillograms is constant to within 20 percent at 125 kv (pressures 0.06 to 0.3 mm) and varies linearly with applied potential at constant pressure (0.145 mm). The ratio of the charge entering the tube during the progress of the wave from input to output end to the total charge decreases with increasing pressure. If the progressive breakdown traverses only part of the tube (very short applied impulses), the previously described[3] contracted luminous column is observed to have a diffuse head about two meters long (0.044 mm pressure).

* Coffin Fellow.
[1] L. B. Snoddy, J. R. Dietrich and J. W. Beams, Phys. Rev. **52**, 739 (1937).
[2] J. R. Dietrich, L. B. Snoddy and J. W. Beams, Phys. Rev. **53**, 923 (1938).

8. The Separation of Gases by Centrifuging.* J. W. Beams, *University of Virginia.*—The air-driven vacuum-type tubular centrifuge was used to test the theoretical equation of Lindemann and Aston for the separation of gases at equilibrium in a centrifugal field. A mixture of CO_2 and N_2 at slightly above atmospheric pressure entered the spinning tube at the top and was collected at the bottom in two equal fractions by volume, one taken from

the axis, the other from the periphery of the tube. The chrome-molybdenum steel tube was 14″ in length, 4″ in external diameter, ¼″ in wall thickness and capped at both ends. It spun in a vacuum at room temperature. The rotational speed was constant to at least 0.2 percent during an experiment. At speeds of 1000 r.p.s. with steady rates of flow up to 500 cm³/min., the observed separation agreed with the equilibrium theory, within a few percent. At rates of flow of 1000 and 2000 cm³/min. the observed separations were 85 and 68 percent of the theoretical equilibrium values, respectively. It is believed that a part of this reduction, at least, is due to stirring at the exits of the tube. At a series of rotational speeds from 500 r.p.s. to almost 1100 r.p.s., with steady rates of flow of about 100 cm³/min., the theory was verified within the limits of experimental error (three percent).

* Supported by a grant from the Research Corporation.

9. A Possible Cause of the Glow to Arc Transition. F. A. MAXFIELD, H. R. HEGBAR, AND J. R. EATON, *University of Wisconsin.*—Further experimental studies with an unstable glow discharge in mercury vapor lend support to the theory proposed by Maxfield and Fredendall[1] that the causes initiating glow to arc transitions are probably bursts of gas non-uniformly emitted from small patches on the electrode surface. Tests showed that transition probability continually decreased when the electrode was kept hot and bombarded with positive ions over a period of several days. Two quite different curves of transition probability as a function of vapor pressure were obtained. With moderate values of glow current the probability of a transition increases with pressure but with very low values of glow current the probability of a transition decreases with an increase of pressure. These effects, as well as many other well-known glow or arc discharge phenomena, can be explained by the gas burst theory. Calculations have been made which show that even if less than 10^{10} atoms of gas are emitted in a burst a sufficient amount will have been emitted to initiate the glow to arc transition. This is a much smaller amount of gas than can be detected by ordinary means.

[1] Maxfield and Fredendall, J. App. Phys. 9, 600 (1938).

10. Absorption and Reradiation by Resonators. C. R. FOUNTAIN AND E. G. PIGG, *George Peabody College for Teachers.*—Tuned resonators absorb and reradiate radio wave energy. The equation for the current induced in such a resonator was checked experimentally for 3.9 meter waves. The induced current varies inversely with the distance and the energy varies inversely with the square of the distance as expected. Another tuned resonator, placed anywhere in the field, also absorbs and reradiates according to these laws. The additional current induced in the first receiver by radiation from the second resonator can also be represented by an equation and checked by experiment. However, there is a change in phase of half a wave-length when the energy is reradiated. Maximum effects are found when the sum of the distances from transmitter to resonator and from resonator to receiver are an odd number of half-wave-lengths greater than the direct distance from transmitter to receiver. Under these conditions the total energy induced in the receiver seems to be far greater than expected from the inverse square law. Such resonators seem to absorb all the energy within a wave-length on either side of them. Two such resonators, each four λ from the transmitter and $\frac{3}{4}\lambda$ from the receiver, more than doubled the normal energy at the receiver.

11. Decay of Phosphorescence After Electron Bombardment. R. B. NELSON* AND R. P. JOHNSON, *General Electric Co.*—An apparatus has been constructed for measuring the luminous output of phosphors under electron bombardment as a function of time, during a cycle in which the exciting beam is turned on and off for any desired intervals. The phosphorescence of green willemite decays approximately exponentially with time, the decay rate being independent of current density, voltage, and duration of the exciting beam. The time constant of the decay varies from seven milliseconds, just after excitation, to 14 milliseconds in the later stages. A simple picture of the luminescence process in willemite is proposed which is consistent with the exponential decay and the observed saturation of steady light output with increasing current density. A sample of pure $CaWO_4$ shows no detectable phosphorescence lasting 10^{-4} seconds, the resolving time of the apparatus. For two samples of ZnS activated with Ag the first part of the decay follows the law $L=A/(t+b)$, where L is the light output, t is the time, A and b are constants. Later, the luminescence falls faster than this. For a ZnS : CdS activated with Ag $L=A/(t+b)^2$. The shapes of the decay curves for sulphides are independent of voltage, but dependent on current density.

* Now at Massachusetts Institute of Technology.

12. On the Mechanism of Air-Blast Atomization (Air-Injection; Ante-Chamber Methods). R. A. CASTLEMAN, JR., *Falls Church, Virginia.*—It is well known that Diesel was side-tracked from his original partial success with a coal-dust internal-combustion engine by discovering that liquid fuel could be efficiently atomized directly into the cylinder by applying behind it a pressure considerably in excess of the momentary cylinder pressure. For years this has remained the favorite method of injection and atomization of liquid fuel in great stationary Diesels, but, since a two or three stage air compressor must be carried along, solid injection has largely displaced this in the vehicle Diesel. It was early observed that this method, when, as is customary, some thirty atmospheres *net* injection pressure was used, gave a spray of uniform fineness comparable to that yielded by air-stream atomization (successfully used for years in carburetors). As the N.A.C.A. has shown, this is quite insufficient to give uniform fineness in solid injection, so that the fuel is not atomized by being pushed ahead of the compressed air. However, the air is blown in at a velocity, relative to the liquid, which is quite sufficient for air-stream atomization. The uniform fineness of the spray formed in air injection is thus explained. This explanation also applies to ante-chamber methods, where the blasting

pressure is furnished by a preliminary partial explosion in a small ante-chamber in the cylinder head.

13. On the Statistical Theory of Rubber Elasticity and Related Experiments. EUGENE GUTH, *University of Notre Dame.*—The high reversible elasticity and the thermoelastic behavior of rubber can be explained in terms of the molecular structure of rubber. Rubber consists of large chain molecules which can exhibit two kinds of Brownian motion: 1. An intramolecular one due to the possibility of free rotations around single C−C bonds and giving rise to a more or less kinked form of the chain molecule; 2. An intramolecular one due to the possibility of a motion of the chain as a whole. Reversible rubber elasticity results if the intermolecular motions are not hindered above a certain degree, and if, at the same time, the translatory intermolecular Brownian motion is completely hindered. The kinked form due to the intramolecular Brownian motion is the most probable one according to the statistical interpretation of the second law of thermodynamics. If a stress is applied, these curved molecules will be straightened, thus giving a transition to a less probable state. When the stress is released the thermal agitation causes a retraction. A predominance of this statistical mechanism gives rise to the anomalous thermoelastic behavior (e.g., stress a constant length rises with increasing temperature) of certain rubber samples. A simple theoretical equation of states holding for this case will be presented.

$$z = a(L) + b(L)T; \quad b(L) = Pl\frac{2}{nl_a}k\left(L - \frac{3}{2L}\right).$$

L, relative length; P, number of chains per cc; n, number of C−C bonds per chain; $l_a = l\cot^2\alpha/2$; l, C−C distance; α, valence angle (approx. 109 deg.). For such a "quasi-ideal" rubber, the specific heat at constant length depends only upon the temperature and not upon the elongation. Generally, the thermal and the caloric equations of state together completely determine the thermodynamics of stretched rubber.

The normal thermoelastic behavior of certain other rubber samples can, on the other hand, be caused by the predominance of the inter- and intramolecular forces. Generally, both the statistical and the force mechanisms can be present. A dynamometer giving directly the stress of a stretched rubber sample in dependency upon the temperature, i.e., the thermal equation of state, will be described and the results obtained by another automatic stress-strain apparatus will be discussed.

14. Effect of Gas Pressure on the Point-to-Plane Discharge in Several Gases. H. C. POLLOCK AND F. S. COOPER, *General Electric Company.*—A maximum in the breakdown voltage *vs.* pressure curve with point-to-plane electrodes, reported in N_2 by Goldman and Wul,[1] has been observed also in O_2, CO_2, SO_2, SF_6, and CCl_2F_2. No effect was observed in A or He up to 300 lb./sq. in. pressure, although with the three-mm gap used, maxima occurred below 120 lb./sq. in. for the other gases. With a fixed voltage between electrodes, corona currents decrease as gas pressure increases until a critical pressure is reached. Above this pressure, no corona is observed preceding spark discharge. An oscillograph indicates a change in the type of positive corona in some gases, at a voltage slightly above that at which corona starts. As Kip[2] found, a very steep rise in current occurs when corona starts from a positive point. These effects have not been observed with negative corona.

[1] Goldman and Wul, Tech. Phys. U. S. S. R. **1**, 497 (1936).
[2] Kip, Phys. Rev. **54**, 139 (1938).

15. Effect of Hydrostatic Pressure on the Resistance of Single Crystals of Selenium. R. M. HOLMES AND H. W. ALLEN, *University of Vermont.*—Single crystals of the hexagonal type about 1 cm long and 0.5 mm in diameter were grown in a partial vacuum by condensation from the vapor phase. Resistances between points a few mm apart were measured using potential leads to a vacuum tube circuit. The crystals were in an insulating oil under pressures up to 700 kg/cm². The resistances decrease with increasing pressures but there is a marked hysteresis effect, the resistances at decreasing pressures falling below the corresponding values at increasing pressures. If the crystals are kept at each pressure for about 30 minutes then values of resistances at both increasing and decreasing pressures fall on a straight line within this pressure range. The value of $\Delta R/R_0\Delta p$ is -3.1×10^{-6}. This is believed to be the largest resistance pressure coefficient so far reported. If the pressure on a Se crystal is quickly increased from atmospheric to 700 kg/cm² the resistance decreases rapidly at first, then at a lower rate and finally attains a constant value after about 30 minutes. When pressure is reduced the increase in resistance is similar in behavior. Oil temperatures were read. The resistance temperature coefficient for Se crystals was found to be 2.4×10^{-3} at 21.5°C. Illumination decreases the resistance pressure coefficient.

16. The Ultrasonic Method for the Determination of Elastic Properties of Solids. H. LUDLOFF, *Cornell University. (Introduced by H. A. Bethe.)*—A method of investigating elastic properties of solids has been devised. The method involves the piezoelectric excitation of spatial ultrasonic wave gratings and the irradiation of the solid with visible light. Interference patterns obtained in this way uniquely determine the elasticity and symmetry behavior of the solid. If the solid is transparent, the action on the light is that of a *spatial* grating. If the solid is opaque, the interference pattern appears in reflected light, the diffraction taking place on the oscillating surface. The interference patterns can be understood and derived quantitatively by integration of the wave equations of the system; it must be taken into account that a *great number* of spatial gratings are excited for each frequency, and that all these gratings will influence the interference pattern. In this respect, the situation is quite different from that encountered in the diagrams in the x-ray range. From our interference pictures one can determine simultaneously all the elastic constants with an accuracy hitherto unattained. From the intensity distribution in the interference pattern, one can draw conclusions concerning the energy distri-

bution of ultrasonic waves of a given frequency; there exists a certain analogy with the equipartition theorem for thermal waves.

17. An X-Ray Investigation of Crystallinity in Rubber. S. D. GEHMAN AND J. E. FIELD, *The Goodyear Tire and Rubber Company, Akron, Ohio.*—X-ray diffraction evidence has shown that a crystalline structure can be produced in rubber by stretching or by freezing. In the former case, a fiber diagram is generally secured, in the latter, Debye-Scherrer rings. When raw rubber was stretched to moderate elongations and frozen, an intense fiber diagram was found, showing that the crystallization proceeded from the nuclei set up by the stretching. A series of diffraction patterns illustrating the effect are reproduced. The geometrical conditions of stretching under which "higher orientation" occurs in stretched rubber were studied by photometric measurements of the relative densities of the first two equatorial spots. Graphs are included demonstrating the effect of variations in gauge, width, length and elongation of the specimens. The different physical structures of vulcanized pure gum stocks became apparent in the "higher orientation" characteristics, although the same diffraction pattern was secured. A correlation of the results with current views on the micellar or secondary structure of rubber and the crystallization of super-cooled liquids is attempted.

18. Negative Power Factors in Air Capacitors. ALLEN V. ASTIN, *National Bureau of Standards.*—Using a method* which permits absolute evaluation of power factors as small as 0.5×10^{-6}, it has been found that certain guard ring capacitors when in an atmosphere of high humidity will occasionally show definite negative power factors. The observed negative values are a maximum at about 80 percent relative humidity and the largest negative value recorded is 70×10^{-6} at 60 cycles. The values are stable provided the capacitor is not disturbed and a constant humidity is maintained, but cleaning and reassembling the electrodes may cause the negative values to disappear.

The capacitors were well shielded so that there was no possibility of capacitative coupling to some other source. The values were independent of the voltage across the capacitor and of the wave form of the voltage. The negative value for two capacitors in parallel, each of which had a negative power factor, agreed with the value computed from the individual values. The negative values decreased as the frequency of the applied voltage is increased. No d.c. effects were observed with capacitors which showed a negative power factor.

* This method is described in detail in the Nat. Bur. Standards J. Research 21, 425 (1938).

19. An Explanation of the Negative Power Factors in Air Capacitors. HARVEY L. CURTIS AND ALLEN V. ASTIN, *National Bureau of Standards.*—In order to explain the negative power factor of an air capacitor it is necessary to assume some source of energy in the capacitor itself or in an electric circuit connected with the capacitor. A source of energy in the capacitor itself is the latent heat of the water vapor, since negative power factors are only observed when there is moisture in the capacitor. An explanation of negative power factors can be based on the assumption that the latent heat of water vapor is converted directly into electrical energy. The second possible source of energy is in the guard circuit of the capacitor since all capacitors in which negative power factors have been observed have been shielded capacitors. By assuming certain conditions in connection with the shield it is possible to explain negative power factors by this method. Neither of the proposed explanations has received a definite experimental proof.

20. The Thermal Distribution and Temperature Gradient in the Arc Welding of Cylindrical Tubing. W. A. BRUCE, *The Carter Oil Company, Tulsa, Oklahoma.*—The assumption is made that the n welders move their electrodes at a constant speed on a circle of a right cylindrical shell, and with a uniform separation w cm between welders. The method of stationary sources, as developed by Kelvin and described by Rayleigh,[1] is used. By integration of the effect of the stationary sources, the general effect of a moving welder is obtained. Similarly, the effect of the n welders is obtained. Demonstration of the validity of this summation is given. Proof is given that an infinite plate with an infinite number of sources w cm apart along a line in the plate is equivalent to a thin right cylinder with n sources separated w cm on a circle of the cylinder. The solution is in the form of a sum of definite integrals. It is shown that under certain conditions these definite integrals may become Bessel functions of the second kind. The temperature gradient and rate of cooling at any point may be obtained by partial differentiation under the definite integral. Experimental results which verify the equation are shown.

[1] Rayleigh, Phil. Mag. 22, 381 (1911).

21. Quiet Boiling. N. ERNEST DORSEY, *National Bureau of Standards.*—The use of more or less rounded points for reducing the severity of such bumping as occurs when air-free water is boiled in clean glass vessels is common practice, but the results so obtained are seldom satisfactory. It seems not to have been recognized that if the material of which the points are made is such that it is perfectly wetted by the liquid at the temperature considered, then the point cannot be efficacious, as it will have no effect whatever upon the form or size of the incipient bubble of vapor. On the other hand, the presence in the liquid of a substance that is completely unwetted by the liquid at the temperature concerned will be efficacious, whatever its shape. Since in this case the contact angle is 180°, the curvature of the incipient bubble at its very beginning will be slight and will at first increase as the volume increases; the first facilitates the formation of the initial bubble, the second stabilizes the initial stages of its growth. Among such substances for water are the stearates of zinc and of aluminum. Each of these is very effective. A simple mechanical device for the prevention of bumping will be described.

22. Reducing the Reflection from Glass by Evaporated Films. C. HAWLEY CARTWRIGHT AND A. FRANCIS TURNER, *Massachusetts Institute of Technology.*—The conditions were investigated for reducing the reflection from optical surfaces by the deposition of evaporated films of LiF, MgF_2, CaF_2, NaF and chiolite. Films of these materials with an optical thickness of 1200A when evaporated under suitable conditions reduced the reflection of visible light from two glass surfaces to about 0.4 percent and resulted in a transmission of about 99.6 percent, as recorded by the Hardy color analyzer. The optical thickness, the geometrical thickness, and the index of refraction of an evaporated film were determined by interference methods and the absolute reflecting power.

23. The Chladni Patterns on Circular Plates. R. C. COLWELL, J. K. STEWART AND A. W. FRIEND, *West Virginia University.*—The solution for the nodal lines on a circular plate appears in the form

$$W = AJ_n(kr)\cos n(\theta-\alpha_n) \pm BJ_m(k'r)\cos m(\theta-\alpha_m) = 0.$$

The first term of this equation has heretofore been given as the complete solution of a vibrating plate. In reality however it represents only circles and radii corresponding to the straight lines on a square plate. If another vibration, which may arise in many ways, is represented by the second term of the equation above, the two terms may be added together with different values of A and B to give the complicated figures which actually appear on circular plates. It is better to add the terms by a graphical method. The mathematical figures will be compared with those obtained experimentally on vibrating plates. The same method may also be applied to circular membranes.

24. Magnetic Moments of the Proton and the Deuteron. J. M. B. KELLOGG, I. I. RABI, N. F. RAMSEY, JR., AND J. R. ZACHARIAS, *Columbia University and Hunter College.*—The molecular beam magnetic resonance method for measuring nuclear magnetic moments has been applied to the proton and deuteron. In this method the nuclear moment is obtained by measuring the frequency of the Larmor precession ($\nu = \mu H/hi$) in a uniform magnetic field. For this purpose HD molecules at liquid nitrogen temperatures are most suitable because they are largely in the ground state of zero rotational moment. This circumstance eliminates disturbing effects which are described in the following paper. The details of the apparatus and method will be described. Very sharp resonance minima were observed which made it possible to show precisely that the observed values of ν/H are independent of H. Observations were also made on a resonance of the CCl_3F_3 molecules in order to connect our results with the measurements made on Li^7, Li^6, and F^{19}. The results obtained for the various moments are

$$_1H^1 \quad 2.780\pm0.02$$
$$_1D^2 \quad 0.853\pm0.007$$
$$_9F^{19} \quad 2.616\pm0.02.$$

The values are in excellent agreement with those obtained by the atomic beam method of Kellogg, Rabi, and Zacharias,[1] which is entirely different in principle, but lie outside of the limit of error of the latest measurement of the proton moment of Estermann, Simpson, and Stern.[2] It is noteworthy that our value of the fluorine moment from CCl_3F_3 agrees with that previously obtained from LiF in a different apparatus.[3]

[1] Kellogg, Rabi, and Zacharias, Phys. Rev. **50**, 472 (1936).
[2] Estermann, Simpson, and Stern, Phys. Rev. **52**, 535 (1937).
[3] Rabi, Millman, Kusch, and Zacharias, Phys. Rev. **53**, 495 (1938).

25. Magnetic Resonance Experiments on H_2 and D_2 Molecules. I. I. RABI, J. R. ZACHARIAS, N. F. RAMSEY, JR., AND J. M. B. KELLOGG, *Columbia University and Hunter College.*—The molecular beam magnetic resonance method applied to H_2 at the temperature of liquid nitrogen reveals a close group of sharp resonance minima. The ratio ν/H for the center of this group is independent of H and thus affords a determination of the proton moment. This value agrees with that obtained using HD molecules. The resonance minima agree in number and in spacing with reasonable predictions based on the assumptions of spin-spin magnetic interaction of the two protons and interaction of the proton moments with the molecular rotation. It will be shown that these experiments yield information with regard to the finer details of molecular dynamics, such as the field produced by the molecular rotation at the positions of the nuclei. In the case of D_2 the resonance minima are not yet completely resolved. The total spread of the group is too great to be accounted for by the theory used successfully for H_2. The center of the group yields a value of ν/H independent of H. The deuteron moment so evaluated agrees with the one obtained with HD.

26. Rotational Magnetic Moment Measurements on H_2 and D_2. N. F. RAMSEY, JR., *Columbia University.*—The molecular beam resonance method for measuring nuclear magnetic moments has been applied to the measurement of the rotational magnetic moments of H_2 and D_2 at liquid nitrogen temperatures. A group of resonance minima has been obtained corresponding to reorientations of the molecular rotational moment rather than of the nuclei within the molecule as in previous experiments. The rotational moment can be evaluated from that member of the group for which ν/H is independent of H. The rotational g and hence the rotational moment of the first rotational state is found to be 0.887 ± 0.018 nuclear magnetons for H_2. This is within the limits set experimentally by Estermann and Stern[1] and theoretically by Wick.[2] A rotational g of 0.445 ± 0.009 nuclear magnetons is found for D_2. This is just half that of H_2 as expected theoretically.[2] At the temperatures used, practically all the H_2 and most of the D_2 is in the zero or one rotational state. The positions and shapes of the different H_2 rotational minima have been studied. The total spread of the rotational group of minima is found to be that predicted by the theory of the nuclear resonance group discussed in the preceding paper.

[1] Estermann and Stern, Zeits. f. Physik **85**, 17 (1933).
[2] Wick, Zeits. f. Physik **85**, 25 (1933).

27. Determination of the Nuclear Magnetic Moment of Caesium by the Molecular Beam Magnetic Resonance Method. P. KUSCH AND S. MILLMAN, *Columbia University.*—An apparatus for the application of the molecular beam magnetic resonance method to the determination of magnetic moments of nuclei in molecules that can be detected by the method of surface ionization has been built. The essential features of the apparatus and the procedure used in obtaining the resonance minima from which magnetic moments are determined will be discussed. A specific application to the case of the nuclear moment of Cs^{133} will be made. A ν/H resonance minimum common to CsCl and CsF and constant, within experimental error, over wide ranges of magnetic field was attributed to the magnetic moment of the Cs^{133} nucleus. The magnetic moments of Li^6, Li^7 and F^{19}, previously determined on another apparatus utilizing the same method, have been redetermined and the values are in agreement with those published.[1] Referred to the published value of the nuclear moment of Li^7, the magnetic moment of Cs^{133} is 2.556 in units of nuclear magnetons.

[1] Rabi, Millman, Kusch and Zacharias, Phys. Rev. **53**, 495 (1938).

28. The Nuclear Magnetic Moments of Na^{23} and K^{39}. S. MILLMAN AND P. KUSCH, *Columbia University.*—The apparatus described in the previous paper has been used to determine the magnetic moments of the Na^{23} and K^{39} nuclei. The molecules used for observing resonance minima for Na were NaF, NaCN and Na_2, and for K were KCN and K_2. From the observed resonance minima the moments of Na^{23} and K^{39} were found to be 2.224 and 0.391 nuclear magneton, respectively, referred to the published value of the nuclear moment of Li^7. Fine structure observed in the resonance minima of Na^{23} and K^{39}, when these resonance minima were observed with homonuclear molecules, will be discussed. It will be shown that the asymmetrical structure sometimes observed in the resonance minima is due to end effects in the wires which produce the radiofrequency oscillating field. Advantage may be taken of this asymmetry to determine the signs of nuclear magnetic moments.

29. The Collimation of Fast Neutrons. PAUL C. AEBERSOLD,* *University of California.* (*To be read by Luis Alvarez.*)—A well-defined, intense beam of fast neutrons has been achieved by using a collimation arrangement in conjunction with a cyclotron. Essentially the collimation is affected by a channel through a tank of water, 55 cm thick, placed in front of the source, a beryllium target bombarded by 8 Mev deuterons. However, this tank becomes a source of gamma-rays by neutron absorption and by scattering from the source. These gamma-rays are greatly reduced by lining the channel with a lead cone having walls 3 cm thick and by putting a 5 cm thick layer of lead on the outside of the tank. Also the radiation coming down the channel is filtered through 3 cm of Pb to suppress the gamma-rays from the source. This arrangement localizes the effect of the fast neutrons to a sharply defined region, and it is particularly well suited for biological and clinical applications. The ionization due to fast neutrons is over a hundred times greater in the beam than outside of it. The ionization produced outside is mainly due to gamma-rays and is only about 5 percent of the total ionization within the beam. As measured in a Bakelite walled thimble chamber the biological effect is smaller per unit of ionization due to the background gamma-rays so that localized biological effects produced by fast neutrons can be observed without significant effects on surrounding regions. Absorption of the beam in various materials corresponds to that given by Dunning for fast neutrons, while the ionization observed in various gases agrees with expectations. The intensity at the end of the cone, 70 cm from the source, using 60 microamperes deuteron current, is 3 e.s.u. per cc of air per min. in a small Bakelite chamber but only 0.6 e.s.u. per cc per min. in a carbon chamber. With such an intensity the epilation of a rabbit requires only a 2-hour exposure.

* Finney-Howell Research Foundation Fellow.

30. The Scattering of Ultra-Slow Neutrons in Ortho- and Parahydrogen. LUIS W. ALVAREZ AND KENNETH S. PITZER, *University of California.*—The three measurements so far reported on the ratio of the scattering cross sections of slow neutrons in ortho- and parahydrogen are not self consistent, due to the "high energy tail" of the cadmium filterable neutrons employed, and also to the difficulties of cooling neutrons. It seemed worth while to repeat this experiment with a source of monochromatic neutrons of low energy, in order to eliminate these two difficulties. In addition, Schwinger and Teller have shown that a measurement of the parahydrogen scattering cross section for neutrons of this type will give a very accurate value for the range of the neutron-proton force. A scattering chamber has been constructed which allows *o*- and *p*-hydrogen to be investigated in the gaseous phase (eliminating any effects due to liquid forces), at the boiling point of hydrogen, to avoid Doppler broadening. Preliminary experiments with gaseous *o*- and *p*-hydrogen cooled to liquid-air temperatures show that the *ortho* cross section is more than five times that of *para* for 30° neutrons. Alterations being made in the cryogenic laboratory have interrupted the work, but results on the scattering of 10°K neutrons in 20°K hydrogen should be available for presentation at the meeting.

31. The Transmission of Medium Fast Neutrons. R. B. ROBERTS* AND P. WANG, *Department of Terrestrial Magnetism, Carnegie Institution of Washington.*—The transmission of the neutrons from carbon bombarded by deuterons has been observed in various elements. Any neutron energy from 275 to 550 kv could be obtained by varying the deuteron energy. It was found possible to restrict the energy spread of the neutron beam to 30 kv by using suitably thin targets and small angles. The transmission of carbon and that of paraffin decreased in a regular way with the energy of the neutrons. The transmission of oxygen also showed a variation with the neutron energy.

* Carnegie Institution Fellow.

32. The Scattering of Neutrons by Protons. V. W. COHEN AND H. H. GOLDSMITH, *Columbia University.*—In order to obtain the free proton-neutron cross section from an experiment in which neutrons are scattered by paraffin it is necessary that the energy of the neutrons be greater than the energy of the lowest vibrational level of the paraffin molecule ($\sim\frac{1}{4}$ volt). This condition is satisfied by resonance neutrons for which the energies are of the order of a few volts. We have performed an experiment in which the transmission of a paraffin sheet for a beam of Rh resonance neutrons was measured. The source of neutrons was 600−300 mC Rn-Be. The detector was a Rh film 45 cm² in area. The beam length was 30 cm with the scatterer placed midway between source and detector. Cd shielding was used to eliminate the effect of thermal neutrons. An Rh filter placed between source and scatterer served to select neutrons of the resonance energy. From the observed transmissions we find the mean free path of these neutrons in paraffin to be 0.56 cm corresponding to a neutron-proton cross section of $20\pm2\times10^{-24}$ cm². This result, though in distinct disagreement with the value of 11×10^{-24} cm² obtained by Amaldi and Fermi, is in accord with recent experiments on the scattering of thermal neutrons by paraffin and by ortho- and parahydrogen.

33. Ultraviolet Microscopy as a Means of Determining Chemical Structure in the Cell. PETER A. COLE, *Washington Biophysical Institute, Washington, D. C.*—The Köhler ultraviolet microscope has been adapted to new radiation sources. Optical problems in connection with its use will be discussed. The relation of microscopic photographs obtained with monochromatic radiation to the major absorption bands of the essential compounds of the cell will be demonstrated. Details of chromosome structure obtained in cooperation with Dr. C. W. Metz, Department of Embryology, the Carnegie Institution of Washington, will be shown in monochromatic ultraviolet microscopic photographs.

34. Absorption and Fluorescence Spectra in Relation to the Photolethal Action of Methylcholanthrene on Yeast. ALEXANDER HOLLAENDER AND PETER A. COLE, *Washington Biophysical Institute and Division of Industrial Hygiene, National Institute of Health.*—The absorption spectrum of methylcholanthrene shows two series of bands in the ultraviolet (2100A to 4000A). The fluorescence spectrum as excited by these bands shows a series of maxima in the short visible region (3950A to 4700A). The use of the fluorescence in detection of small concentrations of methylcholanthrene down to one in 10^7 will be demonstrated. Lethal action by methylcholanthrene (dissolved in physiological salt solution) on a typical microorganism (yeast) is found in the presence of ultraviolet radiation between wave-lengths 3450 and 4500A, whereas, on the contrary, in the dark a stimulative action resulting in the breaking of the early resting phase is produced. It has been possible to detect methylcholanthrene through its toxic action in the presence of near ultraviolet radiation down to one to 10^8 to one to 10^9 parts. Possible photodynamic function of methylcholanthrene will be discussed.

35. A Spherical Coil for a Mass Spectrometer. JOHN A. HIPPLE, JR.,* *Westinghouse Research Laboratories.*—In order to construct a mass spectrometer of high intensity together with considerable resolving power, it was desired to have a rather strong field of great uniformity extending throughout a large volume. It is possible to satisfy these conditions with a large economy in power and copper by employing a spherical coil, in which the current density varies as the sine of the angle θ with respect to the axis of the coil. The variation with respect to r is immaterial. Theoretically, the field of such a coil is uniform throughout the volume. A coil employing these principles has been constructed. Preliminary measurements have shown that the field is uniform to at least 0.3 percent throughout the volume. The coil was constructed by winding $\frac{1}{4}$" square copper tubing to a depth of 5" upon a spherical brass casting of 20" outside diameter. The tubing was wound in conical sections having two layers to each section and maple wedges were placed between the sections. The wedges were varied in size from one section to the next to provide for the variation in current density demanded by the theory. The sphere splits into halves at the equatorial plane, and there are openings 5" in diameter at both ends —the absence of turns in this region having slight effect, since $\sin\theta$ is small in this region. With water circulating through the tubing, it is quite easy to obtain a field of 2500 gauss.

* Westinghouse Research Fellow.

36. Infra-Red Absorption Bands of Some Perturbed Hydroxyl Groups. JOSEPH W. ELLIS, *University of California at Los Angeles.*—The valence band near 1.5μ and the valence-deformation band near 2μ are compared for water in a nonpolar solvent, liquid water, water molecules bound to a protein (gelatin), an alcohol in liquid and nonpolar solution states, crystalline sucrose and cellulose (ramie fibers). The structures of these bands are used to interpret the magnitudes and the types of perturbations to which the OH groups which produce them are subjected. Thus, for example, cellulose has only perturbed OH groups; sucrose has unperturbed and two types of perturbed groups; the bands produced by water bound to gelatin are sharpened on both sides, thus showing that the vapor-like molecules and the very highly perturbed molecules found in liquid water are not present there. An unperturbed state means that no forces greater than van der Waals and Lorentz-Lorenz forces occur, whereas a perturbed state means that relatively large forces enter, usually referred to as arising from hydrogen bonds, but probably really electrostatic in nature.

37. Plasma Oscillations and Scattering in Low Pressure Discharges. HARRISON J. MERRILL AND HAROLD W. WEBB, *Columbia University.*—The velocity distribution of the electrons emitted from the hot cathode in a low pressure (2 to 7 microns) discharge in mercury vapor was studied with a movable probe. The paths of these primary electrons lay within a truncated cone of mean diameter 10 mm and length 16 mm, with the anode and cathode as bases.

With small currents the scattering of these electrons could be followed in detail and was found to occur principally in several distinct approximately plane regions a few tenths of a millimeter thick. Oscillations in the plasma were studied with a crystal detector and a Lecher wire system in the probe-cathode circuit. Corresponding to each of the regions of scattering there were found distinct regions where periodic oscillations existed, the distance between them being approximately that covered by the primary electrons in one half-cycle. The frequencies (about 10^9) agreed well with those given by the formulae of Tonks and Langmuir,[1] and the results agree with their conclusion that the plasma oscillations cause the scattering. The results show further that the oscillations are due to the passage of the fast electrons through the plasma.

[1] Tonks and Langmuir, Phys. Rev. **33**, 195 (1929).

38. Excitation of the New Nitrogen Line. JOSEPH KAPLAN, *University of California, Los Angeles.*—Since the discovery last spring in high pressure nitrogen afterglows of a new line at 3466.3A agreeing with Bowen's predicted value of 3466.4A for the $^2P-^4S$ transition in atomic nitrogen, further studies of this line have been made. The most interesting observation is the remarkably high relative intensity of the line in weak afterglows produced by very weak discharges in nitrogen at about 30 mm, in a tube in which the part showing the glow has a volume of about 100 cc. This is entirely like the excitation of the green auroral line when small amounts of O_2 are added to nitrogen and the afterglow associated with a very weak discharge is observed.[1] The large relative intensity of the new line and the Vegard-Kaplan bands in more intense afterglows in the small tube is also of considerable interest since one would expect radiations from metastable levels to grow weaker as the tube size is diminished. This probably indicates the importance of surfaces for the production of metastable particles. The large relative intensity of the 3466 line points to the high-pressure afterglow as an important source of atomic nitrogen.

[1] Pub. Astronom. Soc. Pac. **47**, 257 (1935).

39. A Self-Consistent Field for Doubly Ionized Chromium. ROBERT L. MOONEY, *Georgetown University.*—A self-consistent field based on Hartree's equations has been calculated for Cr III in the configuration $(3p)^6\,(3d)^4$. The calculations were started by estimating an initial field by a method of graphical interpolation between the results already calculated for other ions. All of the differential equations involved in the computations were integrated numerically with the aid of a calculating machine. Three approximations in the cases of the $(1s)^2$, $(2s)^2$ and $(2p)^6$ groups, and seven approximations for the $(3s)^2$, $(3p)^6$ and $(3d)^4$ groups were made towards self-consistency. Tabulations of the $Z_{a,l}$'s in the last approximations show a divergence from self-consistency of not more than ± 0.004. The normalized wave functions for the individual electrons and the total radial electronic charge density distribution have been plotted as functions of the radius—a spherically symmetrical distribution has been assumed throughout. The results are principally significant in that the self-consistent field for Cr III offers a convenient starting point for calculations of self-consistent fields for singly ionized and for neutral chromium. The tendency toward "over-stability" (in the sense described by Hartree) is strongly marked in the $(3d)^4$ sub-group. Empirical rules are determined for the best method of overcoming the difficulties of the phenomenon of "over-stability."

40. Quantities of Charge Transfers in Lightning Discharges. E. J. WORKMAN AND R. E. HOLZER, *University of New Mexico.*—Five synchronized recording-generating voltmeters developed for indicating electric field intensity under storm conditions (see paper 78) were located at the boundary of a nearly circular area of 25 square miles at Albuquerque. The surface densities of the image charge were obtained from the measured surface field intensities and changes in the contour pattern of the image charge were used to calculate the quantity of charge in observed flashes. More than a thousand discharges of various kinds show on the records of all instruments for the several storms studied. From two to three hundred discharges were observed (visually) as to type and position and may be identified on the records. Seventeen of these discharges were photographed on the high speed lightning camera. Eight simple cloud to ground discharges of one storm have been analyzed and show gross transfers of 26, 54, 50, 37, 100, 30, 33, 29, and 200 coulombs from heights of approximately 1.5 miles. The application of this method to the study of charge development, charge distribution, potential differences, and space charge effects is discussed.

41. Compressibility of Lithium. CONYERS HERRING,* *Massachusetts Institute of Technology.*—Recent calculations of the energy of metallic lithium, made by Bardeen[1] using the method of Wigner and Seitz,[2] yield values for the compressibility which are roughly 15 percent larger than the values observed by Bridgman[3] over a range of pressures. For sodium however the agreement was very good. The most likely source of the discrepancy for lithium seemed to be the failure of the assumption that the energy of an electron with wave vector $\mathbf{k}$ is exactly proportional to k^2. In an attempt to better this assumption, the energies of three excited electronic states have been calculated for a number of values of the lattice constant. To calculate these energies a perturbation method is used starting from free electron wave functions of appropriate symmetry; the convergence is found to be rapid. The correction to be applied to Bardeen's values for the total energy of the electrons can be estimated by interpolation.

* National Research Fellow.
[1] Bardeen, J. Chem. Phys. **6**, 367 (1938).
[2] Wigner and Seitz, Phys. Rev. **43**, 804 (1933); **46**, 509 (1934); Seitz, Phys. Rev. **47**, 400 (1935); Wigner, Phys. Rev. **46**, 1002 (1934).
[3] Proc. Am. Acad. **72**, 207 (1938).

42. The Angular Distribution of the α-Particles from $B+H^1$. R. O. HAXBY[1] AND J. S. ALLEN, *University of Minnesota.*—Measurements have been made of the angular distribution of the α-particles arising from the reactions:

$$_1H^1 + {}_5B^{11} \rightarrow {}_4Be^8 + {}_2He^4 \qquad (1)$$

$$_1H^1 + {}_5B^{11} \rightarrow 3\,{}_2He^4. \qquad (2)$$

These reactions have been studied by Neuert,[2] who found the angular distribution of α-particles from (1) at 200 kv proton energy could be represented approximately by $1+\cos^2\theta$. Those from (2) were found to have a similar distribution for the longest range particles, gradually changing to a uniform distribution for α-particles of less than about 2.4-cm range. At 190 kv proton energy, we found a distribution from reaction (1) which could be represented by $1+0.7\cos^2\theta$. Measurement of the α-particles from (2) within about 1 cm from the end of range gave a similar distribution. Measurements taken at 143 kv, however, gave a uniform distribution for the particles from (2). It was found that the distribution of these α-particles between 143 and 190 kv could be represented by $1+A\cos^2\theta$, where A, as a function of voltage for a thick boron target, showed a similar variation to the efficiency curve of reaction (1).

[1] At present a Westinghouse Research Fellow, Westinghouse Research Laboratories, East Pittsburgh, Pa.
[2] Neuert, Physik. Zeits. 38, 618 (1937).

43. A Precise Measurement of the Mass Difference $_4Be^9-{}_4Be^8$; the Stability of $_4Be^8$. SAMUEL K. ALLISON, ELIZABETH R. GRAVES, L. S. SKAGGS, AND NICHOLAS M. SMITH, JR., *University of Chicago.*—In a previous communication[1] we described an electrostatic analyzer for the energies of short range disintegration particles and reported the energy Q_4 of $_4Be^9(p,\alpha)_3Li^6$ to be 2.152 ± 0.04 Mev. In an extension of these experiments we have now found Q_3 of the concomitant reaction $_4Be^9(p,d)_4Be^8$ to be 0.557 ± 0.006 Mev. This latter value establishes the mass difference $_4Be^9-{}_4Be^8$ as 1.00720 ± 0.00007, and the binding energy of the odd neutron in $_4Be^9$ as 1.651 Mev, which should be the threshold for the photodisintegration of $_4Be^9$. With these precise values, it is now possible to express the masses of $_4Be^9$, $_4Be^8$, $_3Li^6$ *entirely* in terms of $_1H^1$, $_1H^2$, $_2He^4$ and the energies of nuclear reactions which have been measured with high precision. Using Bethe's values for the hydrogen isotopes, Bainbridge's helium[2] as 4.00386, and Q_1 of $_4Be^9(d,\alpha)_3Li^7$ as 6.95 Mev,[3] Q_2 of $_3Li^7(p,\alpha)_2He^4$ as 17.13 Mev,[4] we obtain:

$$
\begin{aligned}
{}_4Be^8 &= Q_1+Q_2-Q_3 &+3{}_2He^4-2{}_1H^2 &= \ \ 8.00739\\
{}_4Be^9 &= Q_1+Q_2-{}_1H^2+3{}_2He^4- &{}_1H^1 &= \ \ 9.01459\\
{}_3Li^6 &= Q_1+Q_2-Q_4 &+2{}_2He^4- &{}_1H^2 = \ \ 6.01655\\
{}_4Be^8-2{}_2He^4 &= Q_1+Q_2-Q_3 &+ {}_2He^4-2{}_1H^2 &= -0.00033.
\end{aligned}
$$

Accepting the author's estimate of their error in Q_1 as 0.04 Mev, the largest error in the above relations arises from the mass of helium and is 0.06 Mev. Thus $_4Be^8$ is stable with respect to two alpha-particles by 0.31 ± 0.06 Mev.

[1] Phys. Rev. 54, 171 (1938).
[2] Phys. Rev. 53, 922 (1938).
[3] Williams, Haxby and Shepherd, Phys. Rev. 52, 1031 (1937).
[4] Oliphant, Kempton and Rutherford, Proc. Roy. Soc. 149, 406 (1935), corrected by Bethe and Livingston.

44. Interactions of Heavy Electrons. J. FRANKLIN CARLSON, *Purdue University.*—The Coulomb scattering in nuclear fields, the collisions with free electrons and with bound electrons, have been studied theoretically for "heavy electrons," "dynatons" or "barytrons," which may be described by a vector wave equation. This vector wave equation, first suggested by Proca,[1] has been developed subsequently from the standpoint of the quantum theory of wave fields as a field theory which among other things gives forces of an exchange nature between nuclear particles.[2] The electromagnetic interactions of these particles will be discussed here. There are peculiarities in the Coulomb scattering by nuclei of these particles, which are intimately connected with their polarization. The points of agreement and difference between the Coulomb scattering by nuclei and the collisions with ordinary electrons of "heavy electrons" describable by a vector wave equation and with those described by a scalar wave equation will be discussed.

[1] Proca, J. de phys. 7, 347 (1936).
[2] Bhabha, Proc. Roy. Soc. 166 (1938). Nature (1938).
[3] Kemmer, Proc. Roy. Soc. 166, 127 (1938); Fröhlich, Heitler and Kemmer, Proc. Roy. Soc. 166, 154 (1938).

45. Design and Construction Features of the Westinghouse Electrostatic Generator. W. H. WELLS, *Westinghouse Research Laboratories.*—The belt type electrostatic generator designed and constructed at the Westinghouse Research Laboratories during the past two years will be described. A fifteen-foot diameter, high voltage terminal is supported inside the spherical thirty-foot diameter dome of a "pear" shaped pressure vessel by a porcelain-steel tower of a new simplified design. The pressure vessel is forty-seven feet in length, is designed for a working pressure of 120 lb./in.^{2} and has been tested at 160 lb./in.^{2}. Two eighteen inch belts give 500 microamperes at atmospheric pressure and after complete installation of the corona rings, seven and one-half foot sparkover occurs from the electrode to the pressure vessel wall. The accelerating tube has been assembled and evacuated under unusual mechanical conditions and preliminary test data will be given.

46. Incoming Cosmic-Ray Energies as Function of Latitude More Accurately Determined. R. A. MILLIKAN AND H. V. NEHER, *California Institute of Technology.*—Ten new flights up to pressure of ten millimeters mercury lead to following tentative conclusions: (1) cosmic-ray electrons enter the atmosphere down to energies of two billion electronvolts but no lower; (2) fluctuations at Bismark amounting to four percent divergence from mean value are greater than observational uncertainties; (3) the energies of the incoming electrons are again found confined to a sharply limited band with a pronounced maximum at about six million electronvolts; and (4) the results at Bismark agree closely with those found by Carmichael and Dymond near the north magnetic pole.

47. An Automatic Apparatus for Recording the History of Shower Phenomena Primarily in Relation to Showers Produced by Penetrating Cosmic Rays. W. F. G. SWANN AND W. E. RAMSEY, *Bartol Research Foundation of the Franklin Institute.*—The apparatus comprises ten trays, each containing eighteen Geiger counters. The trays are

arranged in a vertical column of total length 150 cm, each tray having an area of 400 square cm. A slab of lead 10 cm thick placed between the upper trays limits the phenomena produced below to phenomena of penetrating rays. Each of the remaining trays has a slab of lead 1 cm thick placed above it. Each of the 180 counters is connected to an electroscope provided with a mirror which reflects a spot upon a photographic plate. The electroscopes are only allowed to operate when a ray passes through the whole system; and in that case the record of every counter discharge is automatically imprinted upon the photographic plate and the history of all that has happened in the event is obtained.

48. Cosmic-Ray Measurements in the Stratosphere by Geiger-Müller Counters in an Integrating Circuit. L. F. CURTISS, A. V. ASTIN, L. L. STOCKMANN AND B. W. BROWN, *National Bureau of Standards.*—Earlier measurements by the authors[1] with small Geiger-Müller counters, directly keyed to a radio transmitter and carried aloft by free balloons, have revealed the desirability of observations less affected by statistical errors. These errors were necessary with the previous equipment because of the low maximum counting rate of the radio recording system on the ground. The large numbers of counts required to smooth out the random fluctuations can be obtained conveniently by using a fast counting circuit, such as that of Neher and Harper, and feeding its output to some type of integrating circuit which keys the radio transmitter once for a definite number of pulses. This has been done by a modification of the method reported by Johnson.[2] Approximately 20 successful flights were made from the National Bureau of Standards at Washington during the summer. These observations yield relatively smooth curves of cosmic-ray intensity *versus* pressure. The decrease in intensity beyond the maximum was not found to be as great as the single counter measurements seemed to indicate. By repeated observations with the identical balloon equipment some evidence has been obtained of variations in the shape of the intensity curve at different times.

[1] Phys. Rev. **53**, 23 (1938).
[2] Phys. Rev. **53**, 914 (1938).

49. Absence of Solar Component of Cosmic Radiation at High Elevations. S. A. KORFF AND T. H. JOHNSON, *Bartol Research Foundation of the Franklin Institute.*—Measurements of the total intensity of the penetrating radiation at high elevations have been carried out by the radio-balloon method, with single Geiger counters. The counters were of large area, and operated at a high counting rate in the upper atmosphere, the pulses being scaled 50 : 1 before transmission. The counting rates of the instruments used on the several flights were calibrated with a standard radium source. Flights have been made both during the day and the night. No significant difference between daytime and nighttime intensities was found, greater than the experimental uncertainty, amounting to five percent of the total intensity, up to elevations of 24 km (19 mm Hg). Flights three months apart show good agreement. The observations indicate the absence of any solar component in the penetrating radiation at 24 km, of more than five percent of the total intensity at that level. One daytime flight was caused to level off at 20 km, and remained at that level for about seven hours. During this time a prominent solar flare took place. No increase in counting rate as great as two percent was observed. It is concluded that the radiation from a solar flare is not sufficiently penetrating to enable it to reach a depth of 0.5 m water equivalent in the atmosphere.

50. Difference in the Absorption of Cosmic Rays in Air and Water and the Mean Life of the Barytron. T. H. JOHNSON AND M. A. POMERANTZ, *The Bartol Research Foundation of the Franklin Institute and the University of Pennsylvania.*—The intensity j_1 of the hard component of the cosmic radiation after passage through the atmosphere and an additional 8.9 meters of water contained in a large cylindrical tower has been compared with the intensity j_2 of the same radiation after passing along an inclined path at 58° from the zenith through an equal mass of air. A quadruple coincidence train of aperture less than that of the tower was mounted in a room beneath and counting rates were recorded alternately in the two positions. Lead plates of total thicknesses 17 cm and 38 cm, respectively, were interposed between the counters in two independent experiments. The ratio of counting rates in the two positions had the values $j_2/j_1 = 0.60 \pm 0.02$ with 17 cm lead; and 0.68 ± 0.02 with 38 cm lead. The lower intensities from the air path agree with Ehmert's experiments and may be interpreted as suggested by Heisenberg and Euler by the higher probability of spontaneous disintegration of the barytrons during the longer time required for traversal of the inclined path. The values of j_2/j_1 which we have measured give the mean life of a barytron at rest between 2 and 4×10^{-6} sec. depending upon our choice of rest mass, energy distribution and rate of loss of energy in air, water and lead.

51. Band Spectra in Nitrogen at Atmospheric Pressure. A Source of Band Spectra Excitation. OLIVER R. WULF AND EUGENE H. MELVIN, *Bureau of Chemistry and Soils, Washington, D. C.*—An apparatus, essentially an ozonizer, consisting of a condenser, a portion of the dielectric of which is a gas, has been used as a source of band spectra excitation. In such a source the temperature of the gas remains practically that of the walls. Nitrogen bands $A \rightarrow X$ have been photographed in emission at atmospheric pressure under resolution sufficient to permit measurement of part of their rotational structure. In this source the first positive group is considerably weaker relative to the second positive group than in an ordinary glow discharge. The rather striking difference between this type of source and a high voltage low current arc at atmospheric pressure is illustrated by some band spectra in oxygen containing a small amount of nitrogen.

52. Raman Spectra of Phenyl-1-Propyne-1 and Chloro-2-Phenyl-1-Acetylene. FORREST F. CLEVELAND AND M. J. MURRAY, *Lynchburg College.*—Previous work[1] on the Raman

spectra of derivatives of phenylacetylene has been extended to include (I) $C_6H_5C{\equiv}CCl$ and (II) $C_6H_5C{\equiv}CCH_3$. Interest has been focused primarily upon the lines in the neighborhood of 2220 cm^{-1} and the technique of diaphragming the camera lens to improve the definition and thus to detect possible splitting of lines in this region has been continued. Two lines have been observed in this region for I, 2203(2) and 2222(10), and four lines for II, 2210(8), 2230(4), 2246(10), and 2262(6). A total of 22 frequencies were observed for I. Fourteen of these agree with the results of Bourguel and Daure.[2] Additional frequencies, 334(3), 654(1), 754(2), 1208(1), 1224(2), 2203(2), 2977($\frac{1}{2}$), and 3079(2), have been observed in the present work, while the frequency 766, listed by Bourguel and Daure, has not been observed. A total of 36 frequencies have been observed for II. Sixteen of these agree with frequencies obtained by Bourguel and Daure[2, 3] and also by Gredy.[4] Seven agree with values listed by Bourguel and Daure, but not found by Gredy. Three frequencies, 1443, 1493, and 2253, listed as single by Bourguel and Daure and by Gredy, appear as doublets in the present work. Seven frequencies, 953(1), 1053($\frac{1}{2}$), 1245(1), 1286(2), 2231(4), 3111(1), and 3143(1), were not observed by the above workers. Frequencies 2974 and 3017, listed by Gredy, were not found by Bourguel and Daure or in the present work. It is a pleasure to acknowledge grants in aid of this research by Sigma Xi, the Virginia Academy of Science, and the American Association for the Advancement of Science.

[1] Phys. Rev. **53**, 330, 931 (1938); J. Am. Chem. Soc. **60**, 2664 (1938).
[2] M. Bourguel and P. Daure, Bull. Soc. Chim. **47**, 1349 (1930).
[3] M. Bourguel, Comptes rendus **195**, 311 (1932).
[4] Blanche Gredy, Thèses, Paris, 1935; Comptes rendus **196**, 1119 (1933).

53. Van der Waals Forces in the Boron Molecule. JULIAN K. KNIPP, *Purdue University*.—A very important class of molecules arises from atoms not having spherical symmetry. An example is the boron molecule which dissociates into two boron atoms in normal P states. The interaction energy of these molecules depends on the relative orientation of the atomic angular momenta and at large interatomic distances is due to the quadrupole-quadrupole term in the molecular Hamiltonian. At smaller distances the van der Waals forces become important. The quadrupole-quadrupole energy is a first-order effect with an inverse fifth dependence on the interatomic distance and the van der Waals energy is a second-order effect coming from the dipole-dipole term in the Hamiltonian and having an inverse sixth power dependence. These effects are treated simultaneously. Potential energy curves are followed from large separation distances to distances where exchange and other effects become important. The constants which enter are estimated with the aid of the Hartree-Fock atomic model.

54. On Depolarization of Neutrons Passing Through Ferromagnetic Media. O. HALPERN AND TH. HOLSTEIN, *New York University*.—A beam of neutrons which is partially polarized undergoes depolarization when passing through a nonsaturated ferromagnetic medium. This is because of the existence of randomly oriented domains of spontaneous magnetization in the material. These haphazardly directed magnetic fields lead to a "Brownian movement" of the spin axis of the neutrons. The treatment is straightforward in the case that the period of the Larmor precession is large compared to the time spent in one domain of magnetization. If this condition is not satisfied, more complicated phenomena obtain. Under simple conditions the original polarization decreases as $e^{-(\omega^2\delta d/3v^2}$ (ω=Larmor frequency, v=neutron velocity, δ=thickness of domain, d=total thickness traversed). Observations in this field could lead to a new estimate of the size of these "Barkhausen domains" and to information about the amount of spontaneous magnetization. The phenomena are also of interest in connection with observations on the polarization of neutrons transmitted through, or scattered by a ferromagnet.

55. Depolarization Effects in the Double Scattering of Electrons. M. E. ROSE AND H. A. BETHE, *Cornell University*.—In an attempt to explain the discrepancy between Mott's theory[1] and Dymond's experiments[2] on the polarization of electrons, we have investigated theoretically the depolarizing effect of (1) multiple elastic scattering, (2) inelastic scattering with spin change, (3) exchange scattering with spin change. Multiple scattering is no doubt present with the 2.5×10^{-5} cm Au foils used by Dymond, but the depolarizing effect caused by such scattering is negligible. For a screened Coulomb field the depolarization is of order one percent whereas 90–100 percent is needed to reconcile theory and experiment. The depolarization arising from inelastic scattering, in which the incident electron changes spin direction, and from exchange scattering, in which the exchanged electrons have opposite spin directions, is much smaller than the depolarization caused by multiple scattering. This is largely because of the fact that for the inelastic scattering, the scattering angles and energy losses are small; and for the exchange scattering only the valence electron of Au can participate in the exchange process.

[1] N. F. Mott, Proc. Roy. Soc. **135**, 429 (1932).
[2] E. G. Dymond, Proc. Roy. Soc. **145**, 657 (1934).

56. Retarded Interaction Between Electrons. IRVING S. LOWEN, *New York University*.—The expression for the retarded interaction between two electrons, first given by Breit,[1] can be obtained without the use of the perturbation theory in the following fashion. If in the Hamiltonian for the interaction of matter with the radiation field, from which the longitudinal waves have been eliminated, the term quadratic in the transverse field amplitudes be combined with the term giving the interaction with matter, which is linear in the field amplitudes, by completing the square, one has left over a term in which the field amplitudes do not appear and which is just the expression for the retarded interaction between two electrons given by Breit. The new field Hamiltonian can then be transformed back into its original form by a contact transformation.

[1] Phys. Rev. **39**, 616 (1932).

57. Catalytic Activity and Crystal Orientation of Metal Films. OTTO BEECK, A. WHEELER AND A. E. SMITH, *Shell Development Company*.—Metal films of high and reproduc-

ible catalytic activity were prepared by condensation of their vapors on glass in an atmosphere of an inert gas (N_2, A, etc.) at low pressures and room temperature. Nickel films thus prepared in 1 mm Hg of N_2 or A were shown by electron diffraction (see also following abstract) to be completely oriented with their (110) plane parallel to the backing, the two remaining axes showing random distribution. Iron films were oriented with their (111) plane parallel to the backing. Unoriented nickel films of 5.5 times lower activity were obtained by condensation of nickel vapor in high vacuum, the films showing a slight orientation when more than 10,000 atoms thick. The high vacuum films possess four times the electrical conductivity of the films condensed in gas and one-half of their surface as found by adsorption measurements of H_2 at room temperature and of CO at liquid-air temperature. For both film types catalytic activity, surface area and conductivity increase with film thickness, the last two being linear functions of the thickness. This shows that the interior of the film is accessible through pores. After elimination of the surface factor the oriented gas-condensed films have still more than two and one-half times the catalytic activity of the unoriented high vacuum films. The larger distances between the nickel atoms in the (110) plane are probably the seat of this greatly enhanced catalytic activity. The investigation was extended to Fe, Pd and Pt with essentially similar results.

58. Preparation and Structure of Oriented Metal Films. A. E. SMITH AND OTTO BEECK, *Shell Development Company, Emeryville, California.*—Although the tendency for metal films prepared by condensation to take preferred orientation has long been observed, conditions during deposition that produce this effect are not well understood. The observation that metal films of high catalytic activity prepared by condensation on glass at room temperature in an inert gas (N_2, A, etc.) of low pressure also exhibit a high degree of orientation (see also preceding abstract) has helped considerably to clarify this problem. The degree of orientation induced by the presence of an inert gas during condensation increases with the pressure from high vacuum to 1–2 mm Hg. Film thickness has an important influence on the degree of orientation. On glass surfaces which are well baked out nickel films 3000 atoms thick are completely oriented when deposited in 1 mm Hg of N_2 or A, whereas films of the same thickness deposited in high vacuum are unoriented, though they show a slight orientation with increasing thickness. The influence of air, oxygen, and water vapor on the formation of oriented films will be discussed. Besides nickel, various other metals—iron, cobalt, palladium, platinum, and also copper and gold—have been investigated. It is of special interest that iron (cubic body centered) orients with the (111) plane parallel to the backing whereas Ni (cubic face centered) exhibits the (110) plane. A possible mechanism for the orientation has been deduced from these results.

59. Double β-Disintegration and the Theory of the Neutrino. W. H. FURRY, *Harvard University.*—There are two possible general theories of β-disintegration. If the neutrino obeys the same sort of Dirac theory as the electron, one may suppose that the emission of a neutrino accompanies that of a positron, and an antineutrino must accompany the emission of an electron. In Majorana's modification of the Dirac theory there are no antineutrinos, and the emission of either an electron or a positron has associated with it the emission of a neutrino. Both pictures give the same results for ordinary β-disintegration. In the case of double β-disintegration, however, there is a marked difference. On the original Dirac theory the emission of two electrons (or positrons) must be accompanied by that of two antineutrinos (neutrinos), and, for $\Delta M \sim 0.002$ mass unit, the lifetime is of the general order of magnitude 10^{24} years. On the Majorana theory the disintegration can take place without any neutrino emission, and the lifetime, for $\Delta M \sim 0.002$ mass unit, is something like 10^{16} years (Fermi Ansatz) or 10^{9} years (K-U Ansatz). More accurate investigation of the masses and stabilities of isobars may accordingly make possible a decision between the two theories.

60. Thermal Equilibrium and Microscopic Entropy. EDWIN C. KEMBLE, *Harvard University.*—Exceptions to the second law of thermodynamics due to fluctuation phenomena can be eliminated by two modifications of procedure. The first is to replace assertions regarding individual systems in thermodynamics by corresponding statements regarding Gibbsian assemblies of identical independent systems similarly prepared. The second is to discard the common definition of thermodynamic equilibrium as the ultimate state approached by any system isolated for a long period of time. We redefine thermodynamic equilibrium as follows. Let each member of an assembly of systems A be placed in thermal contact with a corresponding member of an assembly of constant temperature baths of very large heat capacity, the combined system being isolated. The baths must have a common initial temperature T as measured by a thermometer. The ultimate state of the assembly of systems A is then called a state of thermodynamic equilibrium at temperature T. The redefinition of thermodynamic equilibrium obviates difficulties encountered by von Neumann in connection with his "microscopic" definition of entropy in quantum statistical mechanics. The state of thermodynamic equilibrium becomes identical with the canonical assembly of Gibbs and with the state of maximum microscopic entropy S_m for the appropriate energy. A redefinition of the reversible path gives

$$dS_m = (dQ/T)_{rev}.$$

61. On the Derivation of Nuclear Forces from Field Theories. EUGENE FEENBERG, *Washington Square College, New York University.*—The Hamiltonian for a system consisting of a Yukawa field and heavy particles (neutrons, protons) contains (a) a field Hamiltonian which is quadratic in the field amplitudes, (b) a coupling term linear in the field amplitudes, (c) the Hamiltonian operators of free heavy particles. Nuclear forces may be computed by a perturbation method[1] or by applying a canonical trans-

formation[2] to the Hamiltonian of the total system. The two methods do not yield the same forces in all cases, but do agree when the heavy particles are constrained to move in a prescribed manner (in this case, Part (c) of the Hamiltonian is omitted, which amounts to neglecting the reaction of the field on the heavy particles when they absorb or emit quanta of the field). Parts (a) and (b) can be combined into one term by completing the square and subtracting a function which is identical with the nuclear potential given by the second order perturbation calculation when recoil effects are neglected. A canonical transformation then reduces the Hamiltonian to the form (a) plus a sum of interaction potentials between pairs of particles. If Part (c) is included in the Hamiltonian a modified form of this procedure yields forces which agree, where comparison is possible, with the approximately relativistic forces computed by Breit.[3]

[1] N. Kemmer, Proc. Roy. Soc. **166**, 127 (1938).
[2] E. C. G. Stueckelberg, Comptes rendus **207**, 387 (1938).
[3] G. Breit, Phys. Rev. **51**, 248 (1937).

62. Nuclear Reactions Produced by 6.5 Mev Protons. L. A. DuBridge, *The University of Rochester.*—A survey of the radioactivities induced by 6.5 Mev protons in all the readily available elements of the periodic table has been partially completed by the members of the Rochester group. Definite activities are observed in elements as heavy as $_{76}$Os and there is some evidence for a reaction in $_{90}$Th. Most of the elements above $_{52}$Te, however, show no activity. Where identification is possible the reactions are found to be of the $p-n$ type in nearly all cases. An interesting reaction of the (p,p) type leading to a radioactive excited state of In^{115} has been found by Barnes.[1] Over 30 $(p-n)$ reactions leading to radioactive isotopes already produced by other methods and 20 leading to new isotopes have been found and will be summarized. The thick target yields have been determined in many cases and are found to decrease regularly with increasing atomic number. The actual values range from 500 radioactive atoms per 10^6 protons for $Li^7(p-n)Be^7$ down to 0.1 per 10^6 for $W(p-n)Re$.

[1] Chicago Meeting abstracts, 1938.

63. Proton-Proton Scattering. N. P. Heydenburg, L. R. Hafstad and M. A. Tuve, *Department of Terrestrial Magnetism, Carnegie Institution of Washington.*—During the past year we have made a new series of observations on the scattering of protons by protons in the range 700 kv to 900 kv, using the linear amplifier for detection. A completely new scattering apparatus was used, the voltmeter was recalibrated, and the scattering from gold was used as a current-integrator. The calibration was reduced to absolute values by observing the scattering of protons by spectroscopically pure argon. Although completely independent, the results are in agreement with our observations of two years ago. The Mott-ratios differ at most by five percent from our earlier values, which were subject to fluctuating errors arising from the current measurements.

64. The Kinetic Energy of the Electrons in the Wigner-Seitz Theory. R. Landshoff, *University of Minnesota.*—The total energy of a system as calculated from approximate wave functions is a much better approximation to the actual energy than either the kinetic or the potential energy is to its actual values. The comparison of the theoretical and experimental values of the kinetic energy is thus a better criterion for the degree of approximation attained by a given wave function than the comparison of the values of the total energy. Bridgeman and Slater have pointed out the value of the virial theorem for the calculation of the kinetic energy. The application of this theorem on solids under stress leads to the expression

$$T=-E-(X_x+Y_y+Z_z)V$$

for the kinetic energy. The electronic constitution of metals in the theory of Wigner and Seitz will be discussed from this aspect. It is necessary to modify the theory slightly. As long as only the calculation of the total energy was desired, it was sufficient to express the interaction of the electrons in the atom by means of a simple potential function. The calculation of the kinetic energy requires a more thorough consideration of the electronic interaction. The change does not affect the basic idea of the Wigner-Seitz scheme.

65. The Scattering of Protons by Protons. R. G. Herb, D. W. Kerst, D. B. Parkinson and G. J. Plain, *University of Wisconsin.*—The cross section for scattering of protons by protons has been measured for angles from 15° to 45° at voltages of 860, 1200, 1390, 1830, 2105, and 2392 kv. The general design of the scattering chamber follows that used by Tuve, Heydenburg, and Hafstad.[1] However, modifications were made in many details and a different system is used for measurement of incident proton current. The proton beam after traversing the scattering chamber passes through an aluminum foil into an evacuated region and enters a collector cup. Observed scattering cross sections at 15° are close to Mott values for all voltages. Ratios of observed cross section to Mott cross section rise with increasing angle and with increasing voltage. At 45° the ratio rises from 3.90 at 860 kv to 42.9 at 2392 kv. At 1830 kv measurements were made at scattering angles up to 60° and the scattering cross section showed the theoretically expected asymmetry $(\cos\theta)$ about 45°. Precautions were taken to avoid systematic errors due to factors such as generator voltage, measurement of incident proton current, and the counting of scattered protons. As an additional check on the proton-proton measurements the scattering from krypton and argon was investigated for voltages between 850 kv and 2440 kv.

[1] M. A. Tuve, N. P. Heydenburg, and L. R. Hafstad, Phys. Rev. **50**, 806 (1936).

66. Interpretation of Experiments on Proton-Proton Scattering. G. Breit, H. M. Thaxton and L. Eisenbud,* *University of Wisconsin.*—The data of Herb *et al.* give no evidence for the presence of p or d wave anomalies in agreement with theory. The phase shift $|K_1|$ is probably

less than 1° at 2400 kev while a repulsion $38e^{-16r^2}$ n.u. gives $K_1=-0.4°$. The values of the phase shift K_0 are fitted nicely using a constant potential -11.3 Mev superposed on the Coulombian repulsion through a distance e^2/mc^2. This potential is 0.3 Mev shallower than the corresponding $^1S_{\pi\pi}$ value needed for the value 16.5×10^{-24} cm² of the free slow neutron-proton scattering cross section. The data determine the effective range of the $\pi-\pi$ potential with an apparent accuracy of 5 percent. Preliminary probable values are: 0.97 e^2/mc^2 for constant potential; $\alpha=21.(6)$, $A=51.(4)$ for $Ae^{-\alpha r^2}$. Experiment disagrees with $\alpha=16$. For $\alpha=20$: $A_{\pi\pi}=47.4$, $A_{\pi\nu}=48.3$. An error of 1 percent in scattering gives 0.2 percent error in $A_{\pi\pi}$. This range agrees with that suggested by Rarita and Present who used the binding energy of H^3 and, according to them, is in contradiction with He^4. Unpublished results of Tuve *et al.* are taken account of above. Possible velocity dependence: $\delta\alpha=2$ corresponds roughly to $\delta A=0.7$ percent per 2400 kev.

* Now at Princeton University.

67. Proton Induced Activity of Manganese. ARTHUR HEMMENDINGER, *University of Oklahoma.**—The reaction $Cr^{52}(p,n)Mn^{52}$ at 6.6-Mev proton energy produces isomers with periods of 21.3 min. and 7.4 (±1.0) days. These are positron emitters with maximum positron energy of 2.2 Mev (21 min.) and 0.77 Mev (7 days). There is gamma-radiation of energy 1.2 Mev (21 min.) and 1.0 Mev (7 days). By a comparison of the ionization due to the annihilation radiation and that due to the 1.2-Mev radiation (the two are separated by absorption measurements) it can be shown that the 21-min. isomer emits 2 gamma-quanta per positron, and this is just what one would expect as a consequence of the high threshold (6.4-Mev proton energy) for the formation of the 21-min. isomer. The gamma-radiation from the 7-day isomer is 10 times as intense as that from the 21 min. In addition to positron emission followed by the radiation of one gamma-quantum, there must be the alternative mode of disintegration by K-electron capture, leaving the nucleus in the 1 Mev excited state.

* A report on work done at the University of Rochester during the summer of 1938.

68. The Iteration Method. GABRIEL HORVAY, *Columbia University.*—The averages of the powers of H, $\langle H^k\rangle = \int\Psi_0^* H^k\Psi_0 d\tau$, in terms of the approximate wave function Ψ_0, yield valuable information about the eigenvalue problem, $H\varphi=E\varphi$. For example, the variational principle applied to the wave function $\Psi=\Sigma_0^n\lambda_k\Psi_k$ $(\Psi_k=H^k\Psi_0)$ leads to the secular equation of $(n-1)$th order, $|E\langle H^{i+j}\rangle - \langle H^{i+j+1}\rangle|=0$. The lowest root of this equation is an upper bound for the lowest eigenvalue, E_0, of H. If Ψ_0 is a very close approximation to the ground state eigenfunction, then the $\langle H^k\rangle$'s also furnish interesting lower bounds for E_0.[1] Another method of approach is the following. The knowledge of the averages for $k=0, 1, \cdots, n$ permits the determination of the polynomials in η, $K(k,\eta)=\Sigma_0^n c_i^2(E_i-\eta)^k$ $(k=0, 1, \cdots, n)$, where the E_i are the eigenvalues of H and c_i the Fourier coefficients of Ψ_0 with respect to the true eigenfunctions of H. For values of the parameter $\eta>E_0$, there is a marked difference in behavior of K for k odd and k even. For $\eta<E_0$ these differences disappear. Thus a study of the tentative curves $K(k)$ which can be drawn for various η permits an estimate of E_0. This method, when applied to the oxygen problem in Wigner's first approximation, seems to indicate that a binding energy slightly greater than that of four α-particles is not an unreasonable estimate.

[1] Results of Weinstein and MacDonald, discussed in Pauling and Wilson, *Introduction to Quantum Mechanics*, Chapter VII. Further discussion will appear in a forthcoming issue of the *Physical Review*.

69. Complex Roots of Fifteenth-Degree Polynomials. S. LEROY BROWN, *University of Texas.*—A mechanical synthesizer[1] with thirty harmonic elements (fifteen sine and fifteen cosine components) is converted into a multi-harmonograph by communicating the sum of the sine-component motions to vertical motion of a tracing point while the sum of the cosine components produces backward and forward motion of the drawing board in a horizontal direction. Each term $a_n z^n$ of the polynomial may be expanded by DeMoivre's theorem into $a_n r^n(\cos n\theta + i\sin n\theta)$ where r is a modulus of z (complex). When the coefficients a_n are real, set the n harmonic components (sine and cosine) of the machine to the respective amplitudes of $a_n r^n$ and the trace obtained will show all values of $-a_0$ (real, imaginary, and complex) for which $r(\cos\theta + i\sin\theta)$ is a root of the polynomial. The modulus r may be so chosen that the trace goes through a particular $-a_0$ and, thereby, a root (or roots) of a particular polynomial is determined (root of modulus r and angle θ, angle being determined by angle of the fundamental on machine as the trace goes through the position $-a_0$). Since there are fifteen multiple harmonic components in the machine, the complex roots of a 15th-degree polynomial may be determined; and, for lower degree polynomials, only the lower harmonic components of the machine are needed. If the coefficients a_n of the polynomial are complex, as well as the roots, the procedure is similar to the one outlined above except that the so-called sine and cosine components of the machine must each be set to an amplitude (magnitude of $a_n r^n$) and to an angle (angle of a_n).

[1] "A Mechanical Synthesizer-Analyzer," Phys. Rev. **53**, 333 (1938).

70. Soft X-Ray Emission Spectra of Valence Electrons. H. W. B. SKINNER, *University of Bristol*, AND H. M. O'BRYAN, *Georgetown University.*—Emission spectra of simple solid compounds in the region between 18A and 300A indicate that the widths of the energy bands of their valence electrons vary from about 0.5 electron volt for halides to over 30 ev for certain oxides. These soft x-ray spectra show greater detail of the structure and nature of the valence electron states than can be obtained from either optical absorption or ordinary x-ray emission. With sufficient care both contamination and decomposition within the x-ray tube can be avoided for many compounds and spectra obtained which are free from impurity and metallic lines. The halide ions in the very polar alkali halide crystals show, in addition to the structure expected from atomic states, shorter wave-length structure some-

what similar to x-ray satellites. The widths of the halide bands are much less than predicted by theory. Spectra emitted by transitions of the valence electrons into the K shells of both the positive and the negative ions of BeO and B_2O_3 have been observed. There is no close correspondence in the widths and structure of these positive and negative ion spectra of any compound so far studied. This indicates that the distribution and character of the energy states of valence electrons must be quite different in the vicinity of the positive ions from that near the negative ions.

71. Excitation Potential of $L\alpha$ Satellites. R. E. SHRADER AND F. K. RICHTMYER, *Cornell University.*—Coster and Kronig[1] have suggested that the doubly-ionized state required for the production of x-ray satellites can result from an Auger transition. Their theory assumes that the $L\alpha$ satellites arise from the atomic transition, $L_{III}M_{IV,V} \rightarrow M_{IV,V}M_{IV,V}$, and that the initial state is obtained as a result of the Auger transition, $L_I \rightarrow L_{III}M_{IV,V} + \epsilon$, where ϵ represents the kinetic energy of the ejected $M_{IV,V}$ electron. This assumption seems to be confirmed by recent measurements of the intensity (relative to the $L\alpha_1$ line) of the $L\alpha$ satellites of Au(79) as a function of tube voltage. Using a well-filtered voltage supply, the authors have found that at low voltages the satellite intensity decreased with decreasing tube voltage and are not observed for voltages below the excitation potential of the gold L_I state.

[1] D. Coster and R. deL. Kronig, Physica **2**, 13 (1935).

72. Arrangement of Atoms and Molecules in Extremely Thin Films. L. H. GERMER, *Bell Telephone Laboratories, Inc.*—Films of various inorganic substances, produced by vaporization in high vacuum upon organic supporting foils, have been investigated by electron diffraction by the transmission method. Varying amounts of material have been vaporized from V-shaped tungsten ribbons upon foils supported across narrow slits.[1] Mean thickness of each of these films has been calculated from the total amount of vaporized material, distance of the film from the tungsten ribbon, and calibration of the apparatus based upon weighing the material making up a known area of film. Many substances have been studied, from gold (atomic number 79) to beryllium (atomic number 4). For the heavier materials, at least down to copper (atomic number 29), interpretable diffraction patterns can be obtained from films which contain only enough material to form a single layer of atoms or molecules. *In all cases true three dimensional crystals are formed.* In films of caesium iodide, which forms unusually large crystals, the mean linear dimension of a crystal is about 100A in a film having an average thickness of only 1.8A. In films of appreciable thickness ionic compounds form, in general, larger crystals than metals.

[1] See Fig. 4, Proc. Nat. Acad. **23**, 390 (1937).

73. Measurement of the Self-Diffusion of Copper. J. STEIGMAN, *Columbia University*, W. SHOCKLEY AND F. C. NIX, *Bell Telephone Laboratories.*—The high speed rotating cathode technique of electroplating has been applied to the separation from the parent zinc of radioactive copper, transmuted from zinc by neutron bombardment. The radioactive copper, together with a trace of ordinary copper, used as a carrier, is plated upon a copper disk, forming a very thin layer.[1] Spectrochemical tests fail to show the presence of zinc in most instances and in those cases where traces of zinc were found, its presence did not appear to influence the results. Quadrants cut from the disk are clamped face to face between two copper blocks and heated in an evacuated quartz tube, thus permitting the radioactive copper to diffuse into the bulk copper. Measurements of the initial and final activities observed from the surface of the disk supplemented by the known values for the half-life of radioactive copper and the absorption coefficient for the copper radiation in copper yield values for the diffusion constant. The results indicate that the rate of self diffusion of copper is considerably smaller than the value predicted by Rhines and Mehl[2] from an extrapolation to pure copper of the rates of diffusion of small percentages of Si, Al, Zn, Sn and Be in copper.

[1] J. Steigman, Phys. Rev. **53**, 771 (1938).
[2] F. N. Rhines and R. F. Mehl, Am. Inst. Min. and Met. Eng., Technical Pub. No. 883, Class E, Inst. of Metals Div., No. 250. Published in Metals Technology, Vol. 5, No. 1, Jan. 1938.

74. A Dilatometric Study of the Order-Disorder Process in Single Crystals of Copper-Gold Alloys. FOSTER C. NIX AND D. MACNAIR, *Bell Telephone Laboratories.*—Dilatometric studies were made on single crystals of copper-gold alloys, made in a vacuum furnace, containing 22, 28 and 30 atomic percent gold. For temperatures below about 250°C, the temperature where disordering sets in on heating of ordered alloys, the instantaneous or true temperature coefficient of expansion of previously well-ordered alloys is constant. This "disordering" temperature is only slightly dependent on composition for alloys in the composition range from 22 to 30 atomic percent Au. For higher temperatures, the temperature coefficient of expansion increases very rapidly with increasing temperature, passes through a maximum, and then declines until a constant value is again reached. The latter value remains constant up to the highest temperatures studied, which in some cases reached 600°C. The decline to that value above the maximum covers a temperature range varying from 8 to 15°C depending on the composition. Plots of temperature coefficient of expansion-*versus*-temperature for disordered alloys, obtained by quenching in oil from 550°C, display a decrease in the temperature coefficient of expansion near 120°C.

75. X-Ray Atom Factors for Zn in ZnO. K. LARK-HOROVITZ AND C. H. EHRHARDT, *Purdue University.*—Electron diffraction patterns of zinc oxide show an anomalous intensity distribution as compared with the x-ray pattern.[1] As possible explanations were suggested: A shift of the electron cloud,[2] in respect to the nucleus, a distortion of the crystal lattice,[3] a distortion of the electron cloud and particularly of the valence electrons,[4] or dynamical reflection of the electron waves not taken into account in the kinematic theory. As additional experimental evidence x-ray diffraction patterns from a flat sample of zinc oxide

using monochromatic Cu $K\alpha$-radiation have been obtained photographically, and their relative intensities measured. From these results it is possible to calculate the x-ray atom factors for Zn and thus to construct theoretical electron diffraction curves. These reproduce the essential features of the electron diffraction experiments of K. Lark-Horovitz and H. J. Yearian. Therefore, the change in the value of F in the expression for electron diffraction intensity $[(Z-F)/(\sin^2\theta/\lambda^2)]^2$ must be primarily responsible for the observed intensity anomaly and not application of the kinematic theory. This is also in agreement with the explanation by James and Johnson,[4] since the x-ray intensities calculated from our experiments are in better agreement with the theoretical values obtained by using the distorted charge distribution as calculated by James and Johnson than with the symmetrical distribution of Pauling and Sherman.

[1] H. J. Yearian and K. Lark-Horovitz, Phys. Rev. **42**, 405 (1932).
[2] H. J. Yearian, Phys. Rev. **48**, 631 (1935).
[3] V. A. Johnson and L. W. Nordheim, Phys. Rev. **51**, 1002 (1937).
[4] V. A. Johnson and H. M. James, Phys. Rev. **53**, 327 (1938).

76. LiF Achromats for Covering Large Spectral Ranges. C. HAWLEY CARTWRIGHT, *Massachusetts Institute of Technology*.—LiF corrected by SiO_2 is especially suited for an achromatic lens for covering a broad spectral range. This is due to the small dispersion of LiF and the optical constants of SiO_2 (Ord. ray) combining favorably with those of LiF so as to give relatively long focal lengths to the lens elements and $df/d\lambda=0$ for two wave-lengths instead of for only one, as is usual for a combination of two materials. Working with Professor Stockbarger, a corrected doublet was built which is calculated to be achromatic to ± 0.5 percent from 1800A to about 20,000A. A triplet of SiO_2-LiF-SiO_2 corrected for spherical aberration and coma is being built which should be achromatic to ± 0.25 percent from 2300A to 14,000A. A corrected doublet of LiF and CaF_2 was designed and built for the ultraviolet region between 1300A and 1800A.

77. A New Nitrogen Afterglow Spectrum. JOSEPH KAPLAN, *University of California, Los Angeles*.—An interesting spectrum of a nitrogen afterglow at fairly high pressures (about 10 mm) is presented because every hitherto observed feature of nitrogen afterglows is on the plate, as well as two new characteristics. The first of these is the Goldstein-Kaplan band system of nitrogen. These bands correspond to a transition from a level at 12.05 volts to the $B^3\pi$ level (the level on which the well known first-positive bands originate). Their presence in this afterglow in company with the first-negative bands of N_2^+; the new 3466.3 line of atomic nitrogen, the Vegard-Kaplan bands, the second-positive and first-positive bands, indicates that they too may play a significant role in the spectrum of the light of the night sky and in auroral spectra. The second of these characteristics is the diminution with pressure of the two transitions from metastable states, i.e., the 3466.3 line and the Vegard-Kaplan bands. This too will probably be of some interest in the discussion of problems of the upper atmosphere.

78. A Recording Generating Voltmeter for Lightning Studies. E. J. WORKMAN AND R. E. HOLZER, *University of New Mexico*.—An instrument for recording the surface field intensity under active thunder storms is described. The assembly is contained in a weatherproof iron box (10″×10″×12″ high) which has a false top, above the weather lid, under which a plate rotates at 300 r.p.m. The plate consists of two opposite quadrants of a disk and is insulated from the vertical motor shaft which extends through the weather cover. Water baffles are provided. The top cover is cut out in such a way as to expose the quadrants twice during each revolution in which positive ground contact is made. In intermediate positions contact is made to an electrometer needle. The quartz electrometer is a modified quadrant type with deflections in a vertical plane and plates 22 volts above and below ground. The sensitivity of the instrument is adjusted to record fields from +1000 to −1000 volts/cm on a standard 16 millimeter negative which is sprocket fed past a 0.002″ slit at 15 feet per day from 100-foot magazines. Recorded deflections follow field changes with time resolution appropriate to the slit width. Five of these instruments have been used synchronously on storms, and the performance is demonstrated with prints from the records.

79. A Vacuum Interferometric Dilatometer with Photographic Recording for Measuring Thermal Expansion of Metals and Alloys at Elevated Temperatures. FOSTER C. NIX, *Bell Telephone Laboratories*.—A recording dilatometer especially adapted to the precise measurement of thermal expansion of metals at elevated temperatures has been constructed. The two polished fused silica plates of the interferometer are separated by the three small specimens to be studied, and the lower disk serves also as a refraction thermometer.[1] The fused silica plates with specimens are mounted in a vacuum furnace which is heated at any desired predetermined rate. A vacuum of 10^{-6} mm of Hg is maintained throughout the measurement to avoid any disturbance due to oxide formation. The optical system is essentially a Pulfrich viewing apparatus arranged to permit the photographic recording of the fringes produced by the combination of the two plates as well as the fringe system of the refraction thermometer. The fringes are photographed by means of a 16-mm motion picture camera at intervals varying from 10 seconds to 2 minutes; a small electric motor of adjustable speed is employed to trip the single exposure mechanism. The thermal expansion and temperature can be obtained from a knowledge of the number of fringes which pass the fiduciary marks of the two fringe systems.

[1] J. B. Austin, Physics **3**, 240 (1932).

Author Index to Abstracts of Washington Meeting

Aebersold, Paul C.—No. 29
Allen, H. W.—see Holmes, R. M.
Allen, J. S.—see Haxby, R. O.
Allison, Samuel K., Elizabeth R. Graves, L. S. Skaggs and Nicholas M. Smith, Jr.—No. 43
Alvarez, Luis W. and Kenneth S. Pitzer—No. 30
Astin, Allen V.—No. 18
——see Curtis, Harvey L.
——see Curtiss, L. F.

Beams, J. W.—No. 8
——see Skarstrom, C.
Beeck, Otto, A. Wheeler and A. E. Smith—No. 57
——see Smith, A. E.
Bethe, H. A.—see Rose, M. E.
Bramley, Arthur—see Brewer, A. Keith
Breit, G., H. M. Thaxton and L. Eisenbud—No. 66
Brewer, A. Keith and Arthur Bramley—No. 2
Brown, B. W.—see Curtiss, L. F.
Brown, S. LeRoy—No. 69
Bruce, W. A.—No. 20

Carlson, J. Franklin—No. 44
Carr, H. E.—see Skarstrom, C.
Cartwright, C. Hawley and A. Francis Turner—No. 22
————No. 76
Castleman, R. A., Jr.—No. 12
Cleveland, Forrest F. and M. J. Murray—No. 52
Coblentz, W. W. and R. Stair—No. 3
Cohen, V. W. and H. H. Goldsmith—No. 32
Cole, Peter A.—No. 33
——see Hollaender, Alexander
Colwell, R. C., J. K. Stewart and A. W. Friend—No. 23
Cooper, F. S.—see Pollock, H. C.
Curtis, Harvey L. and Allen V. Astin—No. 19
Curtiss, L. F., A. V. Astin, L. L. Stockmann and B. W. Brown—No. 48

Dennison, D. M.—see Fuson, N.
Dietrich, J. R. and L. B. Snoddy—No. 7
Dorsey, N. Ernest—No. 21
DuBridge, L. A.—No. 62

Eaton, J. R.—see Maxfield, F. A.
Ehrhardt, C. H.—see Lark-Horovitz, K.
Eisenbud, L.—see Breit, G.
Ellis, Joseph W.—No. 36

Feenberg, Eugene—No. 61
Field, J. E.—see Gehman, S. D.
Fountain, C. R. and E. G. Pigg—No. 10
Friend, A. W.—see Colwell, R. C.
Furry, W. H.—No. 59
Fuson, N., H. M. Randall and D. M. Dennison—No. 1

Gehman, S. D. and J. E. Field—No. 17
Germer, L. H.—No. 72
Goldsmith, H. H.—see V. W. Cohen
Graves, Elizabeth R.—see Allison, Samuel K.
Gunn, Ross—No. 4
Guth, Eugene—No. 13

Hafstad, L. R.—see Heydenburg, N. P.
Halpern, O. and Th. Holstein—No. 54
Haxby, R. O. and J. S. Allen—No. 42
Hegbar, H. R.—see Maxfield, F. A.
Hemmendinger, Arthur—No. 67
Herb, R. G., D. W. Kerst, D. B. Parkinson and G. J. Plain—No. 65
Herring, Conyers—No. 41
Heydenburg, N. P., L. R. Hafstad and M. A. Tuve—No. 63
Hipple, John A., Jr.—No. 35.
Hollaender, Alexander and Peter A. Cole—No. 34
Holmes, R. M. and H. W. Allen—No. 15
Holstein, Th.—see Halpern, O.
Holzer, R. E.—see Workman, E. J.
Horvay, Gabriel—No. 68

Johnson, R. P.—see Nelson, R. B.
Johnson, T. H. and M. A. Pomerantz—No. 50
——see Korff, S. A.

Kaplan, Joseph—Nos. 38, 77
Kellogg, J. M. B., I. I. Rabi, N. F. Ramsey, Jr. and J. R. Zacharias—No. 24
——see Rabi, I. I.
Kemble, Edwin C.—No. 60
Kerst, D. W.—see Herb, R. G.
Knipp, Julian K.—No. 53
Korff, S. A. and T. H. Johnson—No. 49
Kusch, P. and S. Millman—No. 28
——see Millman, S.

Landshoff, R.—No. 64
Lark-Horovitz, K. and C. H. Ehrhardt—No. 75
Lowen, Irving S.—No. 56
Ludloff, H.—No. 16

MacNair, D.—see Nix, Foster C.
Maxfield, F. A., H. R. Hegbar and J. R. Eaton—No. 9
Melvin, Eugene H.—see Wulf, Oliver R.
Merrill, Harrison J. and Harold W. Webb—No. 37
Millikan, R. A. and H. V. Neher—No. 46
Millman, S. and P. Kusch—No. 27
——see Kusch, P.
Mooney, Robert L.—No. 39
Murray, M. J.—see Cleveland, Forrest F.

Neher, H. V.—see Millikan, R. A.
Nelson, R. B. and R. P. Johnson—No. 11
Nix, Foster C. and D. MacNair—No. 74
——No. 79
——see Steigman, J.

O'Bryan, H. M.—see Skinner, H. W. B.

Parkinson, D. B.—see Herb, R. G.
Pigg, E. G.—see Fountain, C. R.
Pitzer, Kenneth S.—see Alvarez, Luis W.
Plain, G. J.—see Herb, R. G.
Pollock, H. C. and F. S. Cooper—No. 14
Pomerantz, M. A.—see Johnson, T. H.

Rabi, I. I., J. R. Zacharias, N. F. Ramsey, Jr. and J. M. B. Kellogg—No. 25
——see Kellogg, J. M. B.
Ramsey, N. F., Jr.—No. 26
——see Kellogg, J. M. B.
——see Rabi, I. I.
Ramsey, W. E.—see Swann, W. F. G.
Randall, H. M.—see Fuson, N.
Richtmyer, F. K. and R. E. Shrader—No. 71
Roberts, R. B. and P. Wang—No. 31
Rose, M. E. and H. A. Bethe—No. 55

Shockley, W.—see Steigman, J.
Shrader, R. E.—see Richtmyer, F. K.
Skaggs, L. S.—see Allison, Samuel K.
Skarstrom, C., H. E. Carr and J. W. Beams—No. 6
Skinner, H. W. B. and H. M. O'Bryan—No. 70
Smith, A. E. and Otto Beeck—No. 58
——see Beeck, Otto
Smith, Nicholas M., Jr.—see Allison, Samuel K.
Snoddy, L. B.—see Dietrich, J. R.
Stair, R.—see Coblentz, W. W.
Steigman, J., W. Shockley and F. C. Nix—No. 73
Stewart, J. K.—see Colwell, R. C.
Stockmann, L. L.—see Curtiss, L. F.
Swann, W. F. G. and W. E. Ramsey—No. 47

Thaxton, H. M.—see Breit, G.
Turner, A. Francis—see Cartwright, C. Hawley
Tuve, M. A.—see Heydenburg, N. P.

Wait, G. R.—No. 5
Wang, P.—see Roberts, R. B.
Webb, Harold W.—see Merrill, Harrison J.
Wells, W. H.—No. 45
Wheeler, A.—see Beeck, Otto
Workman, E. J. and R. E. Holzer—Nos. 40, 78
Wulf, Oliver R. and Eugene H. Melvin—No. 51

Zacharias, J. R.—see Kellogg, J. M. B.
——see Rabi, I. I.